7.B.1 Nuclear Physics B30 (1971) 1-67. North-Holland Publishing Company

PHENOMENOLOGY OF BACKWARD PHOTOPRODUCTION*

Edmond L. BERGER
High Energy Physics Division, Argonne National Laboratory, Argonne, Illinois 60439

Geoffrey C. FOX
Lauritsen Laboratory of Physics, California Institute of Technology, Pasadena, California 91109

Received 1 March 1971

Abstract: We investigate backward photoproduction reactions both empirically and in the context of specific models. First, salient features of backward single-pion photoproduction data are examined and contrasted with corresponding properties of purely hadronic data. We show that although γp and πN data are qualitatively similar below 5 GeV/c, remarkable differences become apparent at higher energies. Second, four models are studied in detail to see whether they offer an explanation for the distinctive energy and momentum transfer dependence of photoproduction cross sections. In these models, we include contributions from Regge (moving) and fixed poles, as well as absorptive (moving) and fixed cuts. Satisfactory fits to data are obtained with the fixed-pole model, the strong absorption model and the fixed-cut model of Carlitz, Kislinger, Bardakçi and Halpern. However, none of these profoundly different models is adequately tested by available data. Suggestions for many useful new experiments emerge from our study; the most important are backward $\pi N \to N\rho$, backward $\gamma N \to \Delta\pi$, $\gamma d \to pn$, and the inclusive processes $\gamma p \to h$ + anything ($h = \pi^{\pm}$, $K^{\pm}$, p and $\bar{p}$).

CONTENTS

1. Introduction
2. Comparison of hadron and photon induced backward scattering data
   - 2.1. $\gamma p \to N\pi$
   - 2.2. $\pi p \to N\pi$
   - 2.3. $\pi p \to N\rho$, $pp \to d\pi$ *and* $pp \to d\rho$
   - 2.4. *Suggested experiments*
     - 2.4.1. $\pi p \to N\rho$
     - 2.4.2. Forward ρ-production
     - 2.4.3. $\gamma p \to \Delta^{++}\pi^{-}$ and other photon induced backward reactions
     - 2.4.4. Inclusive reactions
     - 2.4.5. Independent confirmation of $\gamma p \to N\pi$ data
     - 2.4.6. Backward hadronic data

* Work performed under the auspices of the US Atomic Energy Commission.

3. Theoretical models and fits to data
3.1. $\Delta\alpha_{\text{eff}}$
3.1.1. Data
3.1.2. Theory
3.2. *Pure Regge-pole model*
3.2.1. Energy dependence
3.2.2. Momentum transfer dependence
3.2.3. Predictions
3.2.4. Vector dominance
3.2.5. Pole extrapolation
3.3. *Fixed-cut (HIPPIE) model*
3.3.1. General motivation
3.3.2. Previous development
3.3.3. Behavior as a function of momentum transfer
3.3.4. Behavior as a function of energy
3.3.5. Fits to data
3.3.5a. Trajectories
3.3.5b. Curves
3.3.6. Analysis and predictions
3.3.7. Unitarity in the u-channel
3.4. *Fixed-pole model*
3.4.1. Fits to data
3.4.2. Predictions
3.4.2a. s-dependence
3.4.2b. t- and u-dependence
3.4.2c. Quantum numbers and exotic exchange
3.4.3. Pole extrapolation
3.5. *Strong-absorption model*
3.5.1. Fits to data
3.5.2. Predictions
3.6. *Other models*
3.6.1. Absorption of fixed singularities
3.6.2. Complex poles
4. Comparison of models and suggestions for new experiments
4.1. *Energy dependence of* $\gamma N \to N\pi$
4.1.1. Experiments: verification of E_{lab}^{-3} behavior
4.2. *Reactions* $\gamma n \to p\pi^-$, $\gamma p \to \Delta^{++}$ *and* $\gamma d \to np$
4.2.1. Other charge states in $\gamma N \to N\pi$
4.2.2. $\gamma d \to np$ and $\gamma p \to \Delta^{++}\pi^-$; decisive tests of models
4.2.2a. u-dependence
4.2.2b. s-dependence
4.2.2c. Isoscalar-isovector interference
4.3. *Polarization measurements in* $\gamma N \to N\pi$, $\gamma N \to \Sigma K$ *and* $\gamma N \to \Lambda K$
5. Conclusions
Appendix A. Photoproduction kinematics and Regge-pole formalism
Appendix B. HIPPIE model
Appendix C. Fixed-pole model
Appendix D. Strong-absorption model
References

1. INTRODUCTION

Differential cross sections for both forward and backward two-body photoproduction processes exhibit little structure as a function of either energy or momentum transfer [1]. For example, at high energies, forward $d\sigma/dt$ scales with energy as E_{lab}^{-2} and backward $d\sigma/du$ scales as E_{lab}^{-3}. Moreover, forward $\gamma p \to \pi^0 p$ is the only photoproduction reaction for which there is a significant dip in the momentum transfer distribution [2]. Strong-interaction data behave very differently. For many purely-hadronic processes, differential cross sections display remarkable structure as a function of momentum transfer; this structure usually varies significantly with energy. Until now, little progress has been made theoretically in achieving even a qualitative understanding of photoproduction phenomena.

In this paper, after a thorough critique of γp data, we examine in detail four phenomenological models for backward single-pion photoproduction. We eschew features of models which are sensitive to subtle variation of parameters. Rather, we concentrate on obtaining a natural explanation for the observed universal dependence of $d\sigma/du$ on energy and momentum transfer.

We consider, in turn, models which employ Regge poles, fixed cuts, fixed poles, and moving Regge cuts generated by absorption. In two of these models (pure Regge pole and strong absorption [4]), no fundamental significance is attributed to observed differences between purely hadronic and photoproduction processes. The differences are associated merely with different *spin* structure of reaction amplitudes, and with values of sundry coupling constants. In the remaining two models, *a basis dynamical difference is postulated* between electromagnetic and hadronic interactions. In these models, fixed singularities are assumed to be present in the complex angular momentum (j) plane. These fixed singularities, forbidden by (u-channel) unitarity for purely-hadronic processes, are assumed to dominate photoproduction amplitudes.

One of these fixed-singularity models was suggested by Carlitz and Kislinger [4] and by Bardakçi and Halpern [5]. In this model, baryon resonances are ensured a unique parity, as observed, by the introduction of a fixed branch-point singularity (cut) in the j-plane. The amplitudes associated with this cut dominate scattering for $u < 0$. The discontinuity across the cut, at $u = 0$, is more singular than allowed by unitarity for purely hadronic processes. As a result, this theory can be applied only to weak and electromagnetic processes, for which no such unitarity constraint exists.

In the fourth model, we postulate the presence of fixed-poles in the j-plane. These poles are located at $j = 0, (-1, -2, \ldots)$ in meson channels and at $j = -\frac{1}{2}, (-\frac{3}{2}, -\frac{5}{2}, \ldots)$ in fermion channels. Again, unitarity forbids fixed poles in purely hadronic processes.

For each model, we begin by studying amplitudes analytically in order to ascertain natural predictions for s- and u-dependence. Amplitudes are then parametrized in economical fashion. We obtain good fits to data on $\gamma p \to n\pi^+$ and $\gamma p \to p\pi^0$ with our versions of the fixed-cut, fixed-pole, and strong-absorption models.

In spite of the high-statistical accuracy of present-data, these three models are not differentiated by the fits. Moreover, even within a given model, coupling-constant parameters are very poorly determined. This is remarkable, in one sense, because structure of basic amplitudes, as a function of both s and u, is radically different in different models. There are two basic reasons for these difficulties. First, the number of independent spin amplitudes (4) is relatively large in single-pion photoproduction. Second, for each spin state, there are three independent isospin amplitudes: $I_u = \frac{3}{2}$, and two $I_u = \frac{1}{2}$ states, formed from the isoscalar and isovector components of the photon. Consequently, further measurements on $\gamma p \to n\pi^+$ and $\gamma p \to p\pi^0$ and, say, $\gamma n \to p\pi^-$, although useful, will not lead to decisive tests of models *.

The reactions $\gamma p \to \Delta^{++}\pi^-$ and $\gamma d \to pn$ have an important simplifying feature; both have unique isospin in the u-channel. *We show that measurements of* $d\sigma/du$ *for these single-exchange reactions will indeed differentiate between models.* Moreover, data for these processes will clarify the interpretation of all photoproduction data (for both forward and backward scattering). This is true because the models studied here can be applied equally well to forward scattering; presumably the same general mechanism governs scattering near both $u = 0$ and $t = 0$. That is to say, if fixed poles, for example, dominate backward photoproduction, then presumably (different) fixed poles also dominate forward γp processes. By contrast with $\gamma p \to \Delta^{++}\pi^-$ and $\gamma d \to pn$, no forward γp process is endowed with a unique exchange in the crossed (t) channel.

Besides $\gamma p \to \Delta^{++}\pi^-$ and $\gamma d \to pn$, we suggest many other experiments which would be valuable in establishing a better understanding of photoproduction. Some of these experiments are motivated on purely empirical grounds; others are suggested by our theoretical analyses. Suggested experiments are listed in sects. 2 and 4.

In sect. 2, we review backward photoproduction data and contrast salient characteristics with those of purely hadronic reactions. Independent of any fits, this study emphasizes the remarkable features of photoproduction data and highlights the need for further experiments. We examine qualitative predictions of vector-meson dominance and find interesting discrepancies at high energy; further experimental study of backward ρ-production in purely hadronic processes seems desirable. We also show that important information will be provided by data on *inclusive reactions* of the type $\gamma p \to h$ + anything, where hadron $h = \pi^{\pm}$, $K^{\pm}$, p and $\bar{p}$.

In sect. 3, we treat our four theoretical models. Technical details are presented in appendices. Because the fixed-pole and fixed-cut models are relatively unfamiliar, we take the opportunity in subsects. 3.3 and 3.4 to discuss some of their qualitative predictions, in a context more general than backward photoproduction.

In sect. 4, we contrast predictions of the models and make specific recommendations for useful experiments. General conclusions are summarized in sect. 5.

* This is true unless, of course, new data indicate behavior which is qualitatively different from current experiments.

Readers interested in an empirical evaluation of γp and hadronic data are directed to sect. 2. However, sect. 2 may be omitted entirely by readers interested primarily in phenomenological models and fits to data. Experimenters interested in a list of valuable new experiments may consult sect. 4 and subsect. 2.4.

2. COMPARISON OF HADRON AND PHOTON INDUCED BACKWARD-SCATTERING DATA

In this section, we describe first the distinctive features of backward-angle photoproduction data * and then contrast these with corresponding properties of backward πN data. Pion-nucleon and γp data are remarkably different in their dependence on both energy- and momentum-transfer variables. Qualitative discrepancies with predictions of vector-meson dominance [6, 7] are also revealed. These observations and other empirical regularities of the data suggest several useful experiments.

2.1. $\gamma p \to N\pi$

In fig. 1, we present measured $d\sigma/du$ for $\gamma p \to n\pi^+$, $\gamma p \to p\pi^0$, and $\gamma p \to \Delta^{++}\pi^-$ [8-10]. We have plotted these data as

$$494\,(\tfrac{1}{5}E_{\mathrm{lab}})^3\,\frac{d\sigma}{du}. \tag{1}$$

The factor $(\frac{1}{5}E_{\mathrm{lab}})^3$ removes obvious energy dependence from the data; the factor 494 is suggested by the vector-meson-dominance model (VDM), in the following way. According to VDM, we may relate the cross section for pion photoproduction $[d\sigma/du(\gamma N \to N\pi)]$ to that for strong-interaction vector-meson production $[d\sigma/du(\pi N \to NV)]$. This relationship is

$$\frac{8}{\alpha}\left(\frac{\gamma_\rho^2}{4\pi}\right)\frac{d\sigma}{du}(\gamma N \to N\pi) = 2\rho_{11}\,\frac{d\sigma}{du}(\pi N \to N[\rho + \tfrac{1}{3}(\omega - \sqrt{2}\varphi)]). \tag{2}$$

In eq. (2), the spin-density matrix element picks out the helicity-one component of the ρ-meson †; γ_ρ^2 is the usual universal ρ-coupling constant [11]; and $(8/\alpha)(\gamma_\rho^2/4\pi) = 494$, if we use generally accepted value $(\gamma_\rho^2/4\pi) = 0.45$.

In order to compare the energy- and momentum-transfer dependences of these γp data, we find it convenient to define the solid curve shown in fig. 1 (and succeeding figures). The solid curve is a representation of eq. (1), for the very accurate 5 GeV $\gamma p \to n\pi^+$ data. In figs. 1a and 1b, by comparing data at various energies with the solid curve, one may see that *both* $n\pi^+$

* A good review of photoproduction is the article by Diebold [1].

† Exact application of VDM is impossible, even if $d\sigma/du$ is available for ρ-, ω- and φ-production. Interference effects remain to be sorted out. In what follows, we assume that the qualitative behavior of ω and φ cross sections is similar to that for ρ-production. Inasmuch as our conclusions, in this section, are based only on qualitative features of data, we deem it satisfactory to refer only to ρ-production when we make VDM comparisons.

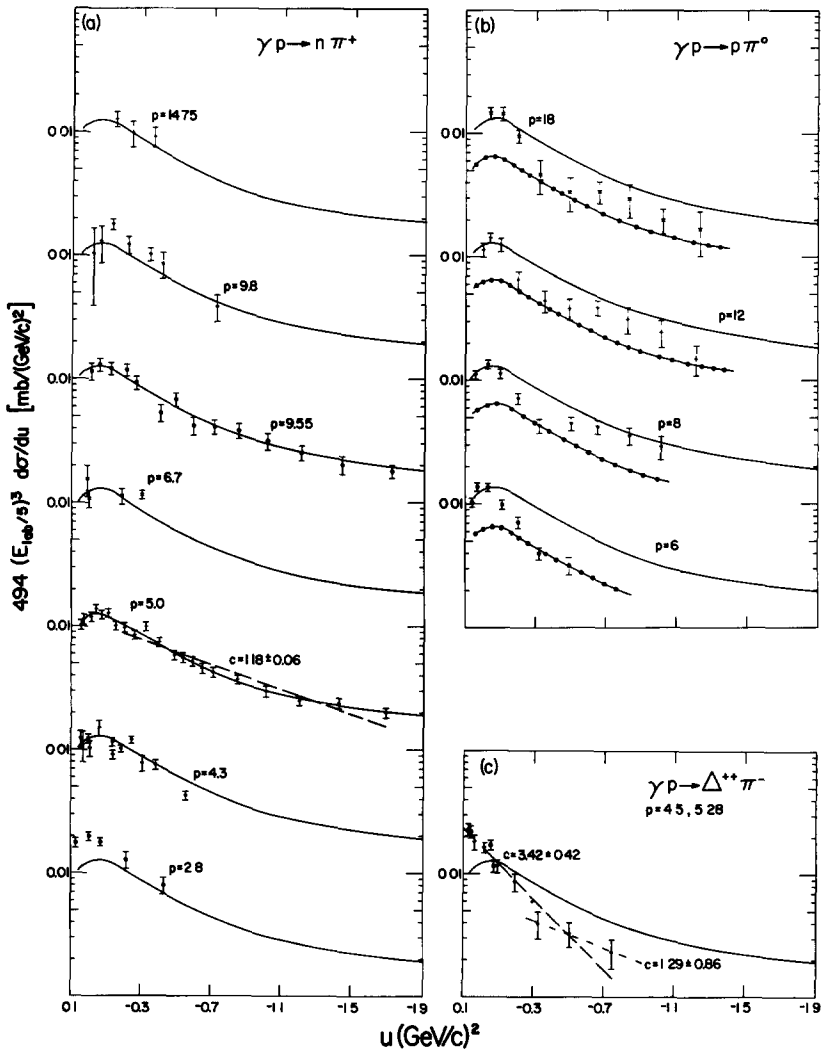

Fig. 1. Single-pion photoproduction data are displayed, p denotes photon lab momentum in GeV. For reasons discussed in the text, we plot 494 $(\frac{1}{5}E_{\mathrm{lab}})^3$ $d\sigma/du$ versus u. In all cases, the solid curve represents (scaled) 5 GeV $\gamma p \to n\pi^+$ data. At each energy, to obtain the dotted curve in (b), we multiply the solid curve by 0.5 Dashed straight lines represent best fits to data with the equation $d\sigma/du = A \exp(cu)$; fitted values of c (in units of $(\mathrm{GeV}/c)^{-2}$) are given in the figure. References for data are (a) $\gamma p \to n\pi^+$ at E_{lab} = 2.8, 4.3, 6.7 and 9.8 GeV [8] and $\gamma p \to n\pi^+$ at E_{lab} = 4.3, 5.0, 9.55 and 14.75 GeV [9], (b) $\gamma p \to p\pi^0$ [10]; (c) $\gamma p \to \Delta^{++}\pi^-$ [9].

and $p\pi^0$ *data scale remarkably with energy* * *as* E_{lab}^{-3}, for all u. There is no shrinkage †. (The deviation at $E_{lab} = 2.8$ GeV in $\gamma p \to n\pi^+$ is a resonance effect; confer fig. 18a.) A second feature of interest is that data for $\gamma p \to n\pi^+$ and $\gamma p \to p\pi^0$ have quite similar u-variation; in both, $d\sigma/du$ falls slowly, approximately as $\exp(u)$. Data for $\gamma p \to \Delta^{++}\pi^-$, which has u-channel isospin $I_u = \frac{3}{2}$, seem to fall off as $\exp(3u)$ (fig. 1c); however, these data are confined to small values of u, at essentially one energy. Finally, the dotted curve in fig. 1b denotes $\frac{1}{2}d\sigma/du(\gamma p \to n\pi^+)$; this would be the value of $d\sigma/du(\gamma p \to p\pi^0)$ if only $I_u = \frac{1}{2}$ exchanges were present in $\gamma p \to p\pi^0$ and $\gamma p \to n\pi^+$.

2.2. $\pi p \to N\pi$

Other significant characteristics of γp data become apparent when contrasted with properties of purely hadronic processes. We turn now to a brief examination of some typical hadronic data; when possible, we select experiments with results extending to large values of $|u|$. We discuss $\pi N \to N\pi$ first, and then go on to $\pi N \to N\rho$, $pp \to d\pi$, and $pp \to d\rho$. In fig. 2, we display a selection of data for the three measured charge states of πp backward scattering. These data are plotted as $(\frac{1}{5}p_{lab})^3\, d\sigma/du$. At each energy, we also show for comparison the $\gamma p \to n\pi^+$ data, scaled as in eq. (1). The most obvious difference in u-dependence between γp data and $\pi^+p \to p\pi^+$ or $\pi^-p \to n\pi^0$ is that backward γp data show no dip structure whatsoever. Second, there is considerable shrinkage in the πp data, whereas none appears in the γp data. Specifically, we note that the u-dependence for $\gamma p \to n\pi^+$ is similar to that of hadronic data for $p_{lab} \lesssim 4$ GeV/c. However, as energy increases, the πp data fade away at large u; thus, at the higher energies, $d\sigma/du \approx \exp(3u)$ for πp, significantly sharper than the $\exp(u)$ characteristic of γp results. Especially noteworthy are $\pi^+p \to p\pi^+$ data at 9.85 and 13.73 GeV/c; near $u = 0$, these data are a factor of 10 above the (scaled) γp results, but by $u = -1.9$ (GeV/c)^2, they lie a decade below ‡.

2.3. $\pi p \to N\rho$, $pp \to d\pi$ *and* $pp \to d\rho$

As expressed through eq. (2), the VDM model postulates close similarity between data for $\gamma p \to N\pi$ and for $\pi N \to N\rho$. Available backward-ρ production data are displayed in fig. 3; shown are examples of $\pi^-p \to p\rho^-$, $\pi^-p \to n\rho^0$, and $\pi^+p \to p\rho^+$. We observe that at low energy, slopes of $d\sigma/du$ for $\pi N \to N\rho$ are similar to those of $\gamma p \to N\pi$. This result is in superficial agreement with VDM. Unfortunately, *no large-u* data exist *at high energy* for reaction $\pi^-p \to n\rho^0$. Therefore, we cannot determine directly whether

* As first remarked by the experimenters, of course [8-10].

† 'Shrinkage' is a property of simple Regge-pole models and of much hadronic data. It indicates that, as a function of E_{lab} at fixed u, $d\sigma/du \propto \exp(g(u)\log E_{lab})$, where $g(u)$ is an increasing function of u. For example, in a single-pole exchange model, $g(u) = 2\alpha' u$, where α' is the slope of the exchanged trajectory.

‡ We remark that if γp cross sections continue to differ by $\exp(2u)$ from πp values, out to even larger u, then at $u \approx -4.0$ (GeV/c)^2, the factor of 494 will be overcome; the cross section for producing photons in πp interactions will then be greater than that for producing hadrons. This is surely ridiculous.

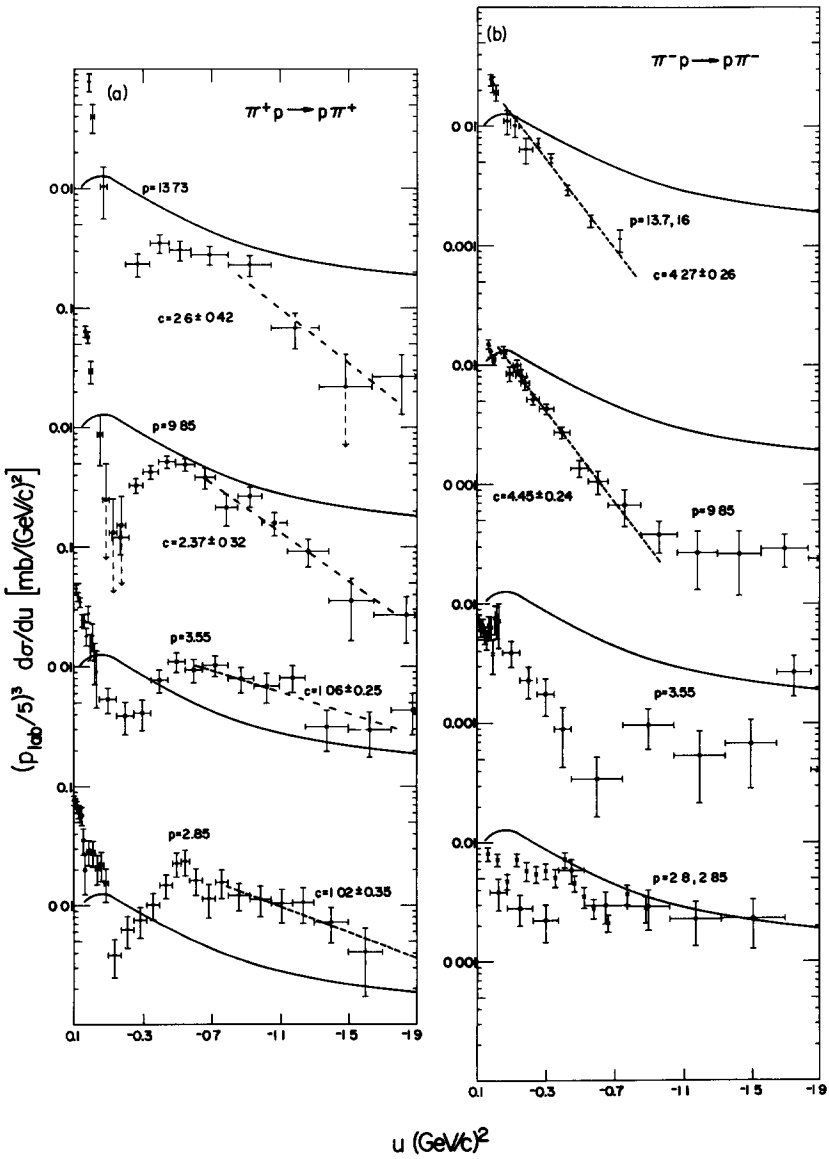
(a)
π⁺p → pπ⁺
p=13.73
c=2.6±0.42
p=9.85
c=2.37±0.32
p=3.55
c=1.06±0.25
p=2.85
c=1.02±0.35
(b)
π⁻p → pπ⁻
p=13.7, 16
c=4.27±0.26
c=4.45±0.24
p=9.85
p=3.55
p=2.8, 2.85
(p_lab/5)³ dσ/du [mb/(GeV/c)²]
u (GeV/c)²

Fig. 2a

Fig. 2b.

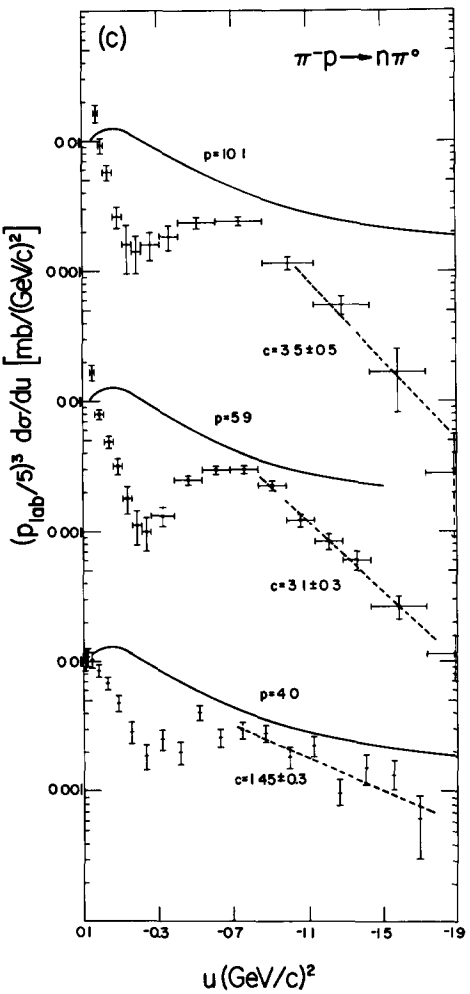

Fig 2c.

Fig. 2. We display a selection of backward data from the three charge states of $\pi p \to N\pi$; p denotes incident pion lab momentum in (GeV/c). In order to compare energy dependence of these data with γp data, we plot $(\frac{1}{5}p_{lab})^3\, d\sigma/du$ versus u. The solid curve is 494 $(\frac{1}{5}E_{lab})^3\, d\sigma/du$ for the 5 GeV $\gamma p \to n\pi^+$ data (cf. fig. 1). Dashed lines here are obtained as in fig. 1. References for data are (a) $\pi^+p \to p\pi^+$ at 2.85 and 3.55 GeV/c [12,13], and $\pi^+p \to p\pi^+$ at 9.85 and 13.73 GeV/c [14]; (b) $\pi^-p \to p\pi^-$ at 2.8 GeV/c [15], $\pi^-p \to p\pi^-$ at 2.85 and 3.55 GeV/c [12], $\pi^-p \to p\pi^-$ at 3.55 GeV/c [13], $\pi^-p \to p\pi^-$ at 9.85 and 13.73 GeV/c [14], $\pi^-p \to p\pi^-$ at 16 GeV/c [16]. In (b), 16 GeV/c $\pi^-p \to p\pi^-$ data have been multiplied by 0.65; consult ref. [17] for a discussion of normalization discrepancies in this reaction. For $\pi^-p \to n\pi^0$, part (c), references are [18] for 4 GeV/c data, and [19] for 5.9 and 10.1 GeV/c.

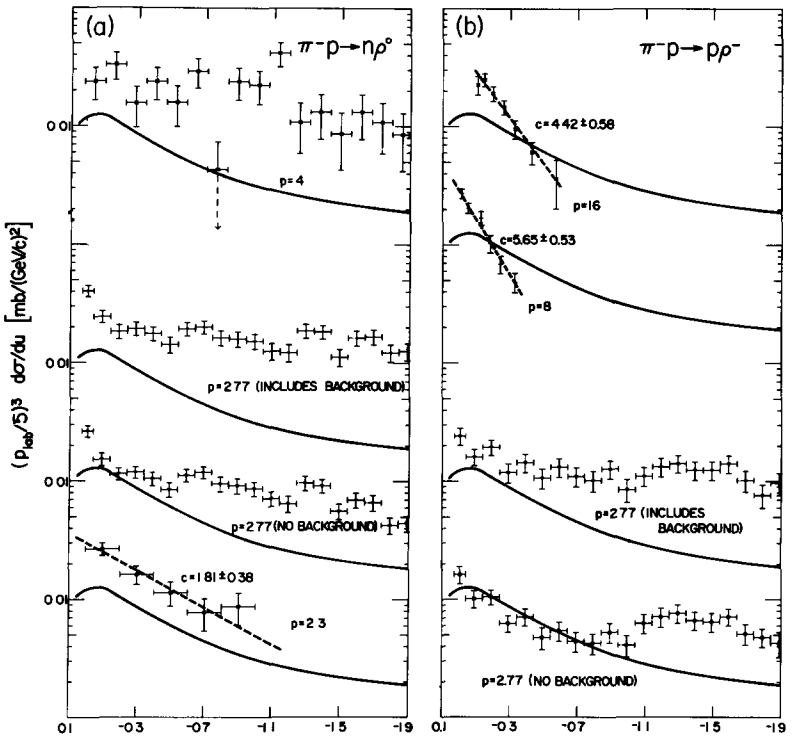

Fig. 3a. Fig. 3b.

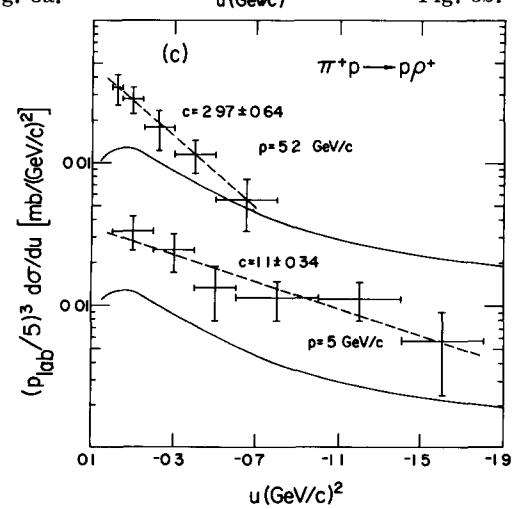

Fig. 3c.

Fig. 3. We display $(\frac{1}{5}p_{\mathrm{lab}})^3\, d\sigma/du$ for three charge states of backward $\pi p \to N\rho$; p denotes incident pion lab momentum. In this figure, solid and dashed curves have the same meaning as in fig. 2. References for data are (a) $\pi^- p \to n\rho^0$ at 2.3 GeV/c [20], at 2.77 GeV/c [21], and at 4 GeV/c [22]; (b) $\pi^- p \to p\rho^-$ at 2.77 GeV/c [21], and at 8 and 16 GeV/c [23], (c) $\pi^+ p \to p\rho^+$ at 5 GeV/c [24] and at 5.2 GeV/c [25].

$\pi N \to N\rho$ data show the same slow $\exp(u)$ behavior as $\gamma p \to N\pi$, as required by VDM, or whether shrinkage is present.

Although not exactly relevant, data for production of charged-ρ, both $\pi^- p \to p\rho^-$ and $pp \to d\rho^+$, do foreshadow difficulties for VDM. Indeed, at 8 and 16 GeV/c, the pure $I_u = \frac{3}{2}$ $\pi^- p \to p\rho^-$ data have a slightly steeper $d\sigma/du$ (for $u \gtrsim -0.6$ (GeV/c)^2) than data for $\pi^- p \to p\pi^-$. (Contrast figs. 2b and 3b.) There is no hint of the flat $\exp(u)$ behavior characteristic of $\gamma p \to N\pi$. A similar effect is observed in the pure $I_u = \frac{1}{2}$ reactions $pp \to d\pi^+$ and $pp \to d\rho^+$. Data are given in fig. 4. At low energy ($p_{lab} \approx 3.5$ GeV/c), $d\sigma/du$ shows a slow $\exp(u)$ behavior characteristic of low energy photonic and hadronic data. However, by 21 GeV/c, shrinkage of $d\sigma/du$ has occurred, and $d\sigma/du \approx \exp(3u)$. We emphasize that $d\sigma/du$ is quite similar, out to $u \approx -1.0$ (GeV/c)^2, for $pp \to d\pi^+$ and $pp \to d\rho^+$.

It appears, therefore, that $d\sigma/du$ for hadronic ρ-production at high energy shows little similarity to the slowly varying ($\exp(u)$) γp data. On the contrary, it is similar to purely hadronic πN data at large u. We have

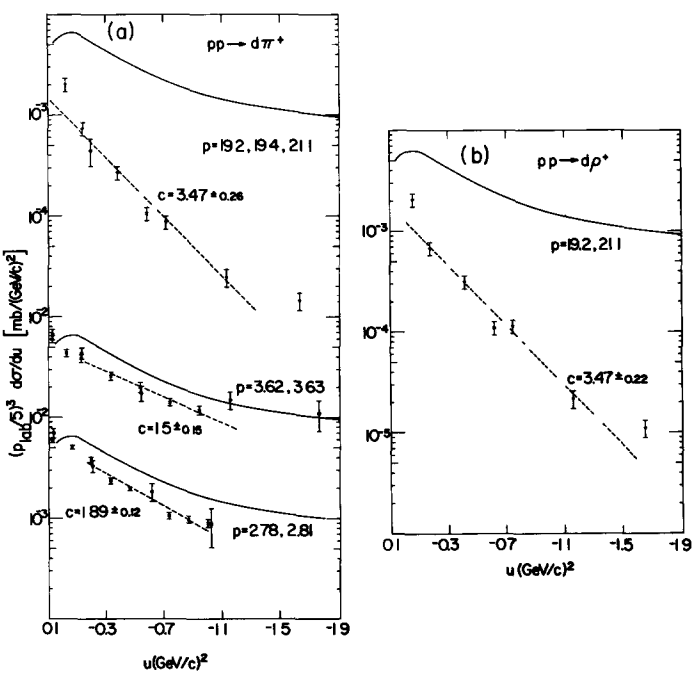

Fig. 4. We display $(\frac{1}{5}p_{lab})^3$ $d\sigma/du$ for (a) $pp \to d\pi^+$ and (b) $pp \to d\rho^+$; symbol p next to data points denotes proton lab momentum in GeV/c. The solid curve is 0.5 times 494 $(\frac{1}{5}E_{lab})^3$ $d\sigma/du$ for 5 GeV $\gamma p \to n\pi^+$ data. Dashed lines have the same meaning as in fig. 1. References for data are (a) $pp \to d\pi^+$ at 2.78 and 3.62 GeV/c [26], at 2.81 and 3.63 GeV/c [27], and at 19.2, 19.4 and 21.1 GeV/c [28]; (b) $pp \to d\rho^+$ at 19.2 and 21.1 GeV/c [28]; (b) $pp \to d\rho^+$ at 19.2 and 21.1 GeV/c [28]. We obtain values of $pp \to d\pi^+$ at 2.81 and 3.63 GeV/c by applying time-reversal invariance to data on $\pi^+ d \to pp$ [27].

shown that this conclusion holds separately for the $I_u = \frac{1}{2}$ and $I_u = \frac{3}{2}$ exchange amplitudes.

2.4. *Suggested experiments*

In this section, we have examined backward γp data and contrasted salient features with those of backward πN data. Quite aside from model-dependent arguments which we consider in sect. 3, this study demonstrates the remarkable energy- and momentum-transfer dependence of photoproduction processes. Especially significant is the energy independent shape of $d\sigma/du$, which behaves roughly as $\exp(u)$ for $0.5 \leq |u| \leq 1.7$ $(\mathrm{GeV}/c)^2$. In the (low) energy range $2 \leq p_{\mathrm{lab}} \leq 5$ GeV/c, a similar u-dependence is observed for the purely hadronic processes, backward $\pi N \to N\pi$ and $\pi N \to N\rho$ (figs. 2,3). Therefore, in this energy region, there is *qualitative* agreement with VDM. However, for $p_{\mathrm{lab}} > 5$ GeV/c, hadronic data exhibit striking shrinkage; all $d\sigma/du$ fall typically as $\exp(3u)$ at large u (figs. 2,4). This is in marked contrast to γp data (fig. 1) which retain an $\exp(u)$ behavior at high energy. The apparent *dis*agreement with VDM will be reversed if, at high energy, the quantity $\rho_{11}\, d\sigma/du$ for $\pi N \to N(p^0, \omega, \varphi)$ is observed to be slowly varying at large u, in contrast to $d\sigma/du$ for $\pi N \to N\pi$.

As a result of this analysis, we can identify several important areas for experimental investigation. (More suggestions are listed in sect. 4, after models have been discussed.)

2.4.1. $\pi p \to N\rho$

Backward ρ-production should be studied at high energy ($p_{\mathrm{lab}} > 5$ GeV/c) from $u = 0$ to $u \approx -1.5$ $(\mathrm{GeV}/c)^2$, in both neutral ($\pi^- p \to n\rho^0$) and charged modes ($\pi^{\pm} p \to \rho^{\pm} p$). Determination of $d\sigma/du$ and of density matrix elements would be valuable. Studies of backward φ and ω cross sections would also be intriguing. In the forward direction, production of φ and ω is suppressed in comparison with ρ; however, all vector-meson amplitudes should be of comparable size in the backward direction.

En passant, we note here that knowledge of density matrix elements (ρ_{ij}) is not as valuable in backward scattering as it is in forward scattering. In forward scattering, the ρ_{ij} are sensitive directly to quantum numbers of exchanges (natural or unnatural parity); this is not the case in backward scattering. Nevertheless, measurements of ρ_{ij} are still useful. For $\pi p \to N\rho^0$, $\rho_{11}\, d\sigma/du$ (rather than simply $d\sigma/du$) is the quantity which is exactly relevant for tests of VDM. Moreover, inasmuch as the ρ_{ij} select out specific (sums of) amplitudes, they serve as more pointed tests of all models. This is true because models predict primarily structure of amplitudes, not* $d\sigma/du$. As an example, it is possible to attribute absence of dip structure in $d\sigma/du$ for $\pi N \to N\rho$ to predominance of the $\rho_{11}\, d\sigma/du$ contribution, which, consistent with $d\sigma/du$ for $\gamma N \to N\pi$, has no dip. However, there may be a dip in $\rho_{00}\, d\sigma/du$, similar to that in $d\sigma/du$ for $\pi^+ p \to p\pi^+$ and $\pi^- p \to n\pi^0$.

* Individual amplitudes may exhibit pronounced structure (e.g., dips or breaks) which occurs at different values of u in different amplitudes. Nevertheless, the resultant $d\sigma/du$, which is a linear combination of absolute squares of amplitudes, can be quite featureless [3,17,53].

2.4.2. Forward ρ-production

Although we have not discussed *forward* scattering results, it is curious that there does not appear to be a striking difference in shape of $d\sigma/dt$, at large t, between photon and hadron induced reactions in the forward direction. This should be contrasted with the backward data we have just reviewed. Indeed, for many hadronic and photonic processes, forward $d\sigma/dt$ falls approximately as $\exp(3t)$, at large t. Examples are forward $\gamma p \to \pi^0 p$ and $\pi^- p \to \pi^0 n$ *. This behavior is similar to that of the backward hadronic processes $\pi^+ p \to p\pi^+$ and $\pi^- p \to n\pi^0$ at large u †. However, tests of VDM require ρ-production data; it must be borne in mind that there is a dearth of good ρ-data at high energy and large momentum transfer. To test VDM, it is vital to measure forward ρ-production at high energies ($p_{lab} \gtrsim 8$ GeV/c) where we have noticed such a marked difference between backward $\gamma p \to n\pi^+$ and backward processes. Thus far, most tests of VDM have been confined to low energy where there are no qualitative differences between γp and πp results.

Our examination of backward data further indicates that discrepancies with VDM are greatest at large $|u|$. In forward scattering, therefore, tests of VDM are also expected to be most decisive at large $|t|$. This suggestion is supported by another argument; specifically, the dominance of π-exchange *at small t* guarantees some agreement with VDM independently of any fundamental validity of the model.

2.4.3. $\gamma p \to \Delta^{++}\pi^-$ and other photon induced backward reactions

The reaction $\gamma p \to \Delta^{++}\pi^-$ provides a possible exception to the universal $\exp(u)$ behavior of $d\sigma/du$ for backward γp data (cf. fig. 1c). It is clearly important to determine whether $d\sigma/du$ for $\gamma p \to \Delta^{++}\pi^-$ continues to fall as $\exp(3u)$ or whether it also levels off at $\exp(u)$, for large values of $|u|$. More generally, it is crucial to confirm or deny the apparent universality of s- and u-dependence of current $\gamma p \to N\pi$ data. Other reactions should be studied; e.g., $\gamma d \to pn$ and $\gamma N \to YK$ [62]. We will consider these again in sect. 4

2.4.4. Inclusive reactions

Inclusive processes of the type $\gamma p \to$ (hadron + anything) deserve special mention.

We have remarked here that $d\sigma/du$, for *backward* $\gamma p \to N\pi$, falls as $\exp(u)$, at large u ($|u| \geq 0.5$ (GeV/c)^2). On the other hand, for photon induced *forward* two-body processes, $d\sigma/dt \propto \exp(3t)$ at large t. In purely hadronic processes, such a marked difference does not exist between

* We remark that $d\sigma/dt$ for forward $\gamma p \to p\pi^0$ falls as $\exp(3t)$, at large t, for $p_{lab} = 6$ and 18 GeV [29, 55]. On the other hand, for $\pi^- p \to \pi^0 n$, good measurements of $d\sigma/dt$ out to large t exist only near $p_{lab} = 6$ GeV [30, 56]. At 6 GeV/c, the t-dependence is similar for the two processes. It is important to measure $d\sigma/dt$ at large t for $\pi^- p \to \pi^0 n$ at $p_{lab} \approx 18$ GeV/c, one should determine whether $\pi^- p \to \pi^0 n$ behaves like $\gamma p \to p\pi^0$, retaining the same slope of $d\sigma/dt$ at both high and low energies, or whether it exhibits shrinkage at large t, as it does at small t.

† Note also that, in all four examples here, there is a pronounced dip in the differential cross section.

large-momentum-transfer behavior of forward and backward two-body reactions. For forward hadronic processes, $d\sigma/dt \propto \exp(3t)$ and for backward reactions, $d\sigma/du \propto \exp(3u)$. These observations can be correlated with available data from inclusive reactions; there seem to be interesting inconsistencies in γp data.

We begin by recalling that, for *hadron* induced inclusive reactions * $d\sigma/dp_T^2 \propto \exp(-3p_T^2)$, *for all types of produced hadrons* †. This universal *behavior is modified* only slightly by a tendency for $\langle p_T \rangle$ to increase with increasing mass of the observed final-state hadron. It seems to us that this universality of the p_T^2 dependence is consistent (and possibly directly connected) with the fact that the differential cross sections for many purely hadronic two-body processes (forward and backward) fall as $\exp(3t)$.

We now use the above information to deduce expected behavior of γp inclusive reactions. Because forward and backward *photon induced* two-body processes differ substantially in behavior at large momentum transfer, we postulate analogous differences in γp inclusive processes. Specifically, for $\gamma p \rightarrow h + \text{anything}$, we expect $d\sigma/dp_T^2 \propto \exp(-3p_T^2)$ if $h = \pi^{\pm}$ or $K^{\pm}$, but $d\sigma/dp_T^2 \propto \exp(-p_T^2)$ if h = proton.

Beam survey measurements provide the only source of photoproduced inclusive data of which we are aware. These studies are performed with a beryllium (Be) target [33]. It turns out that there is not much difference in shape of $\pi^{\pm}$, $K^{\pm}$, and proton spectra at large angles ‡; remarkably, $d\sigma/dp_T^2 \propto \exp(-3p_T^2)$, for all types of secondary particles. This fact that secondary proton and π-spectra are nearly identical in p_T^2 dependence, for $p_T^2 > 0.2\ (\text{GeV}/c)^2$, contrasts sharply with the pronounced difference in large-momentum-transfer behavior of forward and backward two-body photoproduction processes.

It might be argued that inclusive measurements done with a Be target should not be compared directly with results obtained from hydrogen (i.e. proton) targets. However, we note that, for purely hadronic processes at any rate, *shapes* of spectra at large angles (lab frame) are essentially independent of target material [32]. To deduce p_T^2 dependence from this result, one must make a small approximation, because the exact definition of longitudinal direction and thus of p_T is somewhat ambiguous for experiments done with complex nuclei. Nevertheless, if motion of nucleons with the nucleus is ignored, one finds again the universal behavior $\exp(-3p_T^2)$, for all secondary hadrons, a result identical to that for inclusive experiments with proton targets. Therefore, p-Be and pp data are comparable;

* The quantity p_T is the component of three-momentum transverse to the beam direction, $p_T^2 \propto (t - t_{min})$.

† E.g., for $pp \rightarrow h + \text{anything}$ at 12 GeV/c [31] and at 19 GeV/c [32], $d\sigma/dp_T^2 \propto \exp(-3p_T^2)$ for $h = \pi^{\pm}$, $K^{\pm}$, p and p. The result is true for a wide range of values of p_L, the longitudinal momentum of h in the c.m. frame. The proportionality fails for very small p_T^2 ($p_T^2 < 0.2\ (\text{GeV}/c)^2$) and for values of p_L near the kinematic limits.

‡ Consult ref. [33], especially table 3 and figs. 14-19. There is a forward peak in $\pi^{\pm}$ spectra; however, for $0.2 < p_T^2 < 2$, the expression $\exp(-3p_T^2)$ is a good approximation.

correspondingly, it seems legitimate to equate p_T^2 dependence in γ-Be and γp inclusive reactions.

In summary, therefore, the very shallow behavior of $d\sigma/du$ ($\propto \exp(u)$) for $\gamma p \to N\pi$ strikes us as remarkably inconsistent both with hadronic data and with all other photoproduction data. Photon-induced inclusive experiments, done on an hydrogen target, will provide important confirmation (or possible denial) of this conclusion. Therefore, we await with great interest detailed studies of $d^2\sigma/dp_L\, dp_T^2$ for various secondary hadrons (h) produced in $\gamma p \to h$ + anything.

2.4.5. Independent confirmation of $\gamma p \to N\pi$ data

In this section we have pointed out, from several empirical points of view, that $d\sigma/du$ for $\gamma p \to N\pi$ behaves quite anomalously in its dependence on both energy and momentum transfer. The singular absence of shrinkage makes all photoproduction data mysterious. Moreover, as detailed in subsect. 2.4.4, the very shallow $\exp(u)$ behavior of $d\sigma/du$ sets $\gamma p \to N\pi$ apart from all other data, both purely hadronic and photon induced. As we noted, almost all distributions in p_T^2 or t have an empirical slope (on a log plot) of 3; the exception* is $\gamma p \to N\pi$ which has slope 1.

We cannot overemphasize the desirability of confirming existing γp results by using different experimental techniques. Systematic biases may be present which cancel shrinkage and/or result in unusually shallow differential cross sections. In this regard, we note that there are significant differences ($\approx 35\%$) between results of single-arm and double-arm spectrometer studies of $\pi^- p \to p\pi^-$ [14, 16].

2.4.6. Backward hadronic data

In an earlier paper [17], we suggested several specific experiments the results of which should clarify the status of πN backward scattering. Here, we call attention to one general feature of hadronic data which is especially relevant to our analysis of γp data. At low energy ($p_{lab} < 5$ GeV/c), $d\sigma/du$ for available hadronic data (cf. figs. 2-4) may be parametrized as $\exp(u)$, for $|u| > 0.5$ (GeV/c)^2; at higher energies, $d\sigma/du \propto \exp(3u)$. We have attributed this change in $d\sigma/du$ to shrinkage. However, present backward data are really not sufficiently precise to establish a *gradual systematic change* with energy of the slope of $d\sigma/du$. We do not know whether a constant $\exp(3u)$ distribution characterizes hadronic data at *all* (high) energies, or whether canonical shrinkage is indeed present. An understanding of dynamical mechanisms in this region awaits clarification of this point. Precise studies should be made of the energy dependence of $d\sigma/du$, for various hadronic processes (e.g., $\pi N \to N\pi$), for $p_{lab} > 5$ GeV/c, and values of u in the range $0 \leq |u| \leq 1.5$ (GeV/c)^2. Specifically, usual Regge shrinkage predicts that if $d\sigma/du \propto \exp(3u)$ at $p_{lab} = 6$ GeV/c, then $d\sigma/du \propto \exp(5u)$ at $p_{lab} = 18$ GeV/c. Experiments must be designed to distinguish this behavior from the energy independent behavior of photoproduction cross sections at large $|u|$ (and large $|t|$).

* The only other evidence for very shallow dependence on momentum transfer comes from inelastic electron data [34].

3. THEORETICAL MODELS AND FITS TO DATA

We devote this section to a detailed discussion of phenomenological models for $\gamma p \to N\pi$. We examine, in turn, models which employ Regge poles, fixed cuts, fixed poles, and moving Regge cuts generated by absorption. Each model is first studied in an effort to identify its natural predictions for energy- and momentum-transfer dependence of $\gamma p \to N\pi$. Amplitudes are then parametrized and good fits to data are obtained with the fixed-cut, fixed-pole, and strong-absorptive-cut models. As a result of this investigation, we suggest new experiments which would test significant predictions of each model.

We should remark here that, in spite of reservations listed in sect. 2, we take seriously in this section present experimental information on the energy- and momentum-transfer behavior of $\gamma p \to N\pi$.

3.1. $\Delta\alpha_{\text{eff}}$

In sect. 2, we examined the salient features of backward photoproduction data. We pointed out that, as a function of u, $d\sigma/du$ for $\gamma p \to N\pi$ is remarkably slowly varying; over the range $0.5 < |u| < 1.7$ (GeV/c)^2, $d\sigma/du$ is described reasonably well by $\exp(u)$. Furthermore, as a function of energy, $d\sigma/du$ shows no evidence of shrinkage.

For both data and theory, the energy dependence of $d\sigma/du$ is expressed most succinctly in terms of the function $\Delta\alpha_{\text{eff}}(u)$, which we define through the parametrization

$$E_{\text{lab}}^{3}\,\frac{d\sigma}{du} = A(u)\,E_{\text{lab}}^{2\Delta\alpha_{\text{eff}}(u)} \,. \tag{3}$$

Note that $\Delta\alpha_{\text{eff}} = \alpha_{\text{eff}} + \frac{1}{2}$; α_{eff} is defined in ref. [17].

3.1.1. Data

By fitting this expression to data as a function of E_{lab}, at fixed u, we extract $\Delta\alpha_{\text{eff}}$ for $\gamma p \to n\pi^+$ and for $\gamma p \to p\pi^0$. These results are shown in fig. 5. We see clearly that $\Delta\alpha_{\text{eff}} \approx 0$, for all u; this is in agreement with the empirical scaling law $d\sigma/du \propto E_{\text{lab}}^{-3}$, which we discussed in sect. 2.

3.1.2. Theory

In the various theoretical models, different assumptions are made about the dynamical singularity structure of the complex angular momentum (j or α) plane. Singularities in the j-plane are either fixed or move (Regge) as the momentum transfer is varied. Moreover, the singularities may be simple poles or branch points (cuts). These properties of the different theories are displayed easily in a plot of $\Delta\alpha(u) = \alpha(u) + \frac{1}{2}$. Consequently, plots of $\Delta\alpha_{\text{eff}}(u)$ are particularly useful when one is confronting theoretical models with data.

We now turn to a study of available models; we are particularly interested in how each model explains the fact that $\Delta\alpha_{\text{eff}}(u) \approx 0$. In figs. 6a-d, we display the structure of the $\Delta\alpha$ plane predicted by each of our four models. These figures are discussed below. We begin by treating briefly the

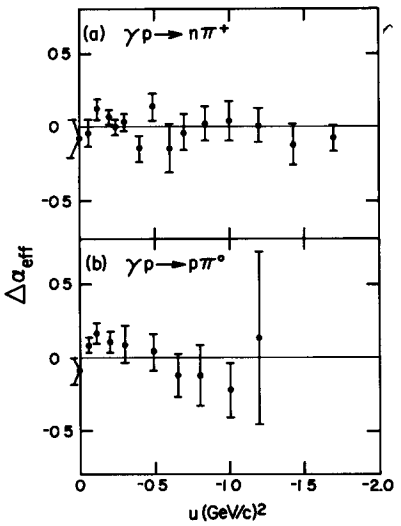

Fig. 5. Experimental j-plane. We show values of $\Delta\alpha_{\text{eff}}$ extracted from data for (a) $\gamma p \to n\pi^+$ and (b) $\gamma p \to p\pi^0$, the function $\Delta\alpha_{\text{eff}}(u)$ is defined in eq. (3) of the text. Where necessary, we extrapolate data from neighboring values of u in order to obtain $\Delta\alpha_{\text{eff}}$ at the values of u shown here.

pure Regge-pole model. Our major emphasis is then devoted to fixed-cut and fixed-pole models. Finally, we also discuss moving-cut approaches.

3.2. *Pure Regge-pole model*

The application of the pure Regge-pole model to backward photoproduction data has been described very well in several previous papers [35-37]. Here, we will not present any new fits with this particular model. However, inasmuch as Regge poles play an important role in all other models, it is necessary to identify qualitative properties of the *pure* Regge-pole approach. These features are independent of details of the various fits to data. We treat formalism only schematically in the text and relegate all kinematical and technical issues to appendices. We begin here by remarking that to each helicity amplitude, a given Regge-pole contributes an expression of the type given in eq. (4).

$$H_i(s,u) = h_i(u)\frac{[1+\tau\,\exp(-i\pi\bar{\alpha})]}{\Gamma(1+\bar{\alpha})\,\sin\pi\bar{\alpha}}\left(\frac{s}{s_0}\right)^{\alpha(u)} . \tag{4}$$

Here, $\bar{\alpha} = \alpha(u) - \frac{1}{2}$, where $\alpha(u)$ is a baryon Regge trajectory; index i labels the helicity state, and τ is signature. Function $h_i(u)$ is a slowly varying* regular function of u; s_0 is the usual scale constant. Our expression displays explicitly all wrong-signature nonsense zeroes (WSNZ) †.

* Apart from kinematic factors.

† Obviously, eq. (4) pertains to the dual or exchange-degenerate version of Regge-pole theory. However, only minor changes in our treatment are required to accommodate versions in which some or all WSNZs are absent. We discuss the SCRAM approach (*all* WSNZs absent) in subsect. 3.5.

3.2.1. Energy dependence

If only one Regge pole is exchanged, this theory predicts

$$\Delta\alpha_{\text{eff}}(u) = \alpha(u) + \tfrac{1}{2} \ . \tag{5}$$

Because trajectories are observed to have slopes $\alpha' \approx 0.9$ (GeV)$^{-2}$, eq. (5) implies marked shrinkage of $d\sigma/du$, in complete disagreement with experiment. However, reactions $\gamma p \to p\pi^0$ and $\gamma p \to n\pi^+$ allow exchange of both the $I_u = \frac{3}{2}$ trajectory Δ_δ and the $I_u = \frac{1}{2}$ trajectories N_α, N_γ, and N_β. (N_β is the trajectory on which the $D_{15}(1670)$ lies.) These trajectories are illustrated in fig. 6c. From this figure, it is easy to see that one can simulate a flat, $\Delta\alpha_{\text{eff}} \approx 0$ by arranging dominance of the N_α (and N_β, N_γ) exchanges for small u and dominance of Δ_δ exchange for $|u| \gtrsim 0.5$ (GeV/c)^2. However, the figure also makes it obvious that this arrangement can work only for $|u| \lesssim 1.0$ (GeV/c)^2. Beyond that value, shrinkage will necessarily take place; therefore, the observed flatness of $\Delta\alpha_{\text{eff}}(u)$ at large $|u|$ is inexplicable in a pure Regge-pole model.

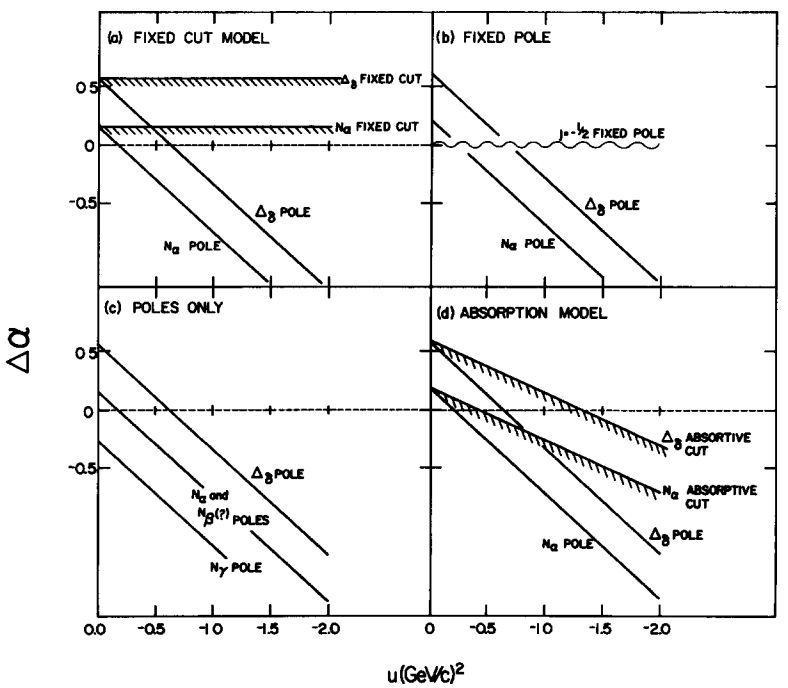

Fig. 6. Theoretical j-plane. Various singularities in the complex angular momentum (j) plane change position (or remain fixed) as u is varied. In this figure, we show $\Delta\alpha(u) = \alpha(u) + \frac{1}{2}$ for dominant singularities in each of the four models. The complexity in this figure should be contrasted with the remarkably constant behavior ($\Delta\alpha_{\text{eff}} \approx 0$) shown in fig. 5.

3.2.2. Momentum-transfer dependence

We turn now to a discussion of the u-dependence of $d\sigma/du$ predicted by pure Regge-pole theory.

Data on backward $\pi^+p \to p\pi^+$ and $\pi^-p \to n\pi^0$ show a pronounced dip in $d\sigma/du$ near $u = -0.15$ (GeV/c)^2. To interpret this phenomenon in a pure Regge-pole model, one assumes that N_α exchange dominates these processes; the dip is then a natural consequence of the first wrong-signature nonsense zero in the N_α amplitude, at $\bar{\alpha}_{N_\alpha} = -1$ ($\alpha_{N_\alpha} = -\frac{1}{2}$).

Backward $\gamma p \to N\pi$ data show no dip structure. Consequently, in a pure pole approach, one must assume that N_α does not dominate $\gamma p \to N\pi$. Rather, other exchanges (N_γ and N_β) must also be large. The dip in the N_α contribution at $\bar{\alpha}_{N_\alpha} = -1$ is 'filled-in' by large N_γ (and/or N_β) contributions. To agree with observed behavior of $\Delta\alpha_{\text{eff}}$, moreover, $\bar{\alpha}_{N_{\gamma,\beta}} \approx \bar{\alpha}_{N_\alpha}$. Unfortunately, as remarked by Kelly et al. [38], a large N_γ contribution disagrees with the factorization property of Regge-pole residues*.

A second difficulty for pure Regge-pole theory is the very flat behavior of $d\sigma/du$ versus u at $|u| \gtrsim 0.5$ (GeV/c)^2. As remarked earlier, in the region $|u| \gtrsim 0.5$ (GeV/c)^2, Δ_δ exchange must be dominant in order to accommodate the observed flat energy dependence ($\Delta\alpha_{\text{eff}} \approx 0$) in that region. Therefore, the u-dependence of $d\sigma/du$ is also controlled by Δ_δ exchange, for $|u| \gtrsim 0.5$ (GeV/c)^2. An indication† of the u-dependence of the Δ_δ contribution is given by data on $\pi^-p \to p\rho^-$, which have an $\exp(3u)$ behavior similar to $\pi^-p \to p\pi^-$ (cf. sect. 2, and figs. 2 and 3). This behavior is too steep to account for the flat [$\exp(u)$] character of $\gamma p \to N\pi$.

In summary, then, pure Regge-pole theory does not account naturally for observed u- or s-dependences of $\gamma p \to N\pi$ data.

3.2.3. Predictions

We judge that pure Regge-pole fits are somewhat artificial. Nevertheless, independent of such philosophy, the model makes clear predictions of canonical shrinkage‡, for all u, in the reactions $\gamma p \to \Delta^{++}\pi^-$ and $\gamma d \to pn$. These processes isolate the $I_u = \frac{1}{2}$ and $I_u = \frac{3}{2}$ exchanges, respectively. There is no possibility of a conspiracy between two sets of exchanges in order to produce a flat $\Delta\alpha_{\text{eff}}$ for these processes.

3.2.4. Vector dominance

In this and the next subsection, we discuss two theoretical questions relevant to all models treated in this paper.

Predictionsof the vector-dominance model are embodied in eq. (2). As discussed at length in sect. 2, there are striking differences between purely hadronic and photoproduction data; these are difficult to understand qualitatively within VDM or, indeed, any model. Until this situation is clarified by further experiments (e.g., those suggested in subsect. 2.4), it seems to us pointless to try to apply quantitative VDM predictions. *Corre-*

* Presence of N_β weakens this conclusion.
† This indication becomes a quantitative prediction if we invoke VDM.
‡ I.e., $\Delta\alpha'_{\text{eff}} \approx 0.9$; see footnote at the end of subsect. 2.1.

spondingly, we have not enforced VDM *constraints in any fits presented in this paper.*

It is also important to note that, in two of four models (the fixed-pole and fixed-cut models), the dynamics of photoproduction are assumed to be profoundly different from purely hadronic reactions. This invalidates VDM automatically.

Predictions of VDM may be applied in the strong-absorption model; in fact, a good simultaneous fit to strong and electromagnetic data was obtained by the Michigan group [38]. However, even in their work, the important qualitative differences between $\gamma p \to N\pi$ and hadronic data, discussed in sect. 2, *are not predicted* by the model. The differences emerge accidentally; they are fitted by adjusting values of various parameters. We are unwilling to state that these differences are merely an accident; therefore in our SCRAM fit (described in subsect. 3.5), we do not enforce VDM.

3.2.5. Pole extrapolation

Regge-pole amplitudes may be extrapolated* from the scattering region ($u < 0$) to the resonance region, where $u > 0$. Near the location of a resonance along a particular trajectory, the amplitude is proportional to $R_J/(u - M_J^2)$, where J denotes the spin of the resonance. Residue R_J is specified completely by the Regge-pole amplitude; physically, R_J is the coupling strength of the resonance. In $\gamma p \to N\pi$, $R_J \propto (\Gamma_{\pi N}\,\Gamma_{\gamma p})^{\frac{1}{2}}$, where Γ_X is the elastic width for decay into channel X. For the nucleon†, $\Delta_\delta(1236)$, $D_{13}(1520)$, $D_{15}(1670)$ and $F_{15}(1688)$, experimental values of R_J are known directly from low-energy phase-shift analysis of photoproduction [39, 40]. Complete vindication of a particular phenomenological model requires that both the scattering data and the coupling strengths of resonances be reproduced in the fits.

In our study of πN backward scattering [17], we learned that no model connects the scattering and resonance regions successfully. Similar discrepancies are found to exist in photoproduction‡.

In conformity with our earlier notation [17], we again use $\gamma_R(\sqrt{u})$ to denote the *reduced* residue function of a Regge-pole amplitude. Values of $\gamma_R(\sqrt{u})$ at discrete values of $\sqrt{u} = M_R$ can be calculated from the R_J defined above; here, M_R denotes the mass of a given resonance along a particular Regge trajectory. If one makes the choice $s_0 = 1\ \mathrm{GeV}^2$ for the Regge-scale factor, then these discrete (resonance) values suggest that $\gamma_R(\sqrt{u})$ is a slowly varying function of $\sqrt{u}$. The value $\gamma_R(0)$ and its derivative $d\gamma_R(0)/d\sqrt{u}$ are determined by fits to scattering data. Just as in πN scattering, Worden finds that $\gamma_R(0)$ is systematically smaller than $\gamma_R(M_R)$. The discrepancy is particularly great for Δ_δ exchange, where $\gamma_R(0) \approx \frac{1}{30}\gamma_R(M_\Delta)$.

In our work on πN scattering, we were forced to use complicated residue

* The remarks of this subsection apply for all models treated in this paper. However, in each model, only the Regge-pole component of scattering amplitudes is extrapolated to the resonance region.

† For the nucleon, of course, the couplings are just the electric charge and magnetic moment.

‡ Private communication from R. Worden, California Institute of Technology.

functions in order to fit scattering and resonance data simultaneously. For example, in a parametrization of the form $\gamma(\sqrt{u}) = a + b\sqrt{u} + cu + d(\sqrt{u})^3$, large values of parameters c and d are necessary in order to obtain respectable fits to resonance widths. However, good fits to scattering data alone are possible with the simpler choice $c = 0$ and $d = 0$. For backward single-pion photoproduction, there are more amplitudes and, therefore, correspondingly more parameters than for πN backward scattering. Furthermore, there are fewer data points. As a result, *we abandon pole extrapolation constraints in all fits to γp data.* To reduce the number of parameters in γp scattering, we elect to keep residue functions as simple as possible.

3.3. *Fixed-cut (HIPPIE) model*

Difficulties inherent in the pure Regge-pole approach suggest that a model with substantially different properties, as a function of *s and u*, is required in order to reproduce $\gamma p \to N\pi$ data. One such possibility is the fixed-cut model first proposed by Carlitz and Kislinger [4] and then generalized by Bardakçi and Halpern [5]. We have already discussed applications of this type of model to backward πp scattering [17]. In this subsection, we begin by describing features of the model in some detail. We establish the characteristic energy- and momentum-transfer dependences expected of amplitudes in the fixed-cut approach. Finally, we present and discuss our fits to photoproduction data.

3.3.1. General motivation

The initial motivation for a fixed-cut model was quite independent of scattering data. Rather, the principal object was to provide a formalism in which fermion poles occur with unique parity.

Simple Regge-pole theory predicts that when the trajectory function $\bar{\alpha}(u) = \alpha(u) - \frac{1}{2} = M$, an integer, then a pair of particles materializes. These two particles have the same spin J and mass, but they have opposite parity. In Nature, at least for small values of J, fermion states do not appear doubled. In simple pole models, with or without absorptive cuts, this can only be parametrized; explicit zeroes are introduced into residue functions of Regge trajectories in order to eliminate the unobserved member of a given parity doublet.

Carlitz and Kislinger showed that one can ensure the observed particle parities, for all states along a trajectory, at the cost of associating a fixed cut with each trajectory $j = \alpha(t)$. The branch point is located at $j = \alpha_0$, the value which the Regge trajectory assumed at $u = 0$. The singularity structure of the resultant j-plane is sketched in fig. 6a; explicit expressions for amplitudes are given in appendix B.

3.3.2. Previous development

In the scattering region, the extent to which the fixed-cut component controls energy- and momentum-transfer dependences of $d\sigma/du$ depends, of course, on the magnitude of the discontinuity across the cut. This changes for different trajectories and for various assumptions made about the resi-

due of the Regge-pole component. Moreover, treatment of signature offers additional freedom.

In our paper on πN backward scattering [17], we defined three versions of the fixed-cut approach. They were denoted FULL HIPPIE, NAIVE HIPPIE and SUPER HIPPIE. In all three, amplitudes are a function of the variable* σ. The discontinuity across the fixed cut is proportional to $(\alpha - \alpha_0)^{\frac{1}{2}\sigma}$.

Attempts to fit (hadronic) πN backward scattering data with fixed-cut models have met with little success. Natural predictions of the approach include (a) relatively slow variation of $d\sigma/du$ versus u and (b) energy dependence of $d\sigma/du$ scaling as $s^{2\alpha_0-2}$ (no shrinkage). These predictions, both of which are in clear disagreement with hadronic data (cf. fig. 2), can be attributed to dominance of the fixed-cut contribution, whose discontinuity varies little with u and is always concentrated near the tip of the cut, at $j = \alpha_0$.

Although the fixed-cut model is unsuccessful for hadronic reactions, we are encouraged to apply it to photoproduction processes where its natural predictions are in qualitative agreement with data. Therefore, we proceed now to a more complete exposition of the characteristic s- and u-properties of amplitudes in the fixed-cut model.

3.3.3. Behavior as a function of momentum transfer

In the HIPPIE approach, scattering amplitudes are given in terms of function $J^i_\sigma(u, s)$. These functions have both a Regge-pole component and a fixed-cut contribution. The pole term has the form

$$-(bu)^{\frac{1}{2}\sigma}\, g_i(u)\, \frac{\pi(1+\tau\, e^{-i\pi\bar{\alpha}})}{2\Gamma(1+\bar{\alpha})\, \sin\pi\bar{\alpha}} \left(\frac{s}{s_0}\right)^{\bar{\alpha}} . \tag{6}$$

Symbols $\bar{\alpha}$, s_0 and τ have the same meaning as in eq. (4); here, b is the slope of the Regge trajectory, $\alpha = \alpha_0 + bu$. Function $g_i(u)$ is a regular function of u; for example,

$$g_i(u) = (a_i + b_i u + c_i u^2 + \ldots) \exp(\mu_i u) , \tag{7}$$

where μ_i, a_i, b_i, c_i, $d_i \ldots$ are constants. Index i labels different spin amplitudes, as described in appendices A and B.

In addition to the pole component given above, J^i_σ also has a contribution from the fixed branch point singularity located at $j = \alpha_0$. This contribution cancels the singular behavior $(bu)^{\frac{1}{2}\sigma}$ of the pole term at $u = 0$. The full function $J^i_\sigma(u, s)$ is analytic at $u = 0$.

In appendix B, we give explicit expressions for $J^i_\sigma(u, s)$. There, we define three versions of the fixed-cut model. All three give the same Regge-pole term, eq. (6); they differ only in discontinuity across the fixed cut. The NAIVE HIPPIE and SUPER HIPPIE versions, defined in eqs. (B.2) and

* In the Carlitz-Kislinger paper, $\sigma \equiv -1$, we follow the Bardakçı-Halpern scheme in which σ is a variable.

(B.3), respectively, involve relatively simple analytic expressions for $J_\sigma(u, s)$. In FULL HIPPIE, a fairly complicated integral (eq. (B.5)) is involved in the definition of $J_\sigma(u, s)$. This integral is both time consuming to compute and obscures predictions of the theory.

Typical behavior of HIPPIE models as a function of u and σ is illustrated in fig. 7. We have computed $d\sigma/du$ for πN backward scattering using N_α and Δ_δ exchanges, separately, and various values of σ. Formalism for backward $\gamma N \to N\pi$ differs from that for backward $\pi N \to N\pi$ only by a trivial kinematic factor *, common to all versions of HIPPIE; therefore, the curves in fig. 7 are also relevant to our analysis of $\gamma N \to N\pi$.

Before analyzing the πN results shown in fig. 7, we first identify explicitly how they are obtained. Curves shown in fig. 7, are based on the follow-

* See discussion in appendix A.

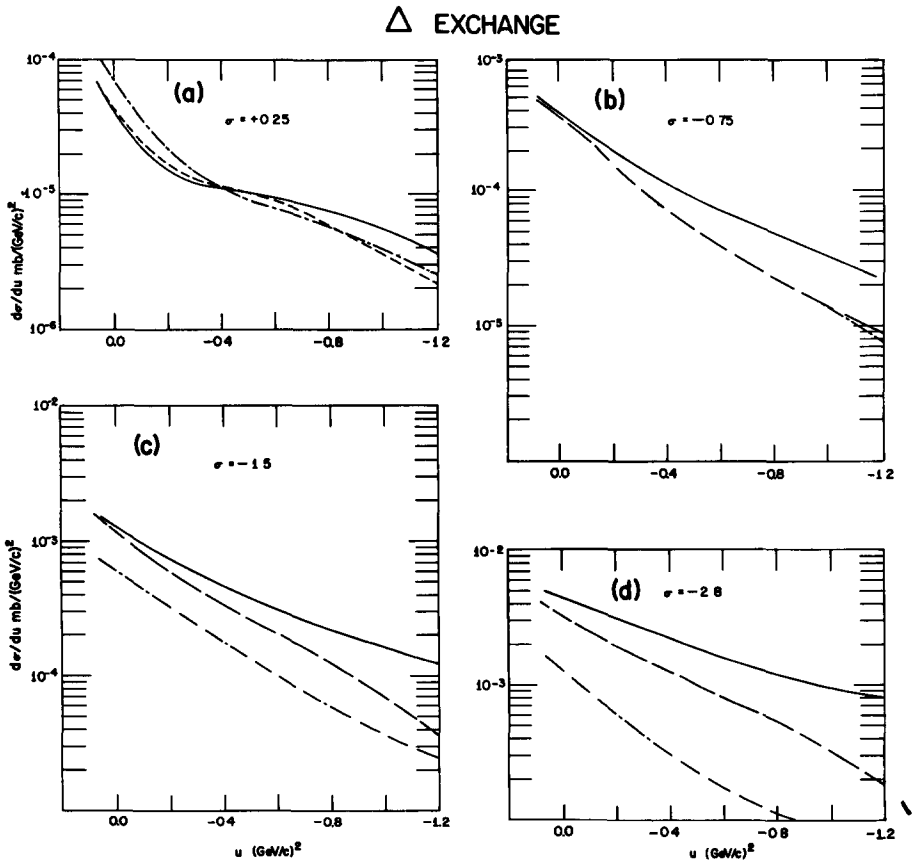

Fig. 7a. Fig. 7b. Fig. 7c. Fig. 7d.

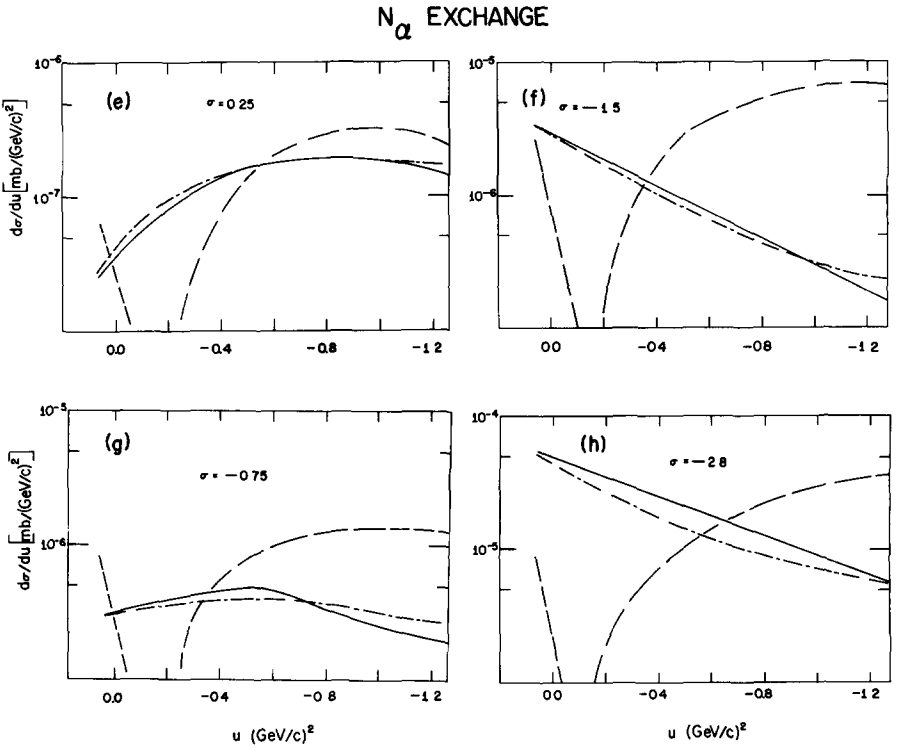

Fig. 7e. Fig. 7f. Fig. 7g. Fig. 7h.

Fig. 7. For πN backward scattering, we present a series of $d\sigma/du$ curves which show variation of u-dependence of HIPPIE models as σ is changed. Two different exchanges are illustrated; Δ_δ results are computed at p_{lab} = 5.91 GeV/c, and N_α values at 6.0 GeV/c. In all graphs, the solid line is FULL HIPPIE, the dashed line is SUPER HIPPIE, and the dot-dashed line is NAIVE HIPPIE. The reduced residue function g_B = 1 for both N_α and Δ_δ exchange.

ing specific choices in our expression for the Regge-pole term *, eq. (6): s_0 = 1 (GeV)^2 and g_B = 1. In our treatment of πN scattering [17], we parametrize invariant amplitudes A and B. Therefore, g_B denotes the residue of the B-amplitude. The residue g_A, of the other πN invariant amplitude, is fixed in terms of g_B by the requirement that parity doubling be abolished †. We set g_B = 1 simply in order to examine natural predictions of the model, unencumbered by complicated reduced residue functions. Once trajectories have been specified, these choices of g_B and s_0 determine HIPPIE results completely.

The curves in fig. 7 demonstrate several points about u-dependence of $d\sigma/du$. First, the NAIVE HIPPIE and FULL HIPPIE models are always qualitatively similar. Obviously, the additional cut contribution in the

* For motivation of the choice s_0 = 1 GeV^2, see subsect. 3.2.5.
† Details are given in ref. [17].

FULL version is relatively unimportant; the most important features of the HIPPIE model are represented by the (analytically simpler) NAIVE version. Second, for the N_α exchange, figs. 7e through 7h, we call attention to the fact that no evidence of dip structure near $u = -0.15$ (GeV/c)^2 is apparent in the FULL HIPPIE and NAIVE HIPPIE results. This is true in spite of the fact that the input N_α Regge-pole term does vanish at a WSNZ point $\bar{\alpha}_{N_\alpha} = -1$ ($u \approx -0.15$ (GeV/c)^2). The smooth fixed-cut contribution is obviously overwhelming*, even at a value of u as small as -0.15 (GeV/c)^2. On the other hand, the SUPER HIPPIE curves do show dip structure at WSNZ points†. Unfortunately, however, figs. 7e through 7h also show that SUPER HIPPIE predicts that $d\sigma/du$ has a larger value at $u \approx -1$ (GeV/c)^2 than at $u = 0$. This anti-peripheral aspect is in clear disagreement both with data, of course, and with predictions of simple pole models, as shown in fig. 8b. Inasmuch as WSNZ dips are not observed in backward γN data, we deem our SUPER HIPPIE version irrelevant for this problem. Its anti-peripheral nature makes it suspect also for studies of purely hadronic processes.

Finally, we note that the shape of $d\sigma/du$ curves shown in fig. 7 varies very slowly as σ is changed. Although the fixed cut becomes weaker as σ is increased (i.e., σ made more positive), $d\sigma/du$ does not become significantly more peripheral. This is superficially contrary to what might be expected. However, we note that the pole residue is proportional to $u^{\frac{1}{2}\sigma}$. Therefore, the contribution from the pole term becomes more suppressed at small u (and, thus, less peripheral) as σ is made more positive. It is also interesting to see explicitly that, in the HIPPIE model, $d\sigma/du$ is always less peripheral than corresponding results from a simple Regge-pole model. This latter result is illustrated in fig. 8a, where HIPPIE results are contrasted with two versions of a pure-pole model of Δ_δ exchange. In the first (solid line), the Δ_δ reduced residue is adjusted to abolish the parity twin of the $J^P = \frac{3}{2}^+$ $\Delta(1238)$; normalization is fixed by the choice $g_B = 1$. In the second version (dashed line, spin-flip), $g_B = 1$ and $g_A = -M$ in order that the s-channel non-spin-flip amplitude $A + MB = 0$.

3.3.4. Behavior as a function of energy

Having just established the salient characteristics of HIPPIE amplitudes as a function of u, we now turn to their s-dependence.

In general, energy dependence of HIPPIE models is quite complicated. As an illustration, we imagine that the discontinuity across the cut is largest near the branch point, at $j = \alpha_0$. The amplitude is then a linear combination of two terms: one with energy dependence s^{α_0}, given by the cut‡, and the second with energy dependence $s^{\alpha(u)} = s^{\alpha_0 + \alpha' u}$, given by the Regge-pole component. As a result, the overall energy dependence $s^{\alpha_{\text{eff}}(u)}$

* In ref. [17], in order to fit backward πN data, we had to reduce the fixed-cut contribution artificially, by parametrizing an extra zero in the N_α reduced residue function.

† Indeed, the choice of acronym SUPER reflected our initial elation at discovering a version of HIPPIE which might reproduce the pronounced dips near $\bar{\alpha}_{N_\alpha} = -1$ in backward $\pi^+ p$ and $\pi^- p$ CEX.

‡ In this description, we ignore powers of $\log s$.

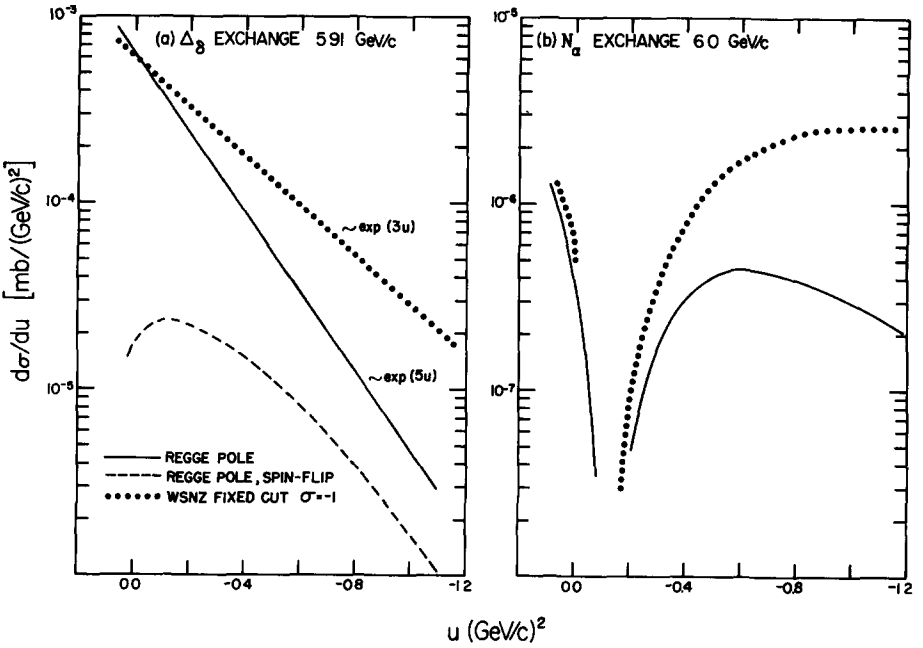

Fig. 8. In this figure, we compare magnitudes and shapes of $d\sigma/du$ obtained from our SUPER HIPPIE model with those from simple Regge-pole models. Parameters used to compute our curves in part (a) are detailed at the end of subsect. 3.3.3, for SUPER HIPPIE curves in both (a) and (b), parameter $\sigma = -1$. In (b), the invariant amplitude B for N_α Regge-pole exchange has reduced residue $g_B = 1$, moreover, in the pure-pole model, residue $g_A = 0$. In the pure-pole model, this latter choice guarantees unique parity at the nucleon pole position, a result which is automatic in HIPPIE models.

depends upon the relative *strength* of the pole and cut contributions, as a function of u.

The strength of the cut contribution is influenced by the value of σ and (for FULL HIPPIE and NAIVE HIPPIE) by the position of the first WSNZ in the basic Regge-pole amplitude. Let us examine σ first. Inspection of eq. (B.1) shows that the cut grows stronger the more negative one takes σ. This effect is also illustrated in fig. 9; there, for values of $u = 0$ and -1.7 (GeV/c)^2, we contrast effective energy dependence of NAIVE HIPPIE models with $\sigma = -0.25$ and -1.5. We evaluate, in turn, pure N_α, Δ_δ, and $D_{15}(N_\beta)$ exchanges. In each case, we plot $E_{lab}^{2-2\alpha_0}\, d\sigma/du$ versus E_{lab} on a log-log scale; therefore, if the dominant singularity were fixed at $j = \alpha_0$, a flat horizontal line would result. We note that for a given exchange and fixed value of u, curves with $\sigma = -1.5$ are closer to flat behavior than those with $\sigma = -0.25$.

Comparison of N_α, Δ_δ and D_{15} results in fig. 9 also demonstrates the effect of WSNZ location on strength of the cut. For Δ_δ, with the first WSNZ at $u \approx -1.7$ (GeV/c)^2, this effect is relatively unimportant; the fixed

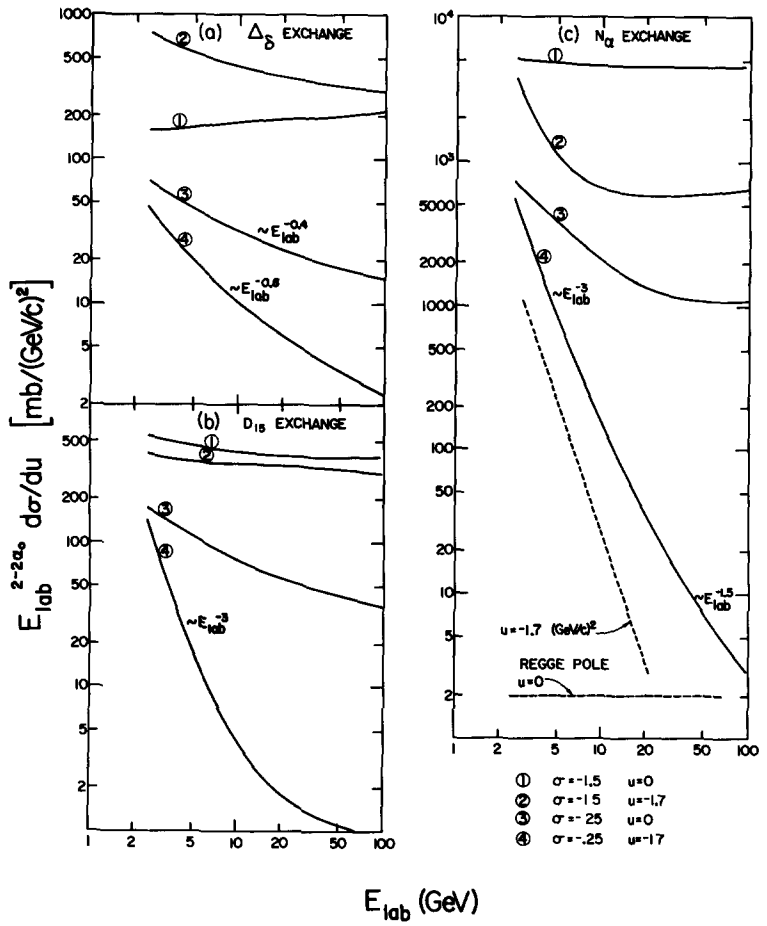

Fig. 9. For various exchanges, solid curves show energy dependence of the quantity $E_{lab}^{2-2\alpha_o}\, d\sigma/du$ predicted by NAIVE HIPPIE; α_o is the intercept of the Regge-pole at $u = 0$. Results are given for two values of u and two values of parameter σ, $\sigma = -0.25$ corresponds to a 'weak' fixed-cut and $\sigma = -1.5$ to a 'strong' fixed-cut contribution. For each curve, only energy variation is significant. Relative normalization between curves is arbitrary. In a simple Regge-pole exchange model, $d\sigma/du \propto E_{lab}^{2\alpha' u}$, where α' is the slope of the Regge-trajectory; dashed curves show predictions of this model, for $\alpha' \approx 1\ (\mathrm{GeV}/c)^{-2}$.

cut is always dominant. However, the strength of the fixed cut is markedly reduced for N_α exchange, whose first WSNZ is located at $u \approx -0.15\,(\mathrm{GeV}/c)^2$. An intermediate case is $D_{15}(N_\beta)$ exchange with a WSNZ at $u = -0.6\,(\mathrm{GeV}/c)^2$. Stated roughly, we see that as we increase σ towards zero and move the location of the first WSNZ toward $u = 0$, the strength of the fixed cut is weakened; a complicated energy dependence results from pole/cut interplay.

We now call attention to a third feature evident in fig. 9. Take, for example, N_α exchange with $\sigma = -1.5$ and $u = -1.7\ (\mathrm{GeV}/c)^2$. We see that after

an initial steep decline, $E^{2-2\alpha_0}\, d\sigma/du$ flattens to a nearly horizontal line above $E_{lab} \approx 10$ GeV. This must happen in all cases simply because the cut term, proportional to s^{α_0}, however small its contribution at low energy, will eventually overtake a pole term proportional to $s^{\alpha_0+\alpha' u}$. On the other hand, note that for N_α with $\sigma = -0.25$ and $u = -1.7$ (GeV/c)^2, flat behavior does not set in until $E_{lab} > 100$ GeV.

Are such subleties of merely academic interest? We make two comments. First, if we plot experimental values of $d\sigma/du$, versus E, at fixed u, on a log-log scale *, then we observe none of the delicate behavior present in curves of fig. 9. However, available data cover a very small range of energy. The fixed-cut approach suggests that by NAL energies, $d\sigma/dt$ for processes like $\pi^- p \to \pi^0 n$ (which now show canonical shrinkage) will gradually stop shrinking. Asymptotic cross sections will be controlled by a highlying fixed cut with small strength.

The second deduction is more relevant to our immediate study of $\gamma p \to N\pi$ Indeed, the absence of subtle energy variation in γp data requires † that $\sigma_{N_\alpha} \lesssim -1.2$. Alternatively (or in addition), a large N_γ contribution ‡ is necessary in the $I_u = \frac{1}{2}$ exchange channel; because the first WSNZ for N_γ is located at much larger $|u|$, the restriction on σ is less severe.

3.3.5. Fits to data

3.3.5a. Trajectories

Comparison of figs. 5 and 6a suggests that the desired energy dependence of $d\sigma/du \propto E_{lab}^{-3}$ ($\Delta\alpha_{eff} \approx 0$) is achieved through dominance of the N_α fixed cut. This implies dominance of $I_u = \frac{1}{2}$ exchange, which, although consistent with $\gamma p \to n\pi^+$ and $\gamma p \to p\pi^0$ data, cannot be proven because two charge states are insufficient to disentangle three possible isospin exchange amplitudes ($I_u = \frac{3}{2}$; $I_u = \frac{1}{2}$, isoscalar γ; $I_u = \frac{1}{2}$, isovector γ).

In addition to N_α, we may include Δ_δ, N_γ and N_β exchanges. There are really too few data points to determine parameters for so many amplitudes; therefore, we ignore N_β entirely. As we will now describe, good fits are possible with either N_α and Δ_δ or with N_α, N_γ and Δ_δ exchanges.

3.3.5b. Curves

Technical details and explicit expressions for amplitudes are relegated to appendices A and B. We have obtained several good fits to data. Parameters and χ^2 for three of these fits are listed in table 1. In fig. 10, we display one of our NAIVE HIPPIE fits to $d\sigma/du$, obtained with parameters of table 1b. Absence of shrinkage is reproduced nicely. In all fits, there is some difficulty in achieving turn-over of $d\sigma/du$, near $u = 0$, for both charge states simultaneously. The two NAIVE HIPPIE fits differ: in the first fit A, only N_α and Δ_δ exchanges are employed, whereas in the other fit B, N_γ exchange is included also.

Parameters for our FULL HIPPIE fit are given in table 1c, and an ex-

* C.f., figs. 18 and 19.
† See fit A discussed in subsect. 3.3.5.
‡ See fit B discussed in subsect. 3.3.5.

Table 1
Parameters of HIPPIE fits.

Table 1a. NAIVE HIPPIE * fit A.

Δ_δ	N_α
$\bar{\alpha} = -0.45 + 0.9u$	$\bar{\alpha} = -0.84 + 0.9u$
$\sigma = -1.75,\ \mu = 1.45$	$\sigma = -1.33,\ \mu = -0.005$
	isovector photon
$g_1 = 0.105\bar{\alpha}$	$g_1 = -9.58 + 0.76u$
$g_2 = -0.625\bar{\alpha}$	$g_2 = 24.5 + 1.05u$
	isoscalar photon
	$g_1 = 1.55$
	$g_2 = -2.42$

$\chi^2(\gamma p \to n\pi^+) = 70$ (on 41 data points),
$\chi^2(\gamma p \to p\pi^o) = 100$ (on 35 data points).

Table 1b. NAIVE HIPPIE * fit B.

Δ_δ	N_α	N_γ
$\bar{\alpha} = -0.45 + 0.9u$	$\bar{\alpha} = -0.842 + 0.9u$	
$\sigma = -1.2,\ \mu = -0.09$	$\sigma = -1.22,\ \mu = 0.614$	
	isovector photon	
$g_1 = 0.141\bar{\alpha}$	$g_1 = -7.88$	$g_1 = -2.79$
$g_2 = -0.616\bar{\alpha}$	$g_2 = 5.73$	$g_2 = 5.14$
	isoscalar photon	
	$g_1 = -1.07$	$g_1 = -0.554$
	$g_2 = 4.42$	$g_2 = 1.92$

$\chi^2(\gamma p \to n\pi^+) = 53$ (on 41 data points),
$\chi^2(\gamma p \to p\pi^o) = 90$ (on 35 data points).

Table 1 (continued)

Table 1c. FULL HIPPIE * fit

Δ_δ	N_α
$\overline{\alpha} = -0\ 45 + 0\ 9u$	$\overline{\alpha} = -0.84 + 0\ 9u$
$\sigma = -1.24,\ \mu = 6.47$	$\sigma = -0.786,\ \mu = 0.909$
	isovector photon
$g_1 = 0.119\overline{\alpha}$	$g_1 = -26.3$
$g_2 = -1.03\overline{\alpha}$	$g_2 = 50.9$
	isoscalar photon
	$g_1 = 1\ 49$
	$g_2 = -0.109$

$\chi^2(\gamma p \to n\pi^+) = 72$ (on 41 data points),
$\chi^2(\gamma p \to p\pi^0) = 85$ (on 35 data points).

* Trajectories are not varied. Amplitudes are given by eqs. (7), (B.1), (B.4), (B.5) and (B.8). For general formalism, see subsect 3.3 and appendices A and B.

ample of $d\sigma/du$ is shown in fig. 11. Our FULL HIPPIE fit exhibits a bit too much shrinkage in $\gamma p \to n\pi^+$; as explained in subsect. 3.3.4, this may be attributed to the fact that the value $\sigma = -0.786$ gives the N_α a 'weak' fixed cut. The addition of some N_γ improves the fit, at the cost of more parameters.

We recall that FULL HIPPIE is more complicated analytically than NAIVE HIPPIE; an additional complicated (cut) integration must be performed numerically. However, as we explained earlier and demonstrated in fig. 7, the additional cut contribution is small for small $|u|$ and does not alter qualitative properties of the theory. We confirm this fact in fig. 11, in which we display a decomposition of our FULL HIPPIE result into its NAIVE HIPPIE component and the remainder.

3.3.6. Analysis and predictions

As forecast above, the contribution of Δ_δ exchange is small in all of our fits; we illustrate this in fig. 12. In the fixed-cut model, this result is forced by the fact that $\Delta\alpha_{\text{eff}} \approx 0$. Aside from this conclusion, however, coupling parameters are not well established. Theory and meagre experimental data determine structure of amplitudes so poorly that we can have no confidence in predicted asymmetries (see sect. 4) for scattering of polarized photons and/or scattering from polarized nucleon targets.

If the Δ_δ contribution were exactly zero, we would predict

$$\sigma(\gamma n \to p\pi^-) = 2\sigma(\gamma p \to p\pi^0)\ , \qquad \sigma(\gamma p \to n\pi^+) = 2\sigma(\gamma n \to n\pi^0)\ .$$

Although the Δ_δ contribution is not zero in HIPPIE fits A and C, these equalities are nevertheless well satisfied in the theory at large $|u|$. In fit B, the Δ_δ contribution is sufficiently large to upset the predictions. Conse-

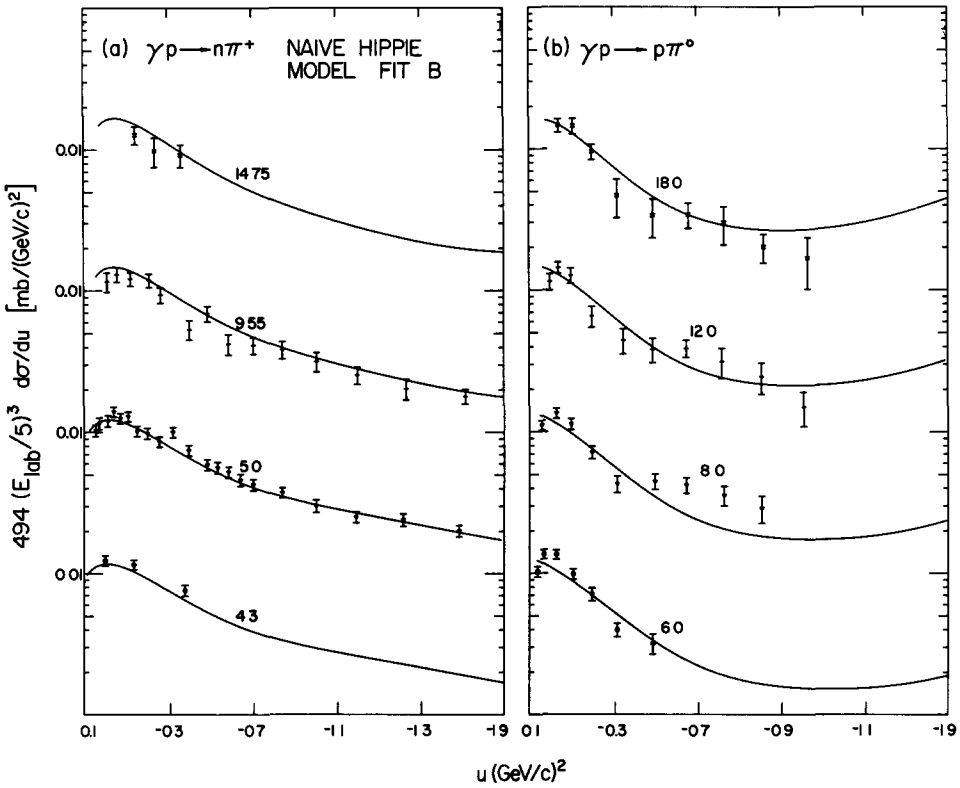

Fig. 10. Curves computed from parameters of our NAIVE HIPPIE fit B (table 1b) are contrasted with data. In (a), we display only the latest SLAC data on $\gamma p \to n\pi^+$ [9], the complete set of data is shown in fig. 1a. Numbers next to curves denote photon lab energy in GeV.

quently, neither measurements of polarization nor of $d\sigma/du$ for these other charge states in $\gamma n \to N\pi$ will provide a decisive test of our HIPPIE models.

The most crucial prediction of fixed-cut models involves energy dependence of processes which have purely $I_u = \frac{1}{2}$ or $I_u = \frac{3}{2}$ exchange. In fact, the model predicts that $d\sigma/du$ for $I_u = \frac{3}{2}$ exchange processes (e.g., $\gamma p \to \Delta^{++}\pi^-$) will have energy dependence E_{lab}^{-2}, for all u, not the E_{lab}^{-3} behavior of present $\gamma p \to N\pi$ data. However, $d\sigma/du$ for $I_u = \frac{1}{2}$ exchange processes (e.g., $\gamma d \to pn$) should scale as E_{lab}^{-3} just as do present data.

3.3.7. Unitarity in the u-channel

As remarked earlier, in HIPPIE models there is a fixed branch-point singularity in the j-plane of the form $(j - \alpha_0)^{\frac{1}{2}\sigma}$. Fits to backward πN data [17] and to backward single-pion-photoproduction data determine that $\sigma < 0$. Values of $\sigma > 0$ lead to unreasonable u-dependence of $d\sigma/du$ (cf. fig. 7). We

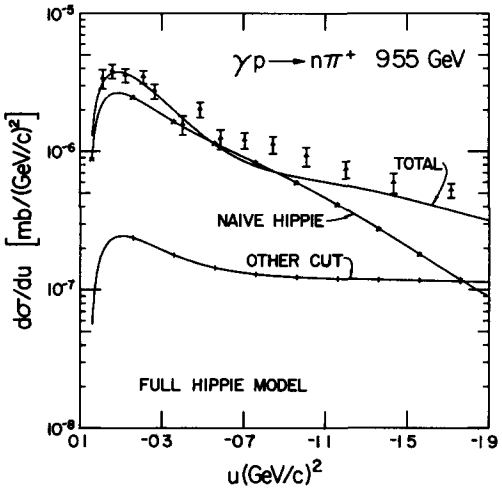

Fig. 11. An example is given of our FULL HIPPIE fit. Parameters are listed in table 1c. Data are from ref. [9]. The curve marked 'total' is the FULL HIPPIE result We show also the portion of $d\sigma/du$ which arises from the NAIVE HIPPIE component of this FULL HIPPIE result. Finally, the curve denoted 'other cut' is the contribution to $d\sigma/du$ of the amplitude which is the difference between FULL and NAIVE HIPPIE amplitudes. Not shown are terms which arise from interference of NAIVE and other cut amplitudes.

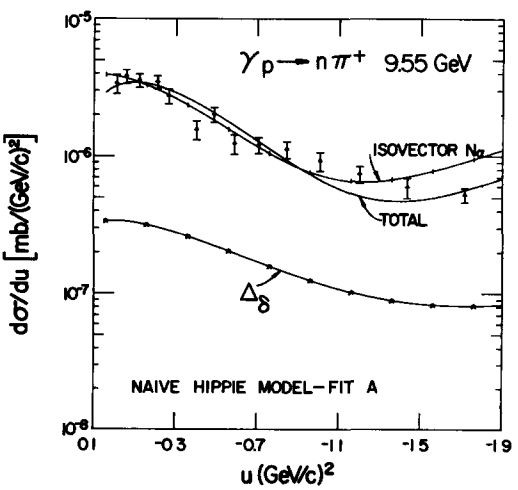

Fig. 12. An example is given of our NAIVE HIPPIE fit A, for which parameters are listed in table 1a. We also show, separately, values of $d\sigma/du$ computed from the $\Delta\delta$ amplitudes and from the $N\alpha$ (isovector photon) amplitudes.

now discuss the fact that unitarity in the u-channel forbids such singular fixed cuts ($\sigma < 0$) in purely hadronic processes [57]. On the other hand, no such theoretical constraint is present for the singly weak process $\gamma p \to N\pi$. Indeed, in $\gamma p \to N\pi$, fixed-*pole* singularities are also allowed, whereas unitarity forbids their presence in purely hadronic reactions [41].

Unitarity in the u-channel offers, therefore, an explanation for the fact that HIPPIE models are successful in reproducing $\gamma p \to N\pi$ data but seriously inadequate for $\pi N \to N\pi$ [17]. Because singular fixed-cuts are forbidden in $\pi N \to N\pi$, current versions of the HIPPIE model should not be expected to work for this reaction. One may surmise that in a correctly unitarized HIPPIE theory for purely hadronic processes, the strong cut at $j = \alpha_0$ will be weakened, thus restoring to amplitudes the marked variation with s and u observed in hadronic data. By contrast, absence of the unitarity constraint in $\gamma p \to N\pi$ justifies the assumption that amplitudes for this process are dominated by a singular fixed-cut contribution. The apparent theoretical dichotomy between $\gamma p \to N\pi$ and $\pi N \to N\pi$ is removed.

For the sake of clarity, we review the usual strong-unitarity arguments for elastic scattering of spinless particles; for treatment of the more general case of coupled-channels with spin, consult the lectures by Oehme [41]. Essential results are unchanged.

Let u_0 denote the elastic threshold in the u-channel, and let u_I denote the first inelastic threshold. For $u_0 < u < u_I$, the strong-unitarity relation for partial-wave amplitude f_j is given by

$$\mathrm{Im}\, f_j = k f_j f_j^* , \tag{9}$$

where k is the u-channel c.m. momentum.

We now define reduced partial-wave amplitudes

$$a(j,u) = k^{-2j} f_j(u) . \tag{10}$$

We set $u^+ = u + i\epsilon$ and $u^- = u - i\epsilon$. Then eq. (9) may be re-expressed as

$$a(j,u^+) - a(j,u^-) = 2ik^{2j+1} a(j,u^+) a(j,u^-) . \tag{11}$$

This equation is true for all real and complex j.

In the neighborhood of a Regge pole,

$$a(j,u) \propto \frac{g(u)}{j - \alpha(u)} . \tag{12}$$

This expression satisfies eq. (11), and we may in fact use eq. (11) to derive the (u-dependent) imaginary part of $\alpha(u)$. In the case where $g(u)$ is real,

$$\mathrm{Im}\, \alpha(u) = g(u) k^{2j+1} . \tag{13}$$

By contrast, near a *fixed-pole* in the j-plane,

$$a(j,u) \propto \frac{1}{j - \alpha_F} . \tag{14}$$

In this case, eq. (11) cannot be satisfied; the left-hand side has a simple pole, whereas the right-hand side has a double pole. Therefore, strong unitarity forbids fixed poles in the j-plane.

Similar analysis shows that eq. (11) also excludes *fixed* branch-point singularities of the form

$$a(j,u) \propto (j - \alpha_F)^{\lambda} , \qquad \text{with} \qquad \lambda < 0 . \tag{15}$$

Consequently, HIPPIE cuts with $\sigma < 0$ are forbidden in strong processes. Those with $\sigma > 0$ are presumably allowed, but, as we demonstrated earlier, they lead to unreasonable u-dependence of $d\sigma/du$.

In weak or electromagnetic processes, *linear* unitarity (more accurately, the absence of bilinear unitarity (cf. eq. (11)) allows fixed poles and/or singular fixed cuts in the j-plane. For reactions like $\gamma p \to N\pi$, with u-channel amplitude $b(j,u)$, unitarity in the u-channel assumes the form

$$b(j,u^+) - b(j,u^-) \propto a(j,u^-)b(j,u^+) . \tag{16}$$

Here $a(j,u)$ is a purely hadronic amplitude*. Note that a fixed singularity may be present in $b(j,u)$, without violating eq. (16).

We remark that eq. (16) cannot be used to prove that fixed singularities exist. Rather, is does not exclude them from processes such as $\gamma p \to N\pi$. In particular, eq. (16) supports our contention that it is not unreasonable to assume that the theoretical j-plane structure of photoproduction processes is very different from that of purely hadronic reactions. We are justified theoretically in advocating HIPPIE models or fixed-pole models (see next section) for photoproduction while excluding their use in hadronic processes. Phenomenologically, these fixed-singularity models offer a natural explanation for the universal behavior ($E_{lab}^{-3}\, d\sigma/du \propto \exp(u)$) of $\gamma p \to N\pi$ data.

3.4. *Fixed-pole model*

For purely hadronic processes, u-channel unitarity forbids the presence of singularities in the j-plane whose position is independent of u. The usual arguments for this assertion were reviewed in subsect. 3.3.7. Therefore, in strong-interaction processes, we do not expect to find fixed-pole type singularities in the j-plane without, for example, compensating or shielding cuts. However, in photoproduction, unitarity does not forbid fixed poles. Generally, these may occur at $j = \frac{1}{2}(2n-1)$ in fermion channels, and at $j = n$ in boson channels; n is an integer which, empirically, is ≤ 0.

In this section, we postulate that fixed poles dominate photoproduction amplitudes. This model has considerable phenomenological appeal. If fixed poles occur at $j = 0, -1, -2, \ldots$, in the meson-exchange model, and at $j = -\frac{1}{2}, -\frac{3}{2}, \ldots$, in the baryon-exchange channel, then we predict directly that $d\sigma/dt$ scales as E_{lab}^{-2}, for forward γp processes, and that $d\sigma/du$ scales as E_{lab}^{-3}, for backward γp reactions. Both predictions are in immediate

* For a more precise equation and other references to unitarity in weak processes, consult ref. [42].

qualitative agreement with data. The difference between the energy dependence of forward and backward processes is explained nicely. By contrast, in all other models, considerable adjustment of parameters is required to reproduce the remarkable energy dependence of photoproduction data. It is only in the fixed-pole model that the energy dependence of $d\sigma/du$ is independent of details of coupling structure and quantum numbers of the exchanges.

Although fixed-pole models are appealing for phenomenology, they are said to be unattractive theoretically. We have met no theorist willing even to discuss the possible validity of these models. Certainly, fixed poles are not expected in theories in which particles are composite*. Moreover, if they *are present* in the j-plane, fixed poles are expected to be associated with elementary particles, e.g., the nucleon or the members of the 0^- meson nonet. Such fixed poles would lie at $j = \frac{1}{2}$ (for backward scattering) or have the coupling structure of the pseudoscalar nonet (for forward photoproduction). The fixed poles necessary to reproduce γp data have neither of these properties.

In order to reproduce energy dependence of $\gamma p \to N\pi$ data, it is clear that the dominant (baryon) fixed pole must be located at $j = -\frac{1}{2}$. However, very little can be said about either the residues of fixed poles or their isospin. We must simply adopt what is required to fit data.

3.4.1. Fits to data

We must specify our choices of both Regge poles and fixed poles. Be-

* See the discussion in ref. [58].

Table 2
Parameters of fixed-pole model † fit.

Δ_δ	N_α	'N_α' fixed pole
$\bar{\alpha} = -0.45 + 0.9u$	$\bar{\alpha} = -0.84 + 0.9u$	$\bar{\alpha} = -1.0$
$\mu = 1.0$	$\mu = 0.853$	$\mu = 0.744$
	isovector photon	isovector photon
$\gamma_1 = 0.847\ (m_\Delta + \sqrt{u})$	$\gamma_1 = -2.07\ (M - \sqrt{u})$	$\gamma_1 = -0.0193\ (M - \sqrt{u})$
$\gamma_2 = 1.36\ \ (m_\Delta + \sqrt{u})$	$\gamma_2 = 1.31\ (M - \sqrt{u})$	$\gamma_2 = -0.0162\ (M - \sqrt{u})$
	isoscalar photon	isoscalar photon
	$\gamma_1 = -0.132\ (M - \sqrt{u})$	$\gamma_1 = 0.0016\ (M - \sqrt{u})$
	$\gamma_2 = 0.897\ (M - \sqrt{u})$	$\gamma_2 = -0.00255\ (M - \sqrt{u})$

$\chi^2(\gamma p \to n\pi^+) = 34$ (on 41 data points),
$\chi^2(\gamma p \to p\pi^0) = 103$ (on 35 data points)

† Trajectories are not varied in the fit. The fixed pole is set at $\bar{\alpha} = -1$. All other numerical values listed here are determined by fitting data. Amplitudes are given in subsect. 3.4 and appendices A and C.

cause such a small quantity of γp data is available, we limit ourselves to the N_α and Δ_δ Regge poles and one fixed pole. For the Regge-pole residues, we restrict functions $\gamma_i(\sqrt{u})$, defined in appendix A, to be linear functions of $\sqrt{u}$. Explicitly,

$$\gamma_i(\sqrt{u}) = (a_i + b_i\sqrt{u}) \exp(\mu u) \ . \tag{17}$$

Moreover, we fix the ratios a_i/b_i, for both Δ_δ and N_α, in order to eliminate parity doubling at the $N_\alpha(938)$ and $\Delta_\delta(1236)$ poles - i.e., we ensure that our amplitudes produce only poles of the observed parity at the nucleon and Δ(1236) positions.

The fixed-pole amplitudes are described in appendix C. For definiteness, in these fits to $\gamma p \to N\pi$ data, we specify a fixed pole of isospin $\frac{1}{2}$. We return to a discussion of isospin later.

Parameters of our best fit with the fixed-pole model are given in table 2. Curves computed with these parameters are compared with $\gamma p \to N\pi$ data in fig. 13. Except for structure in $\gamma p \to p\pi^0$ near $u = 0$, the fit provides a good representation of both s- and u-dependence of data. A particularly interesting feature of the fit is shown in fig. 14. At $u = 0$, the Regge-pole and fixed-pole contributions are of similar size. However, the Regge-pole contribution* falls away rapidly as $|u|$ is increased; the fixed-pole amplitudes dominate the cross section at large $|u|$.

The necessity of fixed-pole dominance at large $|u|$ is obvious from inspection of fig. 6b; to reproduce the empirical result $\Delta\alpha_{\text{eff}}(u) \approx 0$, for all u, we cannot tolerate much contribution from the N_α or Δ_δ Regge-pole exchanges at large $|u|$. Presumably, fixed-pole dominance at large u is a general result; therefore, within this model, all γp backward processes should have universal energy dependence E_{lab}^{-3} and universal u-dependence $\exp(u)$. Correspondingly, unlike the fixed-cut model, we predict that $d\sigma/du$ for $\gamma p \to \Delta^{++}\pi^-$ will scale as E_{lab}^{-3}, not as E_{lab}^{-2}; we also expect the u-dependence of $d\sigma/du$ to change from the present $\exp(3u)$, at small u, to a 'universal' $\exp(u)$ behavior †.

3.4.2. Predictions

A priori, the fixed-pole model is very flexible. Energy dependence is the only distinctive and unambiguous property of the model. To make other predictions, we assume that all characteristic features of present photoproduction data can be attributed to some universal fixed-pole structure. Correspondingly, our predictions for momentum-transfer dependence (sub-

* Note that our 'N_α Regge-pole' contribution does not have a dip near $u = -0.15$ $(\text{GeV}/c)^2$. We deliberately omitted WSNZ factors from our N_α Regge-pole amplitudes. This is equivalent, here, to assuming strong exchange degeneracy of N_α and N_γ poles. We did this in order to make certain that it is the energy dependence of γp data and not its u-dependence which determines the relative contributions of fixed-pole and Regge-pole amplitudes. One can obtain equally good fits with WSNZ factors in the Regge-pole amplitudes.

† This assumes, of course, that the same type of fixed-pole couples to the $I_u = \frac{3}{2}$ and $I_u = \frac{1}{2}$ channels. See below.

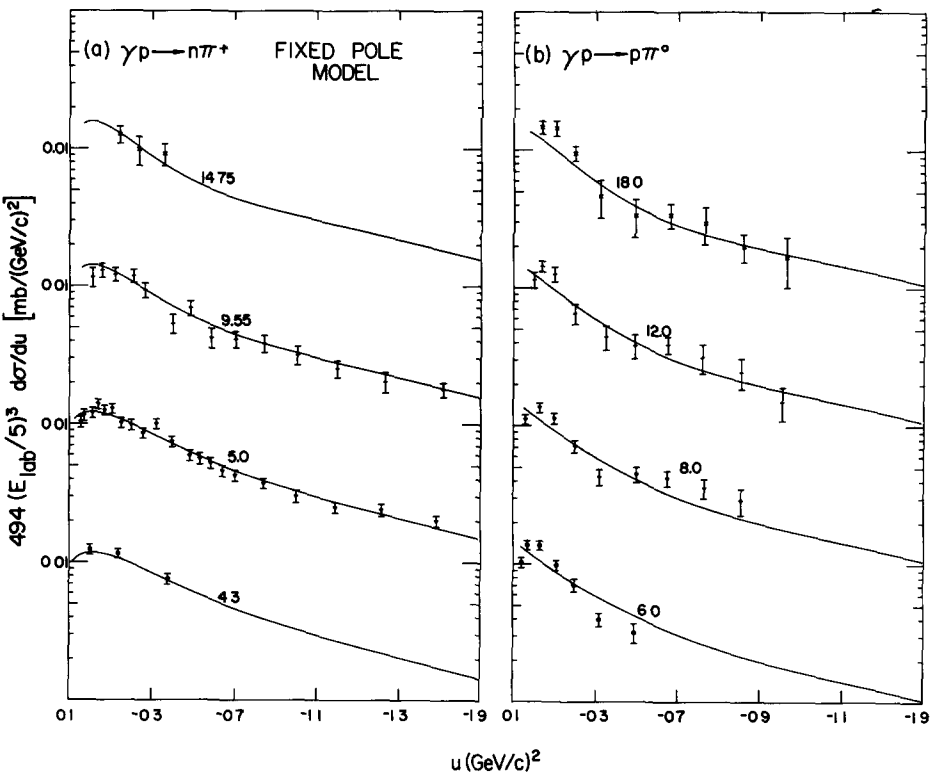

Fig. 13. Curves computed from parameters of our fixed-pole model fit are compared with a selection of data [9,10]. Parameters are given in table 2. Numbers next to data indicate photon lab momentum in GeV.

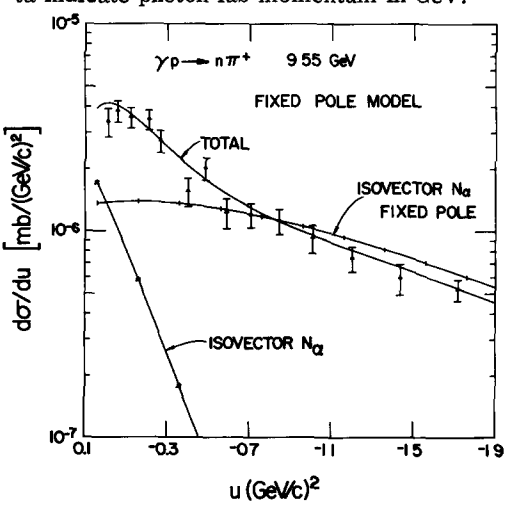

Fig. 14. We give an example of our fixed-pole model fit. We also show the separate contributions to $d\sigma/du$ from N_α Regge-pole and 'N_α' fixed-pole terms in the isovector photon $I_u = \frac{1}{2}$ amplitude.

sect. 3.4.2b) and for quantum numbers of exchange amplitudes (subsect. 3.4.2c) are more speculative than our assertions about s-dependence in subsect. 3.4.2a.

3.4.2a s-dependence

Photoproduction differential cross section should scale as E_{lab}^{-2}, for forward processes, and as E_{lab}^{-3} for backward reactions. These predictions hold for all values of momentum transfer away from the immediate forward and backward peaks (i.e., $|t| > 0.5$ and $|u| > 0.5$ (GeV/c)^2). These assertions are independent of both quantum numbers and spin-coupling properties of the exchanges.

3.4.2b t- and u-dependence

We expect the universal behavior $d\sigma/dt \propto \exp(3t)$ for forward reactions and $d\sigma/du \propto \exp(u)$ for backward scattering. These predictions hold for $|t| > 0.5$ and $|u| > 0.5$ (GeV/c)^2, respectively.

3.4.2c Quantum numbers and exotic exchange

Fixed poles are not expected to have the usual isospin structure of hadrons. In particular, we suggest that large violation* of the pure $I_t = \frac{1}{2}$ rule, observed in $\gamma N \to K\Sigma$ [43], is due to an exotic $I_t = \frac{3}{2}$ fixed-pole amplitude.

To motivate our suggestion, we begin with the remark that the ratio of cross sections for the purely hadronic 'allowed' reaction $\pi^+p \to K^+\Sigma^+$ to that for the exotic process $\pi^-p \to K^+\Sigma^-$ is measured to be approximately 3000 at $p_{lab} = 5$ GeV/c [44,45]. In terms of scattering amplitudes with definite isospin in the t-channel, we write

$$\frac{d\sigma}{dt}(\pi^+p \to K^+\Sigma^+) = \left|\tfrac{2}{3}A^h_{\frac{1}{2}} + \tfrac{1}{3}A^h_{\frac{3}{2}}\right|^2 , \tag{18}$$

$$\frac{d\sigma}{dt}(\pi^-p \to K^+\Sigma^-) = \left|A^h_{\frac{3}{2}}\right|^2 . \tag{19}$$

Superscript h denotes 'purely-hadronic'; subscripts give values of isospin in the t-channel. We deduce that

$$\left|\frac{A^h_{\frac{3}{2}}}{A^h_{\frac{1}{2}}}\right| \sim \frac{1}{80} . \tag{20}$$

We may describe the photoproduction process $\gamma N \to K\Sigma$ in terms of similar t-channel amplitudes. In this case, we find [43]

* It is possible that the evidence for exotic exchange in $\gamma N \to K\Sigma$ and $\gamma N \to \pi\Delta$ is illusory. Perhaps the fault lies in poor understanding of deuteron corrections. Neither theoretical arguments nor experimental evidence is conclusive either way. For our present purposes, we assume that observed effects are interpreted correctly as exotic exchange.

$$\left|\frac{A^{\gamma}_{\frac{3}{2}}}{A^{\gamma}_{\frac{1}{2}}}\right| \gtrsim \frac{1}{10} \tag{21}$$

at $E_{\mathrm{lab}} \approx 11$ GeV. This ratio is an order of magnitude larger than the hadronic ratio.

We conclude that Regge poles present in strong processes have essentially only 'allowed' quantum numbers. The extra measure of exotic exchange present in photoproduction is attributed to fixed poles, which cannot occur in strong processes.

As a consequence of fixed-pole exotic exchange, we suggest that direct production of exotic states is more favored in γp reactions than in purely hadronic processes. In particular, we recommend close examination of the $K^+\pi^+$ mass spectrum in $\gamma p \to K^+\pi^+\Sigma^-$ and of the $\pi^+\pi^+$ mass spectrum in $\gamma p \to \pi^+\pi^+\Delta^-$.

3.4.3. Pole extrapolation

In subsect. 3.2.5, we made several general remarks about extrapolation of Regge-pole residue functions from the scattering to the resonance region. Here, we comment briefly on one aspect of pole extrapolation specifically relevant to the fixed-pole model.

We begin by noting a simple empirical fact. At, say, 10 GeV/c, we define $Q(0)$ to be the quotient of the cross sections at $u = 0$ for reactions $\gamma p \to n\pi^+$ and $\pi^+ p \to p\pi^+$. Similarly, let $Q(M)$ be the quotient of the coupling strengths of the N_α Regge trajectory to $\gamma p \to n\pi^+$ and $\pi^+ p \to p\pi^+$ at $u = M^2$, the nucleon pole position *. Empirically, $Q(0) \approx Q(M)$, to within a factor of two or so. This result suggests that Regge poles make a comparable contribution to $\pi^+ p \to p\pi^+$ and $\gamma p \to n\pi^+$ *at small* u. In other words, we do not expect the small u-behavior of $d\sigma/du$ for $\gamma p \to n\pi^+$ to be dominated by fixed poles (or by any other effect which cannot be present in purely hadronic processes). Conversely, if $\gamma p \to N\pi$ were dominated at small u by some non-strong effect, then we would expect $Q(0) \gg Q(M)$.

As explained in subsect. 3.2.5, we do not enforce pole-extrapolation constraints in our fits. Nevertheless, it is an important consistency check on the validity of our fixed-pole model fit that the *Regge-pole* contribution at $u = 0$ is comparable to the observed cross section there (see fig. 14). Only at larger $|u|$ does the fixed-pole contribution dominate $d\sigma/du$.

3.5. *Strong absorption model*

Motivation for absorption corrections to Regge-pole exchange amplitudes has been reviewed in several articles [3, 46, 47]. Our formalism is described very briefly in appendix D. Essentially, a given input Regge-pole term is modified in such a way that the resulting amplitude has both the

* At $u = M^2$, these couplings are known a priori; they are not determined by extrapolating a high-energy fit to scattering data. For $\pi^+ p \to p\pi^+$, the coupling strength is the πN coupling constant, g^2 ($g^2/4\pi \approx 15$). For $\gamma p \to N\pi$, the couplings are g times the electric charge and magnetic moment of the nucleon.

original Regge-pole term and, in addition, a Regge-cut contribution. The moving branch point singularity in the complex j-plane has a slope α'_C which is approximately one-half that of the input Regge pole. Overall structure in the j-plane is illustrated in fig. 6d.

Insofar as energy dependence is concerned, high-energy scattering amplitudes are a linear combination of a Regge-pole component, with energy behavior $s^{\alpha(u)} = s^{\alpha_0+bu}$, and a Regge-cut term whose energy dependence is $s^{\alpha_C(u)} \approx s^{\alpha_0(u)+\frac{1}{2}bu}$. The relative strength of these pole and cut terms (as a function of u) is specified by the absorption prescription; it depends crucially on assumptions made about u-dependence of the input Regge-pole term. There are also differences of opinion as to how large the 'absorption constant' c should be.

The two main versions of the absorption approach have come to be known as the weak-cut (or Argonne) model and the strong-cut (or Michigan SCRAM) model. In the former, Regge-pole terms have explicitly all WSNZ factors, whereas, in the latter, input Regge-pole terms have no WSNZ factors. Moreover, in the strong-cut version, c is usually about twice as large as in the weak-cut approach.

Comparison of figs. 5 and 6d indicates that the absorption procedure will reproduce empirical result $\Delta\alpha_{\text{eff}} \approx 0$ only if absorption cuts are sufficiently dominant. This is not true in the Argonne model; indeed, the weak-cut model suffers from the same deficiencies outlined in subsect. 3.2 for the pure-Regge-pole approach*. Therefore, we consider only the strong-cut version for the remainders of our discussion.

3.5.1. Fits to data†

Reference to fig. 6d again, indicates that the result $\Delta\alpha_{\text{eff}}(u) \approx 0$, for all u, requires dominance of the Δ_δ absorption-cut term at large $|u|$. This is precisely the opposite of the conclusion we reached in the contest of *fixed*-cut models. In the HIPPIE approach, to achieve $\Delta\alpha_{\text{eff}} \approx 0$, we had to make the N_α contribution dominant.

In addition to Δ_δ, we may choose one or any number of available $I_u = \frac{1}{2}$ trajectories (N_α, N_γ, N_β, ...). Data are relatively meager, so we select only N_α. Moreover, inasmuch as we ignore pole-extrapolation constraints (cf., subsect. 3.2.5), it is sufficient to express reduced pole-residues $\gamma_i(\sqrt{u})$ as linear functions.

$$\gamma_i(\sqrt{u}) = (a_i + b_i\sqrt{u}) \exp(\mu u) \ . \tag{22}$$

Technical details may be found in appendices A and D.

In table 3, we give parameters of our best SCRAM fit to γp data. The fit itself is displayed in fig. 15; agreement with both s and u dependence of data is excellent. In particular, we note that turnover of $d\sigma/du$ near $u = 0$ is

* This was also our conclusion for backward πN scattering [17].

† A strong-cut fit to backward single-pion photoproduction has been published by the Michigan group [38]. Unlike their analysis, however, we do not enforce VDM constraints on our fits. See subsect. 3.2.4 for a discussion of this point.

Table 3
Parameters of SCRAM * fit (absorption constant $c = 1.25$).

Δ_δ	N_α
$\overline{\alpha} = -0.45 + 0.9u$	$\overline{\alpha} = -0.84 + 0.9u$
$\mu = -1.30$	$\mu = 1.17$
	isovector photon
$\gamma_1 = 1.58 + 2.79\sqrt{u}$	$\gamma_1 = -2\ 9 + 11.51\sqrt{u}$
$\gamma_2 = -8.43 - 1.15\sqrt{u}$	$\gamma_2 = -5\ 89 + 5.18\sqrt{u}$
	isoscalar photon
	$\gamma_1 = -0.207 - 0.321\sqrt{u}$
	$\gamma_2 = 5.12 - 7\ 15\sqrt{u}$

$\chi^2(\gamma p \to n\pi^+) = 55$ (on 41 data points),
$\chi^2(\gamma p \to p\pi^0) = 26$ (on 35 data points)

* Trajectories are not varied. Amplitudes are discussed in subsect. 3 5 and appendices A and D.

reproduced for both charge states. For $\gamma p \to p\pi^0$, the change in slope (or break) apparent in $d\sigma/du$ near $u = -0.3$ (GeV/c)^2 is also accommodated nicely. In fig. 16, we present curves which contrast the magnitude of overall ($N_\alpha + \Delta_\delta$) Regge-pole and absorptive-cut contributions. The decomposition of $d\sigma/du$ shows that cancellation is fierce between pole and cut terms; as a result of strong absorption, $d\sigma/du$ is reduced by an order of magnitude from the value it would have if only Regge-*pole* exchange terms were present. The decomposition presented in fig. 17 illustrates the relative importance of N_α and Δ_δ contributions to $d\sigma/du$, as a function of u; this shows the anticipated dominance of Δ_δ at large $|u|$ necessary to achieve $\Delta\alpha_{\text{eff}} \approx 0$.

3.5.2. Predictions

As with other models, fits to data do not determine amplitudes. Therefore, predictions of polarization quantities are meaningless. On the other hand, precise measurements of energy dependence of $\gamma p \to \Delta^{++}\pi^-$ and $\gamma d \to np$ should be clear-cut tests of SCRAM. These reactions isolate $I_u = \frac{3}{2}$ and $I_u = \frac{1}{2}$, as we have emphasized before. If SCRAM is correct, both should exhibit *shrinkage*, unlike present γp data, with effective slope $\alpha' \approx 0.5$ (GeV/c)$^{-2}$.

3.6. *Other models*

Thus far in sect. 3, we have studied four models. These are (i) a model based purely on Regge-pole exchanges; (ii) a model in which both Regge poles and fixed cuts are present; (iii) a model in which there are both Regge poles and fixed poles, but no cuts; and (iv) a model based upon Regge

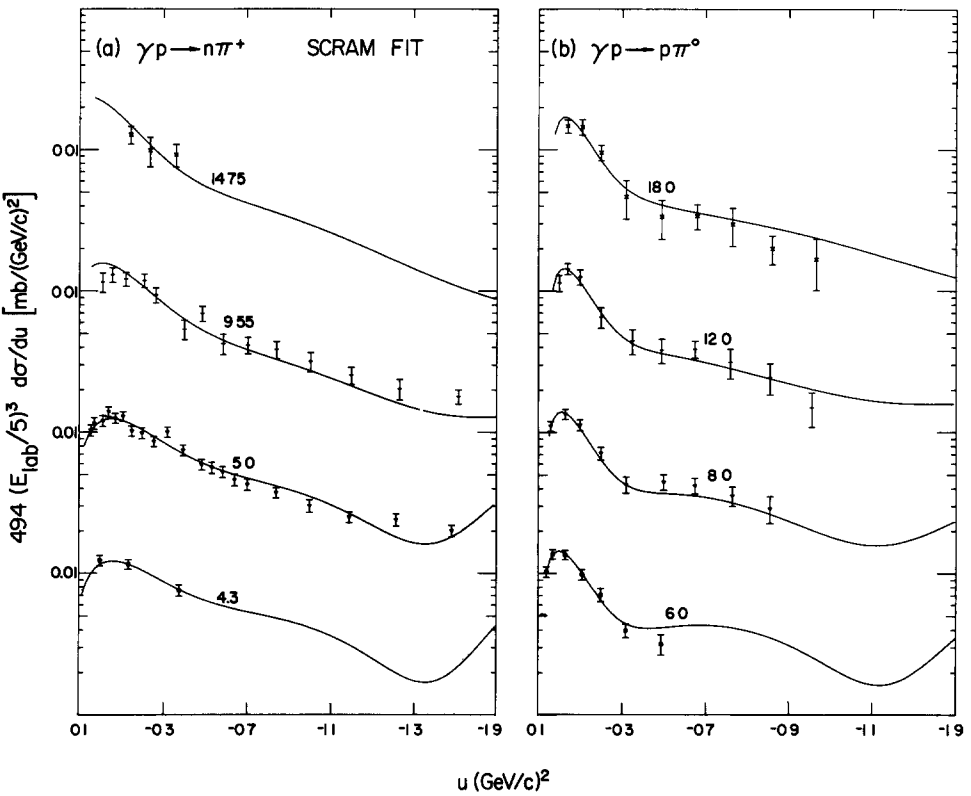

Fig. 15. Curves computed from parameters determined in our SCRAM fit are compared with a selection of data [9,10]. Parameters are listed in table 3. Numbers next to data denote photon lab momentum in GeV.

poles and moving cuts generated by absorption. These four models represent practically all the possibilities for singularity structure in the j-plane. Correspondingly, essentially all conceivable energy dependences of $d\sigma/du$ have been considered.

However, we should mention that a fifth model, based upon complex poles, has also been proposed. Moreover, these five models are not orthogonal. In particular, one may entertain the possibility of absorbing fixed-pole and fixed-cut amplitudes. Let us now turn to an examination of this latter suggestion. Complex poles are treated subsequently.

3.6.1. Absorption of fixed singularities

In SCRAM (cf. subsect. 3.5), we assume, without any compelling theoretical motivation, that one should absorb an input amplitude representing pure-Regge-pole exchanges. However, let us postulate a model in which absorption is applied to a scattering amplitude representing fixed poles and/or fixed cuts. It is evident from the absorption formalism that energy

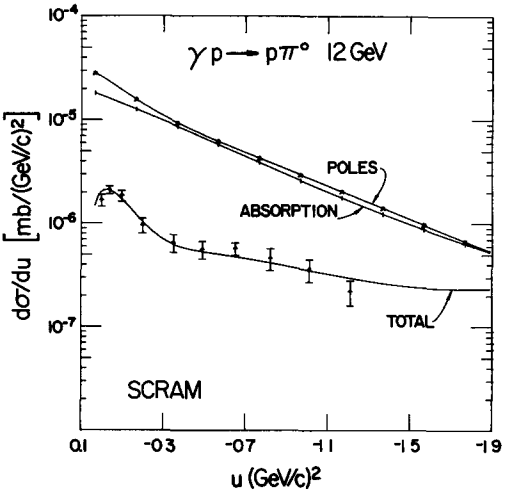

Fig. 16. We give an example of our SCRAM fit to $\gamma p \to p\pi^0$ at 12 GeV. Data are from ref. [10]. We also show values of $d\sigma/du$ computed separately from the unabsorbed net Regge-pole contribution (N_α plus Δ_δ) and from the destructive absorption (moving cut) contribution to scattering amplitudes.

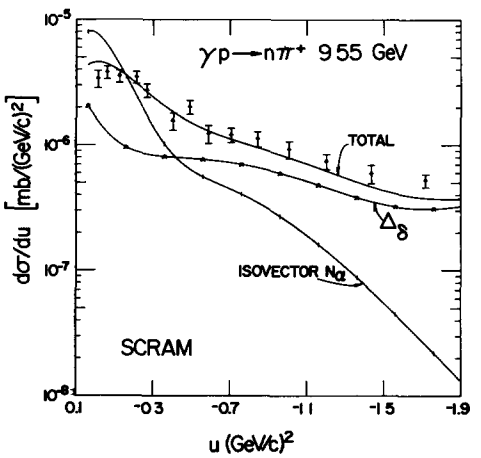

Fig. 17. We present an example of our SCRAM fit to $\gamma p \to n\pi^+$ at 9.55 GeV. Also shown are values of $d\sigma/du$ computed from separate contributions of isovector N_α and Δ_δ exchanges. These N_α and Δ_δ terms are the sum of corresponding Regge-pole and (destructive) absorptive cut amplitudes.

dependence of the final amplitude in this model is essentially the same as that of the input fixed-singularity amplitude. We recall that the only definitive test of a fixed-singularity model is energy dependence of $d\sigma/du$. It is clear that this test is not sensitive to the presence or absence of absorption.

Absorption will alter the u-dependence of amplitudes in the HIPPIE model. However, explicit calculations show that the shape of $d\sigma/du$ is not al-

tered significantly. In particular, for N_α exchange in backward π^+p elastic scattering, no dip in $d\sigma/du$ near $u = -0.2$ (GeV/c)^2 is generated as a result of strong absorption of input NAIVE HIPPIE amplitudes. Although superficially surprising, this result is understood easily. According to folklore, the dip in $d\sigma/du$ near $u = -0.2$ (GeV/c)^2 is expected only if the spin-non-flip amplitude dominates. However, in the HIPPIE model, the flip/non-flip ratio is specified. Whatever the value of σ, we find that the contribution from the spin-flip amplitude fills-in any absorption dip associated with the non-spin-flip amplitude.

3.6.2. Complex poles *

Recently, there have been theoretical developments in the study of Regge trajectories which are complex for u (or t) < 0. It is argued that the phenomenological effects of branch-point singularities in the j-plane (cuts) may be reproduced adequately, over the current range of energies, by a model based on exchange of a pair of complex conjugate Regge poles [48]. The resultant model enjoys the usual technical advantages of pure pole models; in models with cuts, complicated and time consuming numerical integrations must be performed to obtain scattering amplitudes. Furthermore, the complex-pole model is more general than the current crop of cut models (absorption and HIPPIE). Existing cut model give specific expressions for discontinuities across the cut; the complex-pole approach allows more flexibility.

We may distinguish two versions of the complex-pole model. In the first, complex poles replace *moving* (absorptive) cuts. In the second, complex poles substitute for *fixed* (HIPPIE) cuts. Let us examine each of these.

In the usual applications of the first version, complex trajectories have canonical slope ($\alpha' \approx 1$ (GeV/c)^2). They reproduce effects of the weak-cut (Argonne), but not of the strong-cut (SCRAM) model. As we pointed out in subsect. 3.5, only the latter model can fit backward single-pion photoproduction data. Correspondingly, current formulations of 'absorptive' complex poles will not reproduce backward photoproduction data.

The second version seems more promising. In subsect. 3.3, we showed that HIPPIE model can fit current γp data. Therefore, complex pole analogues of HIPPIE models should also be able to reproduce γp data. Unfortunately, the theoretical status of this complex-pole model is unclear; the HIPPIE cut can be calculated explicitly, and it is *not* well approximated by a pair of complex poles.

In view of theoretical uncertainty in its formulation and the large number of parameters involved, we do not present fits with any version of the complex-pole model in this paper.

* Consult ref. [48] for application of complex pole models to forward $\pi^-p \to \pi^0n$. Further references are cited in that paper. GCF is grateful to S. Ellis, R. L. Heimann and P. E. Kaus for helpful discussions of the complex-pole model.

4. COMPARISON OF MODELS AND SUGGESTIONS FOR NEW EXPERIMENTS

In sect. 3, we discussed phenomenological models and presented fits to γp data. Each model was described separately, and adequate fits to the data were obtained in terms of fixed-pole, fixed-cut, and strong-Regge-(moving) cut models. We now turn to a comparative evaluation of features of these models. We contrast the remarkably different ways in which various models reproduce the same data. This confrontation of models with data, and models with each other, demonstrates the clear need for a set of new experiments. The experiments we suggest here are in addition to those we proposed earlier, in subsect. 2.4.

Theoretically, the various models are distinguished on the basis of the dominant j-plane singularities present in each case. 'Exchange' of these singularities (whether poles or cuts, fixed or moving) in each case provides scattering amplitudes with characteristic dependence on s and u. Therefore, in an effort to select a preferred model, we will discuss experiments which would determine more precisely the s- and u-behavior of $d\sigma/du$. Other experiments suggested here are directed to a determination of the s- and u-dependences of amplitudes associated with specific values of exchanged *isospin* I_u. Finally, we also discuss what may be learned from polarization studies.

4.1. *Energy dependence of* $\gamma N \to N\pi$

Of the four models, only the fixed-pole model gives a *natural* explanation of the observed energy behavior $d\sigma/du \propto E_{lab}^{-3}$. To be sure, good or even better fits to data are possible with other models; however, in these models, agreement requires special and, at present, unmotivated values of

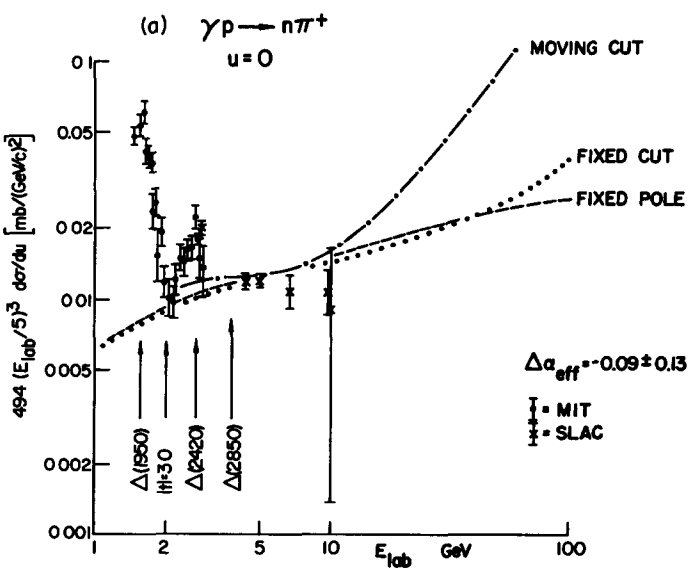

Fig. 18a.

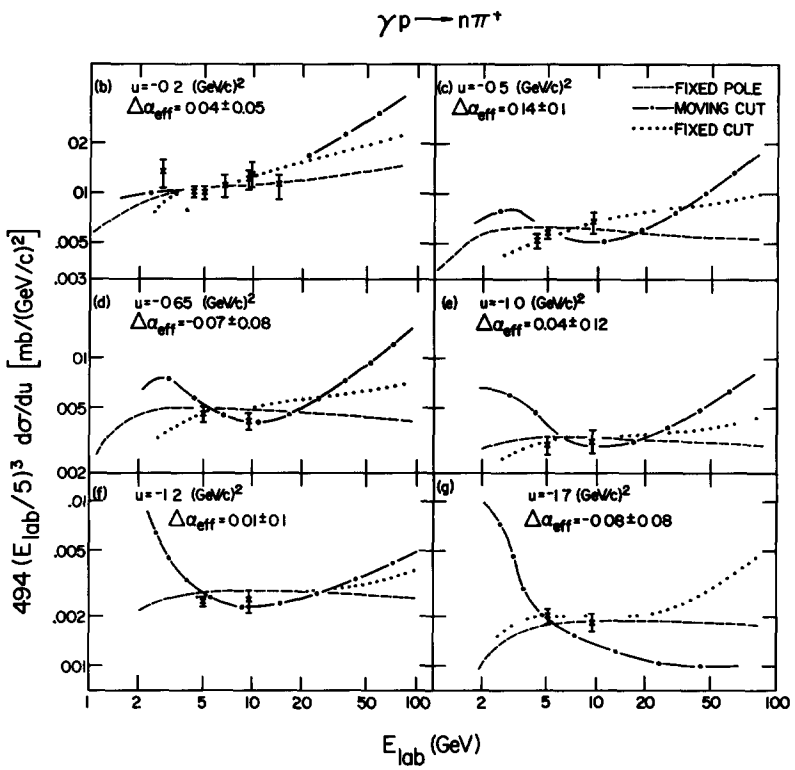

Fig. 18b. Fig. 18c. Fig. 18d. Fig. 18e. Fig. 18f. Fig. 18g.

Fig. 18. Fits and predictions of our models are contrasted with data for $\gamma p \to n\pi^+$. These curves indicate energy dependence at various fixed values of u. Where necessary, we interpolate available data from neighboring values of u in order to present results at the chosen fixed values of u. Points marked with an X are from refs. [8] and [9]; those marked with a large dot are from ref. [49]. For each value of u, we give the experimental value of $\Delta\alpha_{\text{eff}}$, defined in eq. (3) of the text and determined from plotted data above $E_{\text{lab}} = 4$ GeV. Fixed-cut model results shown here are those for our NAIVE HIPPIE fit B, parameters are given in table 1b. Moving-cut and fixed-pole model parameters are found in tables 3 and 2, respectively. In part (a), we mark values of E_{lab} at which prominent resonances occur, also shown is the value of E_{lab} at which $|t| = 3\,(\text{GeV}/c)^2$ coincides with $u = 0$.

parameters. Results are contrasted in figs. 18 and 19. For $\gamma p \to p\pi^0$ and $\gamma p \to n\pi^+$, we plot 494 $(\frac{1}{5}E_{\text{lab}})^3$ $d\sigma/du$ at selected fixed values of u. We call attention to the fact that all theories, except the fixed-pole model, suggest that the observed constancy of $E_{\text{lab}}^3\, d\sigma/du$ is but a local phenomenon, confined to the limited energy range $5 \lesssim E_{\text{lab}} \lesssim 20$ GeV. At $u = 0$, even in the fixed-pole case, $E_{\text{lab}}^3\, d\sigma/du$ grows with increasing E_{lab}, owing to growing importance of Δ_δ Regge-pole exchange at higher energies. Dominance of Δ_δ exchange at $u = 0$ would give $d\sigma/du$ a natural E_{lab}^{-2} behavior near $u = 0$.

The conflict between theories and data is illustrated particularly dramatically in fig. 18a. Scanning from 1.5 GeV to 10 GeV, we observe the da-

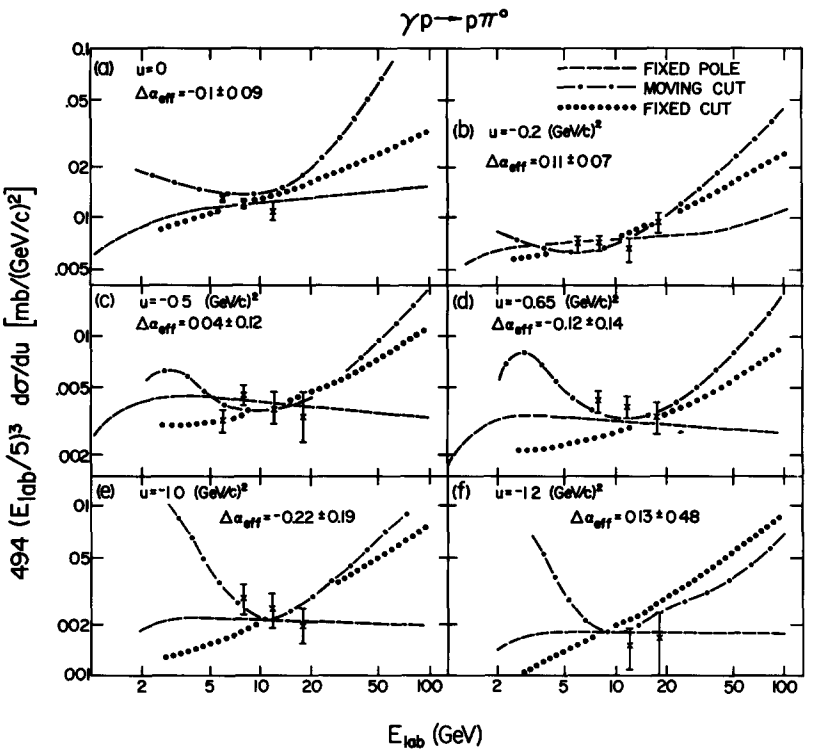

Fig. 19. Fits and predictions of our models are contrasted with data for $\gamma p \to p\pi^0$ at six fixed values of u. Further details are common to fig. 18 and are described in the caption for that figure.

ta falling from the top left to the bottom right of the graph; theoretical curves travel perversely from bottom left to top right. Surely, Nature is not so cruel that the observed constancy of $E_{lab}^3\, d\sigma/du$, above 5 GeV, represents just the irrelevant broad bottom of a bowl, which is bounded by resonance data at low energy, and (for example) by the SCRAM curve at high energy ($E_{lab} \gtrsim 20$ GeV).

In examining energy dependence, we find it also instructive to compare $\gamma p \to n\pi^+$ (fig. 18a) with $\pi^+ p \to p\pi^+$ at $u = 0$ (fig. 20). At low energies, these plots of $E_{lab}^3\, d\sigma/du$ show similar structure for the two reactions*; at high energy, however, data and theories [17] for $\pi^+ p \to p\pi^+$ increase in a cone-shaped fashion, whereas data for $\gamma p \to n\pi^+$ level off.

* For $\pi^+ p \to p\pi^+$, note that the quantity $d\sigma/du\big|_{u=0}$ when plotted as a function of p_{lab} shows a pronounced dip near $p_{lab} = 2$ GeV/c. Recall also that at $p_{lab} = 2$ GeV/c, $u = 0$ corresponds to $t \approx -3$ (GeV/c)^2. For $\pi^\pm p$ elastic scattering, a pronounced dip in the differential cross section near the fixed value $t \approx -3$ (GeV/c)^2 is observed up to $p_{lab} \approx 10$ GeV/c. We remark that at $u = 0$, $d\sigma/du$ for $\gamma p \to N\pi$ also shows a dip near $E_{lab} \approx 2$ GeV. Is there also a fixed $-t$ dip in $d\sigma/dt$ for $\gamma p \to \pi N$ at higher energies? Present data are silent on this subject. It is important to verify or refute this conjecture.

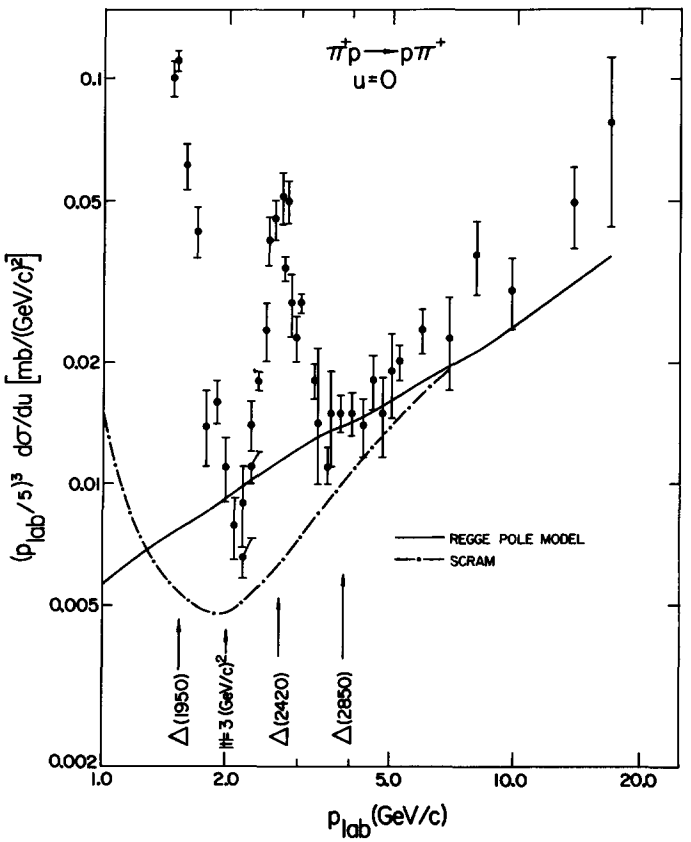

Fig. 20. Data for π^+p elastic scattering at $u = 0$ are contrasted with fits and predictions of two models. Sources of data are legion (cf. the compilation of ref [50]); theoretical curves are obtained from parameters given in ref. [17].

4.1.1. Experiments: verification of E_{lab}^{-3} behavior

The above discussion indicates that the next set of important experiments should be directed to verifying E_{lab}^{-3} behavior of $\gamma p \to N\pi$ for as wide a range of s and u as possible. Our analysis indicates that E_{lab}^{-3} behavior is quite anomalous: we base this conclusion upon results from both a direct empirical comparison of γp data with hadron data and our confrontation of γp data with an essentially complete set of models.

Higher-energy accelerators are required in order to test decisively those theories which predict that $E_{lab}^{-3}\, d\sigma/du$ is a bowl-shaped distribution (as a function of E_{lab}). However, useful clarification is possible also at present energies; for example, extension of present $\gamma p \to p\pi^0$ and $\gamma p \to n\pi^+$ measurements up to, say, $|u| = 3$ (GeV/c)^2 would be useful*. Moreover,

* Recall that if $\exp(u)$ behavior of $d\sigma/du$ persists, cross sections will be relatively large at large $|u|$.

Table 4
Cross sections in nanobarns.

Model	E_{lab} (GeV)	$\gamma p \to n\pi^+$		$\gamma p \to p\pi^0$		$\gamma n \to p\pi^-$	
		$u_{min} \geq u \geq -1.0$	$-1.0 \geq u \geq -2.0$	$u_{min} \geq u \geq -1.0$	$-1.0 \geq u \geq -2.0$	$u_{min} \geq u \geq -1.0$	$-1.0 \geq u \geq -2.0$
NAIVE HIPPIE A	20	0.268	0.0805	0.199	0.105	0.392	0.171
NAIVE HIPPIE B	20	0.304	0.0766	0.217	0.112	0.256	0.0576
FULL HIPPIE	20	0.199	0.035	0.212	0.0459	0.222	0.052
Fixed pole	20	0.249	0.0702	0.169	0.0465	0.391	0.093
SCRAM	20	0.308	0.051	0.212	0.0617	1.04	0.088
NAIVE HIPPIE A	50	0.0253	0.01	0.023	0.0111	0.0333	0.0184
NAIVE HIPPIE B	50	0.0235	0.00621	0.0208	0.0142	0.0206	0.00621
FULL HIPPIE	50	0.0183	0.00365	0.0241	0.0045	0.0187	0.00461
Fixed pole	50	0.017	0.00435	0.0112	0.00288	0.0262	0.00577
SCRAM	50	0.0358	0.00387	0.0292	0.00555	0.0984	0.00587
NAIVE HIPPIE A	100	0.00495	0.00216	0.00538	0.00231	0.00608	0.00362
NAIVE HIPPIE B	100	0.00356	0.00113	0.00389	0.00313	0.00331	0.00131
FULL HIPPIE	100	0.0037	0.000842	0.00546	0.000978	0.00366	0.000989
Fixed pole	100	0.00236	0.000528	0.00136	0.00035	0.00357	0.0007
SCRAM	100	0.00798	0.000603	0.00786	0.000942	0.0183	0.000838

referring to fig. 1a, we note that $\gamma p \to n\pi^+$ data are sparse above 9.55 GeV; we recommend measurement of $d\sigma/du$ at 16 GeV over the range $u_{min} \geq u \geq -3$ $(GeV/c)^2$ *. At $u = 0$, theories predict at least a 30% increase in $E_{lab}^3\, d\sigma/du$ at 16 GeV over its value at 5 GeV (cf., fig. 18a).

In addition to more thorough study of $\gamma p \to p\pi^0$ and $\gamma p \to n\pi^+$, measurements of $d\sigma/du$ for *any other backward photoproduction reaction* would clarify the E_{lab}^{-3} scaling law. Studies of *other charge states in* $\gamma N \to N\pi$ would help a great deal in determining parameters of models. We treat this latter issue in more detail in subsect. 4.2.1. We close our discussion of energy dependence by presenting table 4, in which we give projected cross sections for $\gamma p \to n\pi^+$, $\gamma p \to p\pi^0$, and $\gamma n \to p\pi^-$ at $E_{lab} = 20$, 50 and 100 GeV.

4.2. *Reactions* $\gamma n \to p\pi^-$, $\gamma p \to \Delta^{++}\pi^-$ *and* $\gamma d \to np$

Important reactions are those for which u-channel isospin I_u is unique. For such processes (e.g., $\gamma d \to pn$ and $\gamma p \to \Delta^{++}\pi^-$), measurements of $d\sigma/du$ provide direct information on which type of j-plane singularity is associated with a given I_u. We discuss our expectations for these decisive processes below. However, first we consider briefly other charge states in $\gamma N \to N\pi$.

4.2.1. Other charge states in $\gamma N \to N\pi$

It will be recalled that, in sect. 3, in order to achieve $\Delta\alpha_{eff} \approx 0$ for $\gamma p \to p\pi^0$ and $\gamma p \to n\pi^+$, at large u, we reached contrary conclusions about the isospin of the dominant exchange in different models. For example, in fixed-cut models, $I_u = \frac{1}{2}$ exchange is dominant at large u, whereas, in SCRAM, $I_u = \frac{3}{2}$ is dominant. Because isospin, s- and u-dependences are correlated in this unusual fashion, it becomes especially valuable to measure $d\sigma/du$ for other charge states of $\gamma N \to N\pi$. Ideally, enough charge states should be measured to separate out $I_u = \frac{1}{2}$ and $I_u = \frac{3}{2}$ exchanges †, as well as their interference effects. However, data on even one additional reaction would be quite helpful. To indicate the wealth of possibilities allowed by our good fits to present data, we give our predictions for $\gamma n \to p\pi^-$ at $E_{lab} = 10$ GeV, in fig. 21. Even at $u = 0$, our five fits give cross sections which differ by an order of magnitude. Measurements of $d\sigma/du$ for $\gamma n \to p\pi^-$ would provide a good constraint on parameters in all models and help pin down which isospin exchange is dominant at large u.

4.2.2. $\gamma d \to pn$ and $\gamma p \to \Delta^{++}\pi^-$; decisive tests of models

Several times in the course of sect. 3 we commented upon the special significance of the reactions $\gamma d \to pn$ and $\gamma p \to \Delta^{++}\pi^-$, which have unique

* We note that the statistical accuracy of present data is excellent Further constraints on models will not come from data of increased precision. Rather, measurements are required over a wider range of values of s and u, with accuracy comparable to present experiments.

† Recall, also, that the $I_u = \frac{1}{2}$ exchange amplitude has contributions from both isovector and isoscalar photons. There are effectively three different values of isospin in the exchange channel.

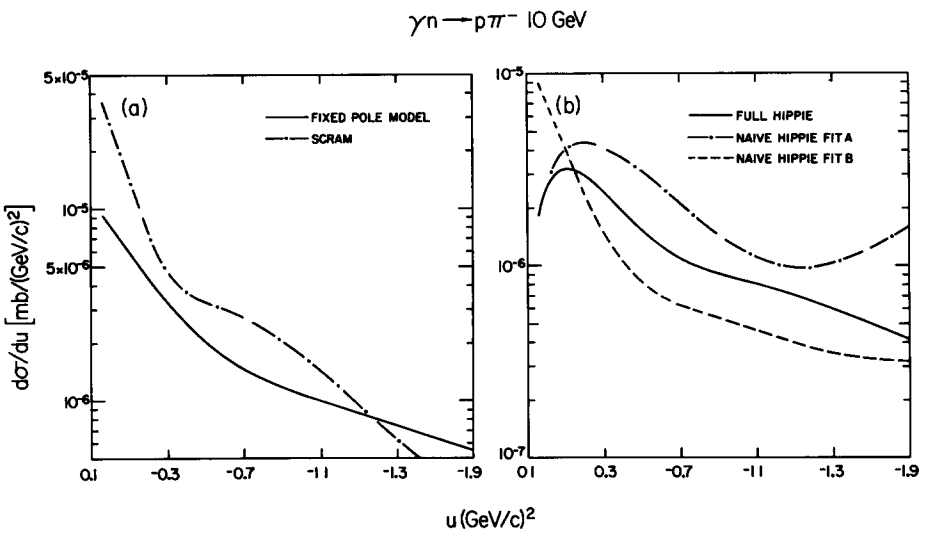

Fig. 21. Predicted values of $d\sigma/du$ are given for reaction $\gamma n \to p\pi^-$ at 10 GeV. The five models are discussed in the text; parameters are found in tables 1-3.

isospin $I_u = \frac{1}{2}$ and $\frac{3}{2}$, respectively *. Determination of the s-and u-dependences of $d\sigma/du$ for each of these processes will distinguish which of the four models † best applied to photoproduction. We recommend measurements of $d\sigma/du$ from $E_{lab} = 5$ GeV to as high an energy as possible; the range of values of u should also be as large as possible, certainly no smaller than $u_{min} \geq u \geq -1.5$ $(GeV/c)^2$.

4.2.2a. The u-dependence

In subsect. 2.4.3, we justified on purely empirical grounds the importance of finding the precise u-dependence of $d\sigma/du$ for $\gamma p \to \Delta^{++}\pi^-$ and $\gamma d \to pn$. Theoretical reasons are more compelling. In fig. 22, data are shown and possible u-dependence are sketched. Essentially two classes of theories must be distinguished. In the first type (fixed-pole and fixed-cut models), observed s- and u-dependences of $\gamma p \to N\pi$ data are deemed to be no accident but, rather, to reflect a new, universal feature of γN processes which is not shared by purely hadronic reactions. Correspondingly, $d\sigma/du$ for $\gamma p \to \Delta^{++}\pi^-$ is expected to have a characteristic smooth behavior at all energies. Presumably, it should level off from its present tumultuous $\exp(3u)$ dependence and, at large $|u|$, exhibit a staid $\exp(u)$ behavior similar to $\gamma p \to N\pi$ data‡. In the second class of theories, we place the moving-(Regge) pole and moving-cut models. These assert that there is nothing

* We are aware, of course, that studies of $\gamma p \to \Delta^{++}\pi^-$ are beset with serious problems, owing to kinematical reflections from the *backward* scattering process $\gamma p \to \rho^0 p$ or, more generally, $\gamma p \to (\pi^-\pi^+)p$ [51, 52].

† Fixed cut, fixed pole, moving (Regge) pole, and moving (Regge) cut.

‡ Footnote see next page.

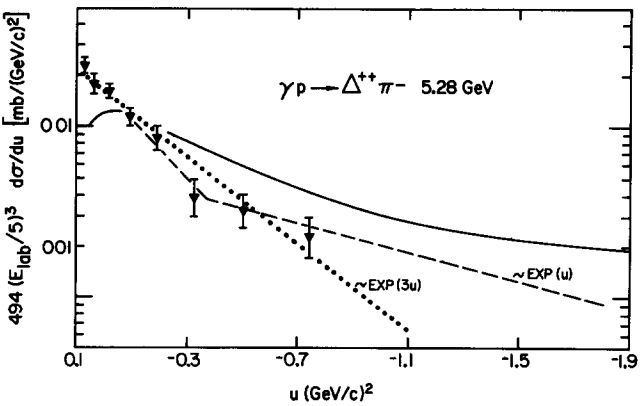

Fig. 22. We present data for $\gamma p \to \Delta^{++}\pi^-$ along with some curves showing typical u-dependences of $d\sigma/du$. The solid curve is the differential cross section for $\gamma p \to n\pi^+$ (cf. fig. 1a). The dashed curve, with a break near $u = -0.3$ $(GeV/c)^2$ represents the prediction of the fixed-pole and fixed-cut models. The behavior of the solid and dashed curves is similar at large $|u|$, both fall approximately as $\exp(u)$. The fixed-pole and fixed-cut models are distinguished by s-dependence of $d\sigma/du$ at large $|u|$; thus, $d\sigma/du \propto E_{lab}^{-3}$ in the fixed-pole model, but $d\sigma/du \propto E_{lab}^{-2}$ in the fixed-cut theory. Finally, the dotted curve, falling as $\exp(3u)$, might be expected in models which suggest $\exp(u)$ behavior of single pion photoproduction data is not universal.

unique about the j-plane for photoproduction. Therefore, any present regularities in γp data have no fundamental significance. Continued $\exp(3u)$ dependence of $d\sigma/du$ would not be unexpected. Indeed, a distribution with any other exponential dependence, or even one with dips or breaks, is quite possible.

Similar remarks to those above hold also for $\gamma d \to pn$, for which no data are available.

4.2.2.b. The s-dependence

For $\gamma p \to \Delta^{++}\pi^-$ and $\gamma d \to pn$, the behavior of $d\sigma/du$ as a function of energy is the most crucial means for distinguishing models. Predictions for the energy dependence of $E_{lab}^3\, d\sigma/du$ are given in fig. 23: (a) and (b) refer to $\gamma d \to pn$, whereas (c) and (d) apply to $\gamma p \to \Delta^{++}\pi^-$. Most critical is the behavior of $d\sigma/du$ for values of u away from the backward peak. In the peak region ($|u| < 0.5$ $(GeV/c)^2$), both kinematic and Regge-pole effects tend to be substantial in all models. However, for u in the range $0.5 < |u| < 2.0$ $(GeV/c)^2$, the characteristic singularity in each model is dominant. For these larger values of $|u|$, moreover, the differences in predicted energy

‡ Caveat We note that our fits determine only that the (isovector) $I_u = \frac{1}{2}$ amplitude should have an $\exp(u)$ dependence. Although not suggested by our present formulation of either the fixed-cut or fixed-pole models, it is *possible* that amplitudes with different isospin also have different u-dependence. Correspondingly, it is *possible* that $d\sigma/du$ for $\gamma p \to \Delta^{++}\pi^-$ behaves as $\exp(3u)$ at large $|u|$. We must await data. In any case, predictions for energy dependence discussed in subsect. 4.2.2b *are an unambiguous signature of models.*

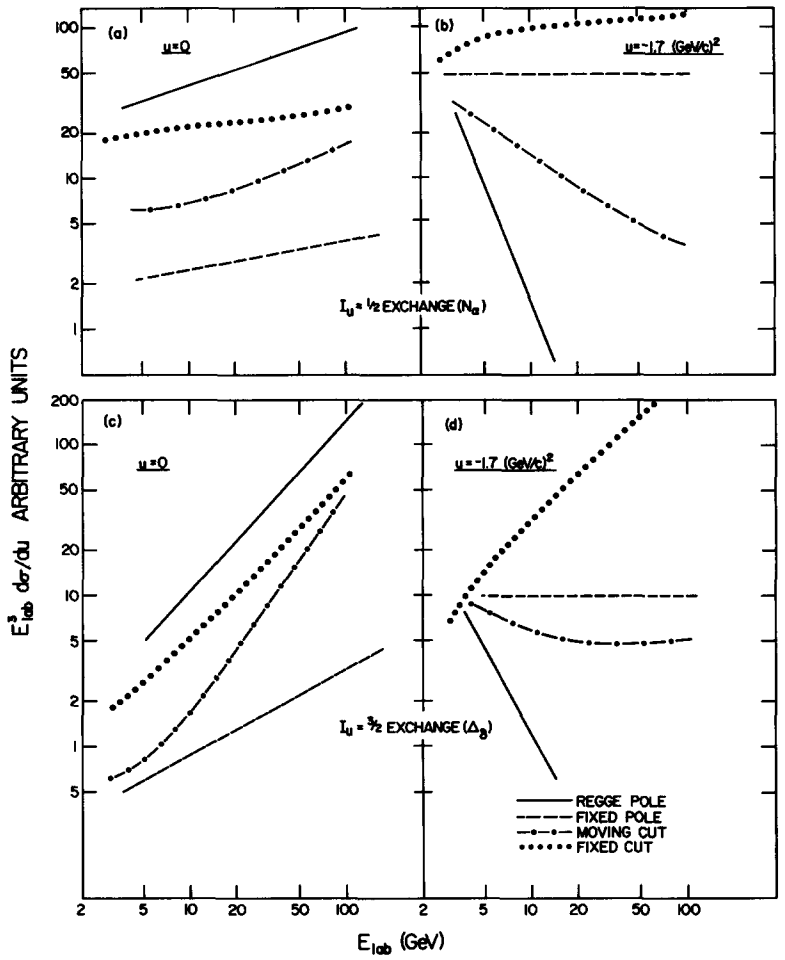

Fig. 23. We contrast predicted energy dependences of $d\sigma/du$ for our four models. Plotted is $E_{\text{lab}}^3\, d\sigma/du$ (arbitrary units) versus E_{lab}, from 2 to 100 GeV. The relative normalization of the four models at a given energy is arbitrary; only the energy dependence of a given curve is significant. In (a) and (b) $I_u = \frac{1}{2}$; physical example is $\gamma d \to pn$. In (c) and (d) $I_u = \frac{3}{2}$, with example $\gamma p \to \Delta^{++}\pi^-$.

dependence of various singularities are enhanced. A pure Regge-pole model predicts shrinkage, with *

$$E_{\text{lab}}^3 \frac{d\sigma}{du} \propto E_{\text{lab}}^{2\alpha_0+1} \exp(2u \log E_{\text{lab}}) \,. \tag{23}$$

In the moving-cut model, there is less shrinkage*; roughly

* Note: α_0 is the $u = 0$ intercept of the exchange; $\alpha_0 \approx 0$ for $I_u = \frac{3}{2}$ ($\Delta\delta$) and $\alpha_0 \approx -0.4$ for $I_u = \frac{1}{2}$ ($N\alpha$). See tables 1-3 for precise values.

$$E_{\text{lab}}^3 \frac{d\sigma}{du} \propto E_{\text{lab}}^{2\alpha_0+1} \exp(u \log E_{\text{lab}}) . \quad (24)$$

In the fixed-pole model,

$$E_{\text{lab}}^3 \frac{d\sigma}{du} = \text{constant} . \quad (25)$$

Finally, in the HIPPIE (fixed cut) model *,

$$E_{\text{lab}}^3 \frac{d\sigma}{du} \propto E_{\text{lab}}^{2\alpha_0+1} . \quad (26)$$

These different predictions are compared quantitatively in fig. 23.

We emphasize that these predictions for energy dependence are based directly on fundamental properties of the models; the predictions are independent of specific values of parameters. Therefore, as shown in fig. 23, measurements of energy dependence of $d\sigma/du$ for $\gamma d \rightarrow pn$ and $\gamma p \rightarrow \Delta^{++}\pi^-$ will determine unambiguously which one, if any, of our four models is correct.

4.2.2c. Isoscalar-isovector interference

Measurements of $d\sigma/du$ for $\gamma d \rightarrow pn$ provide an opportunity to identify interference effects between the two $I_u = \frac{1}{2}$ amplitudes, formed from isovector and isoscalar components of the photon, respectively. We identify two separate reactions †: $\gamma d \rightarrow pn$, which has relatively small momentum transfer u_p from photon to proton, and $\gamma d \rightarrow np$, which has small momentum transfer u_n from photon to neutron. The isovector amplitude contributes to both reactions with the same sign; however, the contribution of the isoscalar amplitude changes. Therefore, $A(u_p) = A^{I\gamma=1} + A^{I\gamma=0}$, but $A(u_n) = A^{I\gamma=1} - A^{I\gamma=0}$. Measurements of $d\sigma/du$, as a function of s and u, are obviously desirable, for both reactions.

4.3. *Polarization measurements in* $\gamma N \rightarrow N\pi$, $\gamma N \rightarrow \Sigma K$ *and* $\gamma N \rightarrow \Lambda K$

Four independent amplitudes are necessary for a complete description of $\gamma p \rightarrow N\pi$. Because each is complex, a total of eight functions of s and u must be determined. Measurement of $d\sigma/du$ provides only one constraint. For this reason, simple agreement with $d\sigma/du$ is no assurance that any of our models is a good representation of $\gamma p \rightarrow N\pi$. Additional progress awaits polarization measurements.

In fig. 24, we give the predictions of our models for two of the polarization observables. Results are given for the three charge states $\gamma p \rightarrow n\pi^+$, $\gamma p \rightarrow p\pi^0$, and $\gamma n \rightarrow p\pi^-$. Quantity Σ refers to experiments done with linearly polarized photons and an unpolarized target. If the photon polarization makes an angle Φ with the production plane, then the observed cross section is

* Note α_0 is the $u = 0$ intercept of the exchange, $\alpha_0 \approx 0$ for $I_u = \frac{3}{2}$ ($\Delta\delta$) and $\alpha_0 \approx -0.4$ for $I_u = \frac{1}{2}$ ($N\alpha$). See tables 1-3 for precise values

† Thus far, in this paper, we have not distinguished the two reactions. All previous references to $\gamma d \rightarrow np$ apply to both.

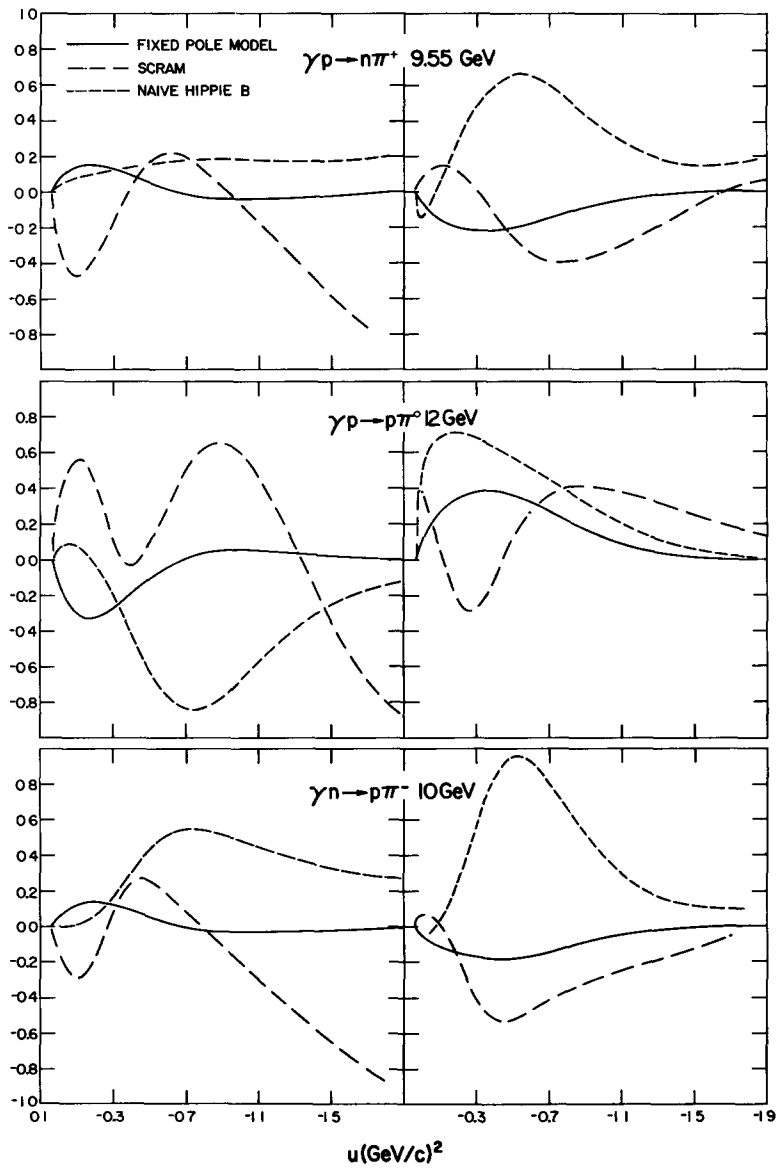

Fig. 24. In the first column, we give predictions for Σ; in the second column, we present values of L. Quantity Σ is the scattering asymmetry of pions produced by linearly polarized photons; L is the left-right asymmetry for photoproduction from a polarized nucleon target. Precise definitions are found in the text.

$$\frac{d\sigma}{du}(\Phi) = \left(\frac{d\sigma}{du}\right)_{\text{unpol.}} (1 - \Sigma \cos 2\Phi) . \tag{27}$$

Quantity L is determined in experiments done with polarized proton targets and unpolarized photons; it measures the left-right asymmetry. If φ is the angle between the target polarization and the normal * to the scattering plane, then

$$\frac{d\sigma}{du}(\varphi) = \left(\frac{d\sigma}{du}\right)_{\text{unpol.}} (1 + LP \cos \varphi) . \tag{28}$$

Quantity P is the initial target polarization. Predictions shown in fig. 24 cannot be taken very seriously. In all models, flexibility is possible in these distributions, without damage to our good fits to $d\sigma/du$. For example, curves for the FULL HIPPIE and NAIVE HIPPIE A models (not shown) differ considerably from those for NAIVE HIPPIE B, shown in fig. 24. We must also admit that measurements of $d\sigma/du$, Σ and L will not necessarily serve to reject any of the current models. To be sure, three quantities will form a tighter noose than just one; however, only a complete set of observables will be conclusive. To establish a complete set, it is necessary to determine final baryon polarization in experiments with polarized photons and polarized proton targets. For $\gamma p \to N\pi$, such an ambitious undertaking is probably not feasible technically at the present time. It certainly should be feasible for the (forward) reactions $\gamma p \to K\Sigma$ and $\gamma p \to K\Lambda$. In these experiments, weak decay of the Σ or Λ can be used to measure final baryon polarization. As a result, all four amplitudes for $\gamma p \to K\Sigma$ or $\gamma p \to K\Lambda$ would be determined, up to a common phase. As we have detailed elsewhere [53], delightful tests of models are possible.

Our main interest in polarization is less prosaic than rejection of models. Rather, it seems to us that if the behavior $E_{\text{lab}}^3 \, d\sigma/du \propto \exp(u)$ is truly universal, then it presumably corresponds to some simple structure of basic amplitudes. Polarization studies will hopefully lead to more profound understanding of the unusual behavior seen thus far in γp experiments. We urge that exploratory polarization studies be undertaken soon.

5. CONCLUSIONS

We have studied backward single-pion-photoproduction data from two points of view. First, we made a purely empirical study of data, comparing features of γp and purely hadronic reactions. Second, we attempted to fit γp data using amplitudes given by four different phenomenological models. These two approaches, empirical and theoretical, are complementary and enrich each other. Our empirical investigation is summarized in sect. 2; models and fits to data are described in sect. 3. The most important practical results of our study are given in sect. 4 and in subsect. 2.4; in those sections, we list valuable new experiments which would clarify outstanding difficulties.

* Normal is in the direction $(\hat{\gamma} \times \hat{\pi})$.

5.1. *Empirical results*

In sect. 2, we discuss the universal scaling law, $E_{lab}^3 \, d\sigma/du \propto g(u)$, which describes $\gamma p \to N\pi$ data. This expression is remarkable for two reasons. First, no shrinkage is observed in the data. Second, the function $g(u)$ falls-off very slowly with increasing $|u|$; for $|u| \gtrsim 0.3$ (GeV/c)^2, $g(u) \propto \exp(u)$. As we demonstrate in sect. 2, this behavior of $\gamma p \to N\pi$ data differs dramatically from that of purely hadronic data. Among other things, these differences cast doubt on the usefulness of the vector-dominance model.

Independently of any particular model, we note that discovery of universal behavior of $d\sigma/du$ (or $d\sigma/dt$) for intermediate values of momentum transfer ($\geq$ 1 (GeV/c)^2) would be of profound importance. It could be interpreted as a universal structure (core) for small impact parameters * [63]. This should be contrasted with high impact parameter behavior which, theoretically, is associated with Regge poles and, experimentally, leads to well-established peripheral peaks at small momentum transfer ($\leq$ 0.5 (GeV/c)^2). It is imperative to investigate several other photoproduction and hadronic reactions. We list specific suggestions in subsect. 2.4. Experiments should be directed towards better identification of precisely what quantum numbers, variables, and amplitudes are important at both small and intermediate values of momentum transfer.

5.2. *Models*

We have examined critically all available models for $\gamma p \to N\pi$. Two of these, the fixed-pole model and the fixed-cut model, are developed here in some detail. We show that these models are not applicable in purely-hadronic processes and, if correct for γp, imply profound dynamical differences between γp and πN reactions.

We confront predictions of each model with data. As we concluded also in our study of πN backward scattering [17], our simultaneous comparative study of several models provides much more insight than can be obtained by examining each model in isolation.

The pure-Regge-pole model is ruled out by present data; a model with Regge poles and weak absorptive cuts is also not tenable. Both models cannot accommodate the singular lack of shrinkage in γp data.

Our strong-absorption model, our fixed-pole model, and our fixed-cut model reproduce $\gamma p \to N\pi$ data. None is decisively successful, however, simply because there is so little experimental information. Nevertheless, these three models are profoundly different; as we illustrate in fig. 23, energy dependence of $d\sigma/du$ for $\gamma p \to \Delta^{++}\pi^-$ and $\gamma d \to pn$ will distinguish them unambiguously. Measurements of $d\sigma/du$ in the energy range $5 < E_{lab} < 15$ GeV would be of immense value; the range of u should be at least $0 < |u| < 1$ (GeV/c)^2.

* Perhaps the difference between photoproduction and purely hadronic interactions stems from greater importance of the low impact parameter core in the former case. It remains an experimental challenge to demonstrate this and for theorists to explain it.

Let us now consider the successful theories in more detail. Although we are able to obtain a good fit with SCRAM, data in no way test the distinctive predictions which this model makes for the *u-position of zeroes* in different helicity *amplitudes*. To test these fundamental assumption in SCRAM, measurements of spin-rotation parameters are essential [53]. We note here that although SCRAM is successful in fitting a variety of forward and backward γp processes, only $d\sigma/dt$ for forward $\gamma p \to \pi^0 p$ shows evidence for the distinctive t-dependent structure of amplitudes in the model [59]. It is not correct prediction of the presence or absence of dips in data which is the reason for the model's success in γp. Rather, it is ability to generate rather flat energy dependence (with little shrinkage) which leads to good fits. By contrast, this prediction of little shrinkage leads to poor fits to much purely hadronic data - e.g., to $\pi^- p \to \pi^0 n$ [60]. Present knowledge suggests that SCRAM is correct only in its prediction for the *imaginary* part of strong interaction amplitudes [53, 61]. Our discussion emphasizes again the need for experiments which will determine u-dependent structure of photoproduction amplitudes [53].

The most significant theoretical aspect of the fixed-cut model is the fact that it predicts no parity doubling for fermions. However, high energy γp and πN scattering data cannot speak to this issue. To test the fixed-cut model, it is essential to extend detailed πN phase-shift analyses up to, say, mass $(\pi^{\pm} p) \approx 3$ GeV. Although present phase-shift results indicate that parity doubling does not occur in Nature for mass $\lesssim 2$ GeV, there are too few resonant states below that value of mass to allow confident generalization [17].

The fixed-pole and the fixed-cut models both offer an appealing phenomenological explanation for the absence of shrinkage in $\gamma p \to N\pi$ data. Unfortunately, there is much freedom in both models; considerable theoretical work is still necessary to eliminate these ambiguities. To motivate such theoretical effort, it is necessary to develop unambiguous experimental evidence for the relevance of models with fixed-singularities. Our specific suggestions are given in sect. 4.

APPENDIX A

Photoproduction kinematics and Regge-pole formalism

(a) *The u-channel helicity amplitudes*. As is customary, we parametrize reduced residue functions of u-channel helicity amplitudes. For the u-channel process $\bar{N}_4 \gamma_1 \to \bar{N}_2 \pi_3$, with helicities $(\lambda_4, \lambda_1 \to \lambda_2, 0)$, we use symbols β_i to denote these reduced residues. The association of subscript index i with helicities is specified in eq. (A.1)

$$\beta_1 = (\tfrac{1}{2}\, 1 \to \tfrac{1}{2}\, 0)\,, \qquad \beta_2 = (\tfrac{1}{2}\, 1 \to -\tfrac{1}{2}\, 0)\,,$$

$$\beta_3 = (-\tfrac{1}{2}\, 1 \to \tfrac{1}{2}\, 0)\,, \qquad \beta_4 = (-\tfrac{1}{2}\, 1 \to -\tfrac{1}{2}\, 0)\,. \tag{A.1}$$

Next we define functions γ and $\bar{\gamma}$ as follows:

$$\gamma_3(\sqrt{u}) = \beta_1 + \beta_2 , \qquad \bar{\gamma}_3(\sqrt{u}) = \beta_2 - \beta_1 ,$$

$$\gamma_2(\sqrt{u}) = \beta_3 + \beta_4 , \qquad \bar{\gamma}_2(\sqrt{u}) = \beta_4 - \beta_3 . \tag{A.2}$$

These are functions of $\sqrt{u}$, which satisfy the MacDowell symmetry constraints:

$$\bar{\gamma}_3(\sqrt{u}) = \gamma_3(-\sqrt{u}) , \qquad \bar{\gamma}_2(\sqrt{u}) = \gamma_2(-\sqrt{u}) . \tag{A.3}$$

As a result, we need consider only the functions $\gamma_2(\sqrt{u})$ and $\gamma_3(\sqrt{u})$. Each of these creates states of $\tau P = -1$ for $\sqrt{u} > 0$, and creates states of $\tau P = +1$ for $\sqrt{u} < 0$ (P is parity, and τ is signature).

(b) *Regge-pole exchange amplitudes.* For each Regge pole, with trajectory $\alpha(u)$ and signature τ, we define a function $\eta(s,u)$ as follows:

$$\eta(s,u) = \frac{-\pi(1+\tau\, e^{-i\pi\bar{\alpha}})}{2\Gamma(1+\bar{\alpha})\sin\pi\bar{\alpha}} \left(\frac{s}{s_0}\right)^{\bar{\alpha}} . \tag{A.4a}$$

Here, as elsewhere in this paper, $\bar{\alpha} = \alpha - \frac{1}{2}$. Furthermore, let

$$\eta_3(s, \sqrt{u}) = \gamma_3 \eta , \qquad \eta_2(s, \sqrt{u}) = \gamma_2 \frac{\eta}{s} . \tag{A.4b}$$

We define $\bar{\eta}_i$ by the equation

$$\bar{\eta}_i(s, \sqrt{u}) = \eta_i(s, -\sqrt{u}) .$$

(c) *Standard invariant amplitudes.* Rather than make explicit the relationship of the functions $\gamma_i(\sqrt{u})$ to the u-channel helicity amplitudes, we choose instead to express the standard CGLN invariant amplitudes [54]* in terms of the γ_i. We thus avoid a multitude of irrelevant kinematic factors of uncertain and confusing sign.

Denote the nucleon mass by M and the pion mass by μ; let $\omega = \sqrt{u}$; $s+t+u = 2M^2 + 2\mu^2$. We find

$$A_2(s,u) = \frac{-\eta_2 + \bar{\eta}_2}{2\omega} , \qquad A_3(s,u) + A_4(s,u) = \frac{(\omega+M)\eta_2 + (\omega - M)\bar{\eta}_2}{2\omega} ,$$

$$A_4(s,u) = \frac{1}{2(u-M^2)} \left[\frac{(\eta_3 - \bar{\eta}_3)}{2\omega} + (u - M^2)(A_3 + A_4) + M(t - \mu^2)A_2 \right] ,$$

$$A_1(s,u) = \frac{1}{2(u-M^2)} \left\{ \frac{(\omega+M)\eta_3 + (\omega - M)\bar{\eta}_3}{2\omega} - (u - M^2)t A_2 - M(t - \mu^2)(A_3 + A_4) \right\} . \tag{A.5}$$

* We follow the modern convention and rename their A-, B-, C- and D-amplitudes as A_1, A_2, A_3 and A_4.

(d) *Parametrization of* $\gamma_i(\sqrt{u})$. Upon defining

$$\gamma_1 = \frac{\gamma_3 + M\gamma_2}{2(u - M^2)} , \tag{A.6}$$

we may see from eq. (A.5) that functions γ_1 and γ_2 are free from kinematic singularities. Therefore, γ_1 and γ_2 are suitable for parametrization as analytic functions of $\sqrt{u}$. For example,

$$\gamma_i(\sqrt{u}) = (a_{1i} + a_{2i}\sqrt{u} + \ldots) \exp(\mu_i u) ,$$

where a_{ji} and μ_i are constants.

We note, furthermore, that γ_2 corresponds to helicity flip $\frac{3}{2}$ in the u-channel; γ_1 is the helicity flip $\frac{1}{2}$ amplitude. If a pole 'chooses sense' at $\alpha = \frac{1}{2}$, one would expect γ_2 to vanish, leaving only γ_1 non-zero there. For the N_α trajectory, explicit calculation indicates this is not true at $\alpha_{N_\alpha} = \frac{1}{2}$ (the nucleon-pole position). Both γ_1 and γ_2 are non-zero at $\alpha_{N_\alpha} = \frac{1}{2}$: they are related to the anomalous magnetic and electric born terms, respectively *. From exchange degeneracy arguments, we expect a similar situation for N_γ; we again allow γ_1 and γ_2 to be non-vanishing at $\alpha_{N_\alpha} = \frac{1}{2}$.

If a trajectory 'chooses nonsense' at $\alpha(u) = \frac{1}{2}$, then γ_1 and γ_2 are zero at that value of u. In dual versions of Regge theory †, this is true for Δ_δ and D_{15} trajectories. Thus, $\gamma_{i,\Delta} \propto \bar{\alpha}_\Delta$; this constraint is imposed in our HIPPIE and fixed-pole-model fits. In SCRAM, such nonsense zeroes are always absent.

(e) *Experimental observables.* For completeness, we present formulas for the usual experimental observables. We choose to do this in terms of s-channel helicity amplitudes ‡. Denote the latter by $H_S(\lambda_\gamma, \lambda_{N_2}, \lambda_{N_4})$, where N_2 is the initial and N_4 the final nucleon. For brevity, we write

$$H_1 = H_S(1, \tfrac{1}{2}, \tfrac{1}{2}) , \qquad H_2 = H_S(1, \tfrac{1}{2}, -\tfrac{1}{2}) ,$$

$$H_3 = H_S(1, -\tfrac{1}{2}, \tfrac{1}{2}) , \qquad H_4 = H_S(1, -\tfrac{1}{2}, -\tfrac{1}{2}) . \tag{A.7}$$

The observables are then

$$\frac{d\sigma}{dt} = \frac{0.3893}{128\pi M^2 E_{lab}^2}\, \mathcal{S} , \qquad \mathcal{S} = [\,|H_1|^2 + |H_2|^2 + |H_3|^2 + |H_4|^2\,] . \tag{A.8}$$

Here, E_{lab} is the incident photon energy, given in terms of s by

* This is not surprising. In forward photoproduction, a similar situation is present for the spin-zero pion pole, which occurs with a t-channel helicity-one $\pi\gamma$ vertex. In general, sense zeroes are absent from photoproduction amplitudes when a trajectory creates an internal particle pole having the same mass as one of the external particles.

† For discussion, see ref. [17].

‡ In our actual fits, we use equivalent expressions in terms of u-channel amplitudes. This saves computer time, but is perhaps more confusing.

$$E_{\text{lab}} = \frac{(s - M^2)}{2M} . \tag{A.9}$$

The asymmetry Σ for photoproduction by polarized photons is

$$\Sigma = 2\ \text{Re}\{H_1 H_4^* - H_2 H_3^*\}/\sigma . \tag{A.10}$$

The left-right asymmetry for scattering from a polarized target is

$$L = 2\ \text{Im}\{H_3 H_1^* + H_4 H_2^*\}/\sigma . \tag{A.11}$$

As mentioned in sect. 4, we have defined the normal to the production place to be $\hat{\gamma} \times \hat{\pi}$, as is natural for the (usual) forward scattering measurements, and *not* $\hat{\gamma} \times \hat{N}_4$.

The relationship of our helicity amplitudes - for which we use the standard Jacob-Wick convention - to the invariant amplitudes is given by

$$\begin{aligned}
H_1 &= -8\sqrt{2}\pi\sqrt{s}\ \sin\tfrac{1}{2}\theta\{F_1 + F_2 + \cos^2\tfrac{1}{2}\theta(F_3 + F_4)\} , \\
H_2 &= 8\sqrt{2}\pi\sqrt{s}\ \cos\tfrac{1}{2}\theta\{F_1 - F_2 + \sin^2\tfrac{1}{2}\theta(F_4 - F_3)\} , \\
H_3 &= 8\sqrt{2}\pi\sqrt{s}\ \sin^2\tfrac{1}{2}\theta\ \cos\tfrac{1}{2}\theta\{F_4 - F_3\} , \\
H_4 &= 8\sqrt{2}\pi\sqrt{s}\ \sin\tfrac{1}{2}\theta\ \cos^2\tfrac{1}{2}\theta\{F_3 + F_4\} .
\end{aligned} \tag{A.12}$$

Here θ is the s-channel c.m. scattering angle, and the F_k of CGLN are given by

$$\begin{aligned}
F_1 &= K\{A_1(s - M^2) + (s - M^2)(\sqrt{s} - M)A_4 - \tfrac{1}{2}(t - \mu^2)(\sqrt{s} + M)(A_3 - A_4)\} , \\
F_2 &= \frac{q}{E + M} K\{-A_1(s - M^2) + (s - M^2)(\sqrt{s} + M)A_4 - \tfrac{1}{2}(t - \mu^2)(\sqrt{s} - M)(A_3 - A_4)\} , \\
F_3 &= qK(s - M^2)\{(\sqrt{s} - M)A_2 + (A_3 - A_4)\} , \\
F_4 &= \frac{q^2 K}{(E + M)}(s - M^2)\{-(\sqrt{s} + M)A_2 + (A_3 - A_4)\} ,
\end{aligned} \tag{A.13}$$

with $K = (1/8\pi\sqrt{s})\sqrt{(E+M)/2\sqrt{s}}$, and $E = (s + M^2 - \mu^2)/2\sqrt{s}$, the final nucleon c.m. energy.

(f) *Isospin conventions.* Amplitudes for scattering in definite charge states are given by

$$\begin{aligned}
A(\gamma p \to n\pi^+) &= \sqrt{\tfrac{2}{3}}(V + \sqrt{3}S - \Delta) , & A(\gamma p \to p\pi^0) &= \tfrac{1}{3}(V - \sqrt{3}S + 2\Delta) , \\
A(\gamma n \to p\pi^-) &= \sqrt{\tfrac{2}{3}}(V - \sqrt{3}S - \Delta) , & A(\gamma n \to n\pi^0) &= \tfrac{1}{3}(V + \sqrt{3}S + 2\Delta) ,
\end{aligned} \tag{A.14}$$

Here, S and V denote isoscalar photon and isovector photon $I_u = \frac{1}{2}$ couplings, and Δ is the $I_u = \frac{3}{2}$ coupling.

APPENDIX B

HIPPIE model

In our paper on πN backward scattering [17], we defined three versions of fixed-cut models. We refer readers to that paper and to subsect. 3.3 of this text for elaboration of results. Here, we collect formulas specifically relevant to the present paper.

We begin by defining, for each Regge pole, the function $N^{\iota}_{\sigma}(u,s)$:

$$N^{\iota}_{\sigma}(u,s) = \tfrac{1}{2}\Gamma(-\bar{\alpha})\,(bu)^{\frac{1}{2}\sigma} g_{\iota}(u) \left(\frac{s}{s_0}\right)^{\bar{\alpha}_\gamma} \frac{\left[-\frac{1}{2}\sigma, bu \log\left(\frac{s}{s_0}\right)\right]}{\Gamma(-\frac{1}{2}\sigma)} \,. \qquad \text{(B.1)}$$

Here, index $\iota = 1, 2$ lables the two-pole couplings. Function $\gamma[-\frac{1}{2}\sigma, \ldots]$ is the incomplete Gamma function (cf. eq. (26) of ref. [17]); $g_{\iota}(u)$ is a regular function of u (e.g., eq. (7) of this paper). As table 1 indicates, in our fits we set $g(u) = (a_0 + a_1 u)\exp(\mu u)$; a_0, a_1 and μ are variable parameters. In some cases, we set $a_1 \equiv 0$.

Amplitudes with signature may be constructed in different ways. To define NAIVE HIPPIE, we set

$$J^{\iota}_{\sigma}(u,s) = N^{\iota}_{\sigma}(u,s) + \tau N^{\iota}_{\sigma}(u, s\ e^{-\iota\pi}) \,. \qquad \text{(B.2)}$$

For SUPER HIPPIE, we set

$$J^{\iota}_{\sigma}(u,s) = \eta_{\tau}(u) N^{\iota}_{\sigma}(u, s\ e^{-\frac{1}{2}\iota\pi}) \,, \qquad \text{(B.3)}$$

where

$$\eta_{\tau}(u) = \begin{cases} 2\cos\tfrac{1}{2}\pi\bar{\alpha} & \text{if} \quad \tau = +1 \,, \\ 2\iota \sin\tfrac{1}{2}\pi\bar{\alpha} & \text{if} \quad \tau = -1 \,. \end{cases} \qquad \text{(B.4)}$$

Both eqs. (B.2) and (B.3) have the same Regge-pole component, given by eq. (6) of this paper.

We use acronym FULL HIPPIE to denote the original amplitude suggested by Bardakçi and Halpern. It differs from eqs. (B.2) and (B.3) by a term which has only a cut singularity at $j = \alpha_0$. In terms of eq. (B.3), we define FULL HIPPIE by

$$J^{\iota}_{\sigma}(u,s) = \eta_{\tau}(u) N^{\iota}_{\sigma}(u, s\ \exp(-\tfrac{1}{2}\iota\pi))$$

$$+ \frac{\sin\frac{1}{2}\pi\sigma}{\pi} (\tilde{s})^{\bar{\alpha}_0} \int_0^{\infty} \frac{d\mu\, \tilde{s}^{-\mu}\, \mu^{\frac{1}{2}\sigma}}{\mu + bu} \left[G_i\left(\frac{-\mu}{b}\right) - G_{\iota}(u) \right] , \qquad \text{(B.5)}$$

where

$$\tilde{s} = \left(\frac{s}{s_0}\right) \exp(-\tfrac{1}{2}i\pi) \qquad \text{(B.6)}$$

and

$$G_\iota(u) = \eta_\tau(u)\, g_\iota(u) \tfrac{1}{2}\Gamma(-\bar{\alpha}) \ . \tag{B.7}$$

In practice, we set $s_0 = 1/b$ wherever it appears; b is the slope of the Regge trajectory $\bar{\alpha} = \alpha - \frac{1}{2} = \alpha_0 - \frac{1}{2} + bu$.

In HIPPIE models, the functions $\eta_\iota(s, \sqrt{u})$, discussed in appendix A, are given by:

$$\eta_\iota(s, \sqrt{u}) = (-\tau P(b)^{-\frac{1}{2}} J^\iota_{\sigma+1}(u, s) + \sqrt{u}\, J^\iota_\sigma(u, s))/s^{\iota-1} \ , \tag{B.8}$$

for $\iota = 1$ and 2. In analogy to eq. (A.6), η_3 is found from

$$\eta_3 = 2(u - M^2)\eta_1 - M\eta_2 s \ . \tag{B.9}$$

As a result, Regge trajectories create only states for which the product (signature × parity) = τP; as observed in Nature, each Regge recurrence has a definite parity.

APPENDIX C

Fixed-pole model

Formalism for the fixed-pole model is essentially identical to that presented in appendix A. We need only specify how we write the fixed-pole contribution to $\eta(s,u)$.

Much arbitrariness is present in the exact choice of fixed-pole formulas. We may define a fixed-pole amplitude to be the function obtained from a Regge-pole amplitude in the limit $\bar{\alpha}_0 \to -1$ and $\alpha' \to 0$. (Regge-pole amplitudes are functions of $\bar{\alpha} = \bar{\alpha}_0 + \alpha' u = \alpha_0 - \frac{1}{2} + \alpha' u$.) Correspondingly, different expressions for fixed-pole amplitudes are obtained for different sets of quantum numbers of the original Regge pole. Because it is adequate here, we adopt only an 'N_α fixed pole'. We calculate its contribution numerically by setting $\bar{\alpha} = -1.01 + 0.01u$ in the formula

$$\eta(s,u) = -\tfrac{1}{2}\pi \frac{(1 + e^{-i\pi\bar{\alpha}})}{\Gamma(1+\frac{1}{2}\bar{\alpha}) \sin \pi\bar{\alpha}} (\alpha' s)^{\bar{\alpha}} \ . \tag{C.1}$$

Our eq. (C.1) is a modification of eq. (A.4); we replace $\Gamma(1+\bar{\alpha})$ by $\Gamma(1+\frac{1}{2}\bar{\alpha})$ in order to remove the (WSNZ) zero present in N_α Regge-pole amplitudes at $\alpha_N = -\frac{1}{2}$. Without this modification, eq. (C.1) would vanish at $\bar{\alpha} = -1$. We will encounter eq. (C.1) again in appendix D; it is the form for an N_α Regge-pole amplitude used in the SCRAM model.

Actually, in our fixed-pole model fit, we use these 'SCRAM amplitudes' also for *Regge*-pole expressions (without the limiting procedure applied, of course). We do so in order to avoid a dip near $u = -0.15$ (GeV/c)^2 in the N_α Regge-pole contribution to $d\sigma/du$. See eq. (D.1) for more details. Both for the Δ_δ and N_α Regge-pole amplitudes and for the fixed-pole amplitudes, we parametrize the reduced residues (defined in appendix A) as

$$\gamma_i(\sqrt{u}) = (a_i + b_i\sqrt{u})\exp(\mu u) .$$

The ratio (a_i/b_i) is then fixed in order to eliminate the wrong parity state at the $N_\alpha(936)$ and $\Delta_\delta(1236)$ resonance-pole positions; i.e. for N_α,

$$\gamma_i(\sqrt{u}) = d_i(M - \sqrt{u})\exp(\mu u)$$

and for Δ_δ,

$$\gamma_i(\sqrt{u}) = d_i(M_\Delta + \sqrt{u})\exp(\mu u) .$$

These choices are made primarily to reduce the number of free parameters. Variable parameters are then d and μ for each exchange. Scale constraint s_0, in Regge-pole expressions, is also fixed; $s_0 = 1/\alpha'$. For reasons now lost in the murky past, we replace s by $\nu = \frac{1}{2}(s-t)$ everywhere it appears; this substitution is inconsequential.

APPENDIX D

Strong-absorption model

Our absorption prescription is similar to that described for backward πN scattering in ref. [17]; we do not repeat details here. In our version of SCRAM, input *Regge-pole* amplitudes have the form

$$\eta(s,u) = \frac{-\pi(1+\tau\, e^{-i\pi\bar{\alpha}})}{2G(\bar{\alpha})\sin\pi\bar{\alpha}} \left(\frac{s}{s_0}\right)^{\bar{\alpha}} , \tag{D.1}$$

with

$$G(\bar{\alpha}) = \begin{cases} \Gamma(\frac{1}{2}(1+\bar{\alpha})) & \text{if} \quad \tau = -1(N_\gamma, \Delta_\delta) , \\ \Gamma(\frac{1}{2}(2+\bar{\alpha})) & \text{if} \quad \tau = +1(N_\alpha) . \end{cases} \tag{D.2}$$

This expression replaces eq. (A.4) of appendix A. The effect of substituting $G(\bar{\alpha})$ for $\Gamma(1+\bar{\alpha})$ is to remove explicitly all WSNZs from the usual simple Regge-pole formula. However, the same phase is retained, as is the presence of recurrence poles at right-signature-sense positions.

Scale constant s_0 is fixed again: $s_0 = 1/b$, where b is the trajectory slope. As in the fixed-pole model, we make the unimportant replacement of s by $\nu = \frac{1}{2}(s-t)$. Parametrization of functions $\gamma_i(\sqrt{u})$ is given in eq. (22) of the text. Absorption is characterized by the s-wave absorption constant c (cf. eqs. (11)-(13) of ref. [17]); we fix c to be purely real and equal to 1.25. This value is close to that determined in our best SCRAM fits to πN backward scattering data [17].

REFERENCES

[1] R Diebold High-energy photoproduction. SLAC-PUB-673 published in Proc of the 1969 Boulder Conf on high-energy physics, eds K Mahanthappa, W Walker and W Brittin (Colorado Associated Univ Press, 1970)

[2] P Joos, Compolation of photoproduction data above 1 2 GeV Report No DESY-HERA 70-1 (September, 1970)

[3] M. Ross F Henyey and G L Kane, Nucl Phys 23B (1970) 269

[4] R Carlitz and M Kislinger, Phys. Rev Letters 24 (1970) 186

[5] K. Bardakçi and M B Halpern, Phys. Rev Letters 24 (1970) 428

[6] Y Nambu and J J Sakurai, Phys Rev Letters 8 (1962) 79

[7] M. Gell-Mann, D. Sharp and W G Wagner, Phys Rev Letters 8 (1962) 261

[8] R. L Anderson, D. Gustavson, J Johnson, D Ritson, R Weinstein, W G Jones and D. Kreinick, Phys. Rev Letters 21 (1968) 479

[9] R. L Anderson, D Gustavson, J Johnson, I Overman, D Ritson and B H Wiik, Phys. Rev Letters 23 (1969) 721

[10] D Tompkins R Anderson, B Gittelman, J. Litt, B H Wiik, D Yount and A Minten, Phys Rev Letters 23 (1969) 725

[11] R. Wilson, Nuovo Cimento Letters 1 (1969) 952

[12] J Banaigs, J. Berger, C Bonnel, J Duflo, L. Goldzahl, F Plouin, W F Baker P J Carlson, V. Chabaud and A Lundby, Nucl Phys B8 (1968) 31

[13] W F Baker P J Carlson V Chabaud A Lundby, J Banaigs, J Berger C Bonnel J Duflo L Goldzahl and F Plouin, Nucl Phys B9 (1969) 249

[14] D P Owen, F C. Peterson, A L Read, J Orear, D G Ryan, D H White, A Ashmore, C J.S. Damerell, W R Frisken and R Rubinstein, Phys Rev 181 (1969) 1794

[15] R. R. Crittenden, K F. Galloway, R M. Heinz, H A Neal and R A Sidwell, Phys Rev D1 (1970) 3050

[16] E W Anderson, E J Bleser, H R Blieden, G. B Collins D Garelick, J Menes, F. Turkot D Birnbaum, R M Edelstein, N C Hien, T J McMahon, J Mucci and J Russ, Phys Rev Letters 20 (1968) 1529

[17] E. L. Berger and G C. Fox, Comparative evaluation of theories of πN backward scattering, Report No ANL/HEP 7019, Nucl Phys B26 (1971) 1

[18] R C Chase, E Coleman, H W J Courant, E Marquit, E W Petraske, H Romer and K Ruddick, Phys Rev Letters 22 (1969) 1137

[19] J P Boright, D R Bowen, D E. Groom, J Orear, D P Owen, A J Pawlicki and D. H White, Phys. Letters B33 (1970) 615

[20] S Hagopian, V. Hagopian, E. Bogart, R O'Donnell and W Selove, Phys Rev. Letters 24 (1970) 1445

[21] J P Baton and G Laurens, Nucl Phys B21 (1970) 551.

[22] P B. Johnson, J A Poirier, N N. Biswas, N M. Cason, T.H Groves, V P. Kenney, J. T McGahan, W D. Shephard, L J. Gutay, J. H Campbell, R L. Eisner, F J. Loeffler, R E Peters, R. J. Sahni, W L Yen, I Derado and Z Guiragossian, Phys. Rev. 176 (1968) 1651.

[23] E. W. Anderson, E J Bleser, H R Blieden, G B Collins, D. Garelick, J. Menes, F. Turkot, D Birnbaum, R. M. Edelstein, N C Hien, T. J McMahon, J. Mucci and J. Russ, Phys. Rev. Letters 22 (1969) 102.

[24] D. J Schotanus, C. L. Pols, D. Z. Toet, R T. Van de Walle, J. V Major, G. E. Pearson, B. Chaurand, R Vanderhaghen, G. Rinando and A. E Werbrouck, Nucl Phys. B22 (1970) 45.

[25] P. J. Carlson, P Fleury, A. Lundby, S. Mukhin and J Myrheim, Phys Letters Letters 33B (1970) 502.

[26] R. M. Heinz, O E. Overseth, D. E. Pellett and M. L. Perl, Phys Rev 167 (1968) 1232.

[27] D. Dekkers, B Jordan, R. Mermod, C C. Ting, G Weber, T. R Willitts, K. Winter, X DeBonard and M. Vivargent, Phys. Letters 11 (1964) 161.

[28] J. V. Allaby, F Binon, A.N Diddens, P. Duteil, A. Klovning, R. Meunier, J P Peigneux, E J Sacharidis, K Schlupmann, M Spighel, J P Stroot, A M. Thorndike and A. M Wetherell, Phys Letters 29B (1969) 198
[29] R Anderson, D. Gustavson J Johnson, D Ritson, B H Wiik, W G Jones, D Kreinick F Murphy and R Weinstein, Phys Rev D1 (1970) 27
[30] P. Sonderegger J Kirz, O Guisan, P Falk-Vairant, C Bruneton, P Borgeaud, A V Stirling, C Caverzasio J P Guillaud, M Yvert and B Amblard, Phys Letters 20 (1966) 75.
[31] C W Akerlof, D. G Crabb, J L Day, N. P Johnson, P Kalbaci, A D Krisch, M T. Lin, M L Marshak J K Randolf, P Schmueser, A L Read, K W Edwards, J G Asbury G J Marmer and L G Ratner, Inelastic high-energy proton-proton collisions Univ. of Michigan Report (1970)
[32] J V Allaby, F Binon A N Diddens, P Duteil, A Klovning, R Meunier, J. P Peigneux E J Sacharidis, K Schlupmann, M Spighel, J P Stroot, A M. Thorndike and A M Wetherell, High-energy particle spectra from proton interactions at 19.2 GeV/c CERN Report 70-12
[33] A. M Boyarski, F Bulos W Busza, R Diebold, S D Ecklund, G E Fisher, J R. Rees and B Richter, article D 6 in SLAC users handbook
[34] M. Breidenback J Friedman, H Kendall, E D Bloom, D H Coward, H DeStaebler J Drees L Mo and R Taylor, Phys Rev Letters 23 (1969) 935
[35] V Barger and P Weiler, Phys Letters 30B (1969) 105 Nucl Phys B20 (1970) 615.
[36] J V. Beaupré and E A Paschos, Phys Rev D1 (1970) 2040
[37] R. P Bajpai and A Donnachie, Nucl Phys B17 (1970) 453
[38] R. Kelly G. L. Kane and F. Henyey, Phys Rev Letters 24 (1970) 1511.
[39] F. A. Berends, A Donnachie and D L Weaver, Nucl Phys. B4 (1968) 1, 54, 103
[40] R. L. Walker, Phys Rev 182 (1969) 1729.
[41] R. Oehme, lectures in Strong interactions and high-energy physics, ed R G Moorhouse (Plenum Press, New York, 1964).
[42] G. C Fox and D. Z. Freedman, Phys Rev 182 (1969) 1628
[43] A. M Boyarski, R Diebold, S D Ecklund G E Fisher, Y Murata, B Richter and M Sands, Phys Letters 34B (1971) 547
[44] C Akerlof, T Coffin, T Kalbaci, D Meyer, K Stanfield and P Schmueser, Small-angle production in the reaction $\pi^+ p \to K^+ \Sigma^+$ Univ. of Michigan preprint (1970) submitted to 15th Int Conf on high-energy physics, Kiev, 1970
[45] C W Akerlof, Double-charge-exchange reactions, invited paper presented at APS-DPF Meeting, Austin, Texas, November, 1970
[46] C B Chiu, Revs Mod Phys 41 (1969) 640
[47] J D Jackson, Revs Mod Phys 42 (1970) 12.
[48] B R Desai, P Kaus, R T. Park and F Zachariasen, Phys Rev Letters 25 (1970) 1389 1686(E).
[49] R. A. Alvarez, G. Cooperstein, K. Kalata, R C Lanza and D Luckey, Phys Rev D1 (1970) 1946
[50] G Giacomelli, P Pini and S Stagni, A compilation of pion-nucleon scattering data, CERN/HERA Report 69-1
[51] E. L Berger, Phys Rev. Letters 23 (1969) 1139
[51] E L. Berger and R. A. Morrow, Phys. Rev Letters 25 (1970) 1136
[53] E. L. Berger and G. C. Fox, Argonne report ANL/HEP 7023, Phys Rev Letters 25 (1970) 1783
[54] G. F Chew, M. L. Goldberger, F. E Low and Y. Nambu, Phys. Rev. 106 (1957) 1345.
[55] California Institute of Technology Users Group, unpublished data on $\gamma p \to \pi^0 p$ in $|t|$ range from 0.5 to 3 (GeV/c)^2 E_{lab} = 6 to 18 GeV.
[56] W.S Brockett, G. T. Corlew, W. R. Frisken, T. L. Jenkins, A. R. Kirby, C. R. Sullivan, J. A. Todoroff and W B Richards, Phys. Rev. Letters 26 (1971) 527.
[57] J. B. Bronzan and C. E. Jones, Phys. Rev. 160 (1967) 1494.
[58] R. Dashen and S Y. Lee, Phys. Rev. Letters 22 (1969) 366

[59] G. L. Kane, F. Henyey, D R Richards, M Ross and G Williamson, Phys Rev Letters 25 (1970) 1519.
[60] G C. Fox, in High-energy collisions, ed C N Yang, J Cole, M. Good, R Hwa and J Lee-Franzini (Gordon and Breach, NY, 1969).
[61] H Harari Elastic hadronic processes, duality and absorption, SLAC-PUB-821 (October, 1970).
[62] R. L. Anderson, D. Gustavson, J. Johnson, I. Overman, D. Ritson and B. H. Wiik, Phys. Rev. Letters 23 (1969) 890.
[63] This idea is both elaborated and applied to forward photoproduction and strong interactions by G. C. Fox and C. B. Chiu (unpublished). This work is reviewed by G. C. Fox in Phenomenology in Particle Physics, 1971 (Caltech 1971).